

İSTANBUL TECHNICAL UNIVERSITY ★ GRADUATE SCHOOL OF SCIENCE
ENGINEERING AND TECHNOLOGY

**DEVELOPMENT OF METHODOLOGIES AND THEIR APPLICATIONS ON
THE IMPROVEMENT OF VEHICLE NVH PERFORMANCE**



Ph.D THESIS

Cem MERİÇ

Department of Mechanical Engineering

Mechanical Engineering Programme

MAY 2018

İSTANBUL TECHNICAL UNIVERSITY ★ GRADUATE SCHOOL OF SCIENCE
ENGINEERING AND TECHNOLOGY

**DEVELOPMENT OF METHODOLOGIES AND THEIR APPLICATIONS ON
THE IMPROVEMENT OF VEHICLE NVH PERFORMANCE**



Ph.D. THESIS

Cem MERİÇ
(503082005)

Department of Mechanical Engineering

Mechanical Engineering Programme

Thesis Advisor: Prof. Dr. Haluk EROL

MAY 2018

İSTANBUL TEKNİK ÜNİVERSİTESİ ★ FEN BİLİMLERİ ENSTİTÜSÜ

**ARAÇ NVH PERFORMANSININ İYİLEŞTİRİLMESİNİ HEDEFLEYEN
YÖNTEMLERİN GELİŞTİRİLMESİ VE UYGULAMALARI**

DOKTORA TEZİ

**Cem MERİÇ
(503082005)**

Makina Mühendisliği Anabilim Dalı

Makina Mühendisliği Programı

Tez Danışmanı: Prof. Dr. Haluk EROL

MAYIS 2018

Cem Meriç, a Ph.D. student of İTÜ Graduate School of Science Engineering and Technology student ID 503082005, successfully defended the thesis entitled “DEVELOPMENT OF METHODOLOGIES AND THEIR APPLICATIONS ON THE IMPROVEMENT OF VEHICLE NVH PERFORMANCE”, which he prepared after fulfilling the requirements specified in the associated legislations, before the jury whose signatures are below.

Thesis Advisor : **Prof. Dr. Haluk EROL**
İstanbul Technical University

Jury Members : **Prof. Dr. Ata MUGAN**
İstanbul Technical University

Dr. Öğr. Üyesi Erdem UZUNSOY
Bursa Technical University

Prof. Dr. İsmail Ahmet GÜNEY
İstanbul Technical University

Prof. Dr. Ayşe Saide SARIGÜL
Dokuz Eylül University

Date of Submission : 04 April 2018

Date of Defense : 21 May 2018





To my family,



FOREWORD

I would like to express my gratitude to all those who gave me the opportunity to complete this thesis.

I am deeply indebted to my supervisor Prof. Dr. Haluk Erol for his guidance, contribution and suggestion during all phases of my study. I would also like to thank all my friends and colleagues Mr. Mustafa Reşit Özer, Mr. Tarık Küçük, Mr. Ziya Girgin, Mr. Halil Ateş, Mr. Ahmet Ayvaz and Mr. Aytekin Özkan especially to for their help and support.

Finally, I should say many thanks to my great family for all their patience and encouragement at every phase of my studies; my mothers Ayşe Meriç, Neziha Kumru, my fathers Sadettin Meriç, Hüseyin Kumru, my sister Sinem Meriç, my brothers Yavuz Akyapak, Tevfik Kumru. I should express my gratitude to my beloved wife Yasemin Meriç, who gave us our meaning of life, our son Batu Meriç, for her support in every phase of my life including this thesis study.

May 2018

Cem MERİÇ
(Mechanical Engineer, M.Sc.)

TABLE OF CONTENTS

	<u>Page</u>
FOREWORD	ix
TABLE OF CONTENTS	xi
ABBREVIATIONS	xiii
SYMBOLS	xv
LIST OF TABLES	xix
LIST OF FIGURES	xxi
SUMMARY	xxiii
ÖZET	xxv
1. INTRODUCTION	1
2. NOISE CONTRIBUTION ANALYSIS OF A VEHICLE PASSENGER COMPARTMENT	9
2.1 Abstract	9
2.2 Introduction	10
2.3 Theory	12
2.4 Experimental Studies	18
2.5 Conclusion	35
3. ON THE SOUND ABSORPTION PERFORMANCE OF A FELT SOUND ABSORBER	37
3.1 Abstract	37
3.2 Introduction	37
3.3 Theoretical Background	38
3.4 Analytical Studies	42
3.5 Experimental Studies	47
3.6 Conclusion	49
4. DESIGN AND APPLICATION OF A COMPACT HELICAL AIR INTAKE SYSTEM RESONATOR FOR BROADBAND NOISE CONTROL	53
4.1 Abstract	53
4.2 Introduction	53
4.3 Theory	55
4.4 Design And Virtual Verification	57
4.5 Experimental Studies	62
4.6 Conclusion	68
5. CONCLUSION	71
5.1 Practical Application of This Study	72
REFERENCES	73
CURRICULUM VITAE	77



ABBREVIATIONS

ASQ	: Acoustic Source Quantification
SEA	: Statistical Energy Analysis
PACA	: Panel Contribution Analysis
TL	: Transmission Loss
TPA	: Transfer Path Analysis
NR	: Noise Reduction
WOT	: Wide Open Throttle
PBN	: Pass-by-Noise
SPL	: Sound Pressure Level
Kph	: Kilometer per Hour
NATF	: Near Field Acoustic Transfer Function
FATF	: Far Field Acoustic Transfer Function
ATF	: Acoustic Transfer Function
VVSS	: Volume Velocity Sound Source
DRE	: Driver Right Ear
AFR	: Air Flow Resistivity
FRFL04	: Front Right Floor 4th Sub-panel
FRFL05	: Front Right Floor 5th Sub-panel
TRUNKFLOR02	: Trunk Floor 2nd Sub-panel
TRUNKFLOR03	: Trunk Floor 3rd Sub-panel
ROOF06	: Roof 6th Sub-panel
ROOF10	: Roof 10th Sub-panel
CAD	: Computer Aided Drawing
FFT	: Fast Fourier Transform
AIS	: Air Intake System



SYMBOLS

\mathbf{p}^{TF}	: Pressure during the reciprocal transfer function measurements
\mathbf{u}^{TF}	: Particle velocity during the reciprocal transfer function measurements
\mathbf{p}	: Pressure during the noise measurements
\mathbf{u}	: Particle velocity during the noise measurements
S	: Defined cavity
M	: Surface of the defined cavity
p_r	: Reference pressure
Q	: Monopole source
P_{target}	: Total calculated sound pressure level at the target position
P_i	: Contribution of each panel to the total noise level at the target position
\dot{Q}_i	: Operational loads of panel i
H_i	: Acoustic transfer function from the panel i to the target position
\ddot{x}_i	: Acceleration of i^{th} panel
A_i	: Area of the panel i
P_{Ti}^{OP}	: Sound pressure level at each indicator microphones in operational conditions
\dot{Q}_{VVSS}^j	: Volume acceleration at VVSS on each engine surface during the ATF measurements
P_{Ti}^{TF}	: sound pressure level at each indicator microphone in the stationary ATF measurements
$P_{\text{TARGET}}^{\text{TF}}$: sound pressure level at the target microphone (DRE: Driver Ear) in the stationary ATF measurements
\dot{Q}_i^{OP}	: Operational loads at indicator i
P_i	: Contribution of each indicator location
P_{target}	: Total calculated sound pressure level at the target position
n_i	: Modal density
ΔN_i	: Number of natural frequencies of a subsystem
Δf	: Interested frequency range
P_{ii}	: Dissipated power inside the system
P_{ij}	: Dissipated power between the subsystems
E_i	: Energy input of the subsystem i
E_j	: Energy input of the subsystem j
P_i	: Power input of the subsystem i
P_j	: Power input of the subsystem j
P_{ii}	: Energy dissipated inside the subsystem i
P_{jj}	: Energy dissipated inside the subsystem j
P_{ij}	: Energy dissipation between the subsystems i and j
P_{ji}	: Energy dissipation between the subsystems j and i
η_{11}	: Damping loss factor of the subsystem i

η_{12}	: Coupling loss factor of the subsystem i
η_{22}	: Damping loss factor of the subsystem j
η_{21}	: Coupling loss factor of the subsystem j
ρ	: Effective density
K	: Bulk modulus
ϕ	: Porosity
α_{∞}	: Tortuosity
Λ	: Viscous characteristic length
Λ'	: Thermal characteristic length
P_0	: Atmospheric pressure
ρ_0	: Density of air
ω	: Angular frequency
γ	: Adiabatic constant
B	: Prandtl number
c'	: Coefficient
c	: Pore shape factor
η	: Dynamic Viscosity
Z_C	: Characteristic impedance
k	: Wave number
R	: Reflection Coefficient
α	: Sound absorption coefficient
p_{xi}	: Pressure at the bottom of the i^{th} layer of a multi layer porous material
u_{xi}	: Particle velocity at the bottom of the i^{th} layer of a multi layer porous material
p_{xi+1}	: Pressure at the bottom of the $(i + 1)^{\text{th}}$ layer of a multi layer porous material
u_{xi+1}	: Particle velocity at the bottom of the $(i + 1)^{\text{th}}$ layer of a multi layer porous material
p_{li}	: Pressure at the top of the i^{th} layer of a multi layer porous material
u_{li}	: Particle velocity at the top of the i^{th} layer of a multi layer porous material
d_i	: Thickness of the layer of a multi layer porous material
ρ_i	: Density of the i^{th} layer of a multi layer porous material
k_{xi}	: Wavenumber for the i^{th} layer of a multi layer porous material
z_{si}	: Impedance of the bottom of the i^{th} layer of a multi layer porous material
z_i	: Characteristic impedance of the i^{th} layer of a multi layer porous material
z_{si+1}	: Impedance of the bottom of the $(i + 1)^{\text{th}}$ layer of a multi layer porous material
x_1	: Position of microphone #1 in impedance tube
x_2	: Position of microphone #2 in impedance tube
p_1	: Sound pressure at microphone #1 in impedance tube
p_2	: Sound pressure at microphone #2 in impedance tube
H_{21}	: Transfer function between the microphones in impedance tube
s	: Distance between the microphones in impedance tube
α	: Normal sound absorption coefficient
l_a	: Length of rigid straight main duct
d_a	: Diameter of rigid straight main duct
l_b	: Length of rigid straight inner duct

d_b	: Diameter of rigid straight inner duct
TL	: Transmission loss of the pipe system
$p(0, t)$: Sound pressure at the input of a pipe
$p(L, t)$: Sound pressure at the output of a pipe
$v(0, t)$: Volume velocity at the input of a pipe
$v(L, t)$: Volume velocity at the output of a pipe
A, B, C, D	: Four-pole parameters
$p(x, t)$: Sound pressure field inside the tube
t	: Time
T	: Transfer matrix of the pipe
S	: Cross sectional area of the pipe
Z_a	: Characteristic impedance at inlet of the pipe
Z_e	: Characteristic impedance at outlet of the pipe
T_{17}	: Transfer matrix of the resonator system





LIST OF TABLES

	<u>Page</u>
Table 3.1 : Material acoustical parameters.....	44
Table 3.2 : Tested configurations.	45
Table 3.3 : Weight and Sound Absorption Performance Comparison (Analytical Studies).....	50
Table 3.4 : Weight and Sound Absorption Performance Comparison (Experimental Studies).....	50





LIST OF FIGURES

	<u>Page</u>
Figure 1.1 : Integration of PACA, ASQ and SEA methodologies.	5
Figure 2.1 : Integration of the PACA, ASQ and SEA methodologies.....	12
Figure 2.2 : Panel contribution systematic.	14
Figure 2.3 : ASQ-Inverse matrix method for determining the engine acoustic contribution (indicator microphones, volume velocity sound source, target position (driver ear)).	15
Figure 2.4 : Power balance equations for a sample system.....	17
Figure 2.5 : Acoustic material characterization test setups.....	19
Figure 2.6 : ATF measurement for the SEA model correlation (left: vehicle cavity, right: engine cavity).	20
Figure 2.7 : ATF measurement for the SEA model correlation (calculated vs. tested).	20
Figure 2.8 : Vehicle SEA (left) and inner-dash isolator optimization model (right). ..	21
Figure 2.9 : Initial vs. final SEA calculated ATFs.	21
Figure 2.10 : Mid/high frequency volume source.	22
Figure 2.11 : Application of engine ASQ, (Left: operational, 2 microphones for each engine face. Right: Positioning of volume source, at least 2 places on each engine face).	23
Figure 2.12 : Low/mid frequency volume source.....	24
Figure 2.13 : MATLAB model flowchart.	25
Figure 2.14 : Application of panel contribution (accelerometers on each subpanel), roof (left) and trunk floor (right).	26
Figure 2.15 : Result of the evaluation.	26
Figure 2.16 : Calculation Result: Major contributors.	27
Figure 2.17 : Subpanels and main contributor subpanels (highlighted in orange). ...	28
Figure 2.18 : Calculation result: Detailed subpanel contribution.	28
Figure 2.19 : Front right floor contributing subpanels-Adding damping pads.	29
Figure 2.20 : Improvement in the front floor contribution (before and after the application of damping pads).	30
Figure 2.21 : Improvement in the roof contribution (before and after the application of damping pads).	30
Figure 2.22 : Trunk floor - detailed contribution analysis.	31
Figure 2.23 : Trunk floor sub-panel #2 operational load and ATF analysis.	32
Figure 2.24 : The decrease in panel vibrations around 260 Hz (old: old exhaust hanger, new: new exhaust hanger with more vibration insulation performance).	33
Figure 2.25 : Improvement in the trunk floor contribution.	33
Figure 2.26 : Calculated initial and final interior noise level.	34
Figure 2.27 : Tested final interior noise level.	35
Figure 3.1 : Representation of the Multilayer Porous Material Structure.....	41

Figure 3.2 : Schematic of the Impedance Tube.	42
Figure 3.3 : Sound Absorption Coefficient Curves Calculated with the Analytical Model (Solid Red Curve: Configuration-0, Dashed Red Curve: Configuration-1, Solid Orange Curve: Configuration-2, Solid Blue Curve: Configuration-3, Solid Green Curve: Configuration-4, Solid Black Curve: Configuration-5).	46
Figure 3.4 : Schematic of the Initial One-layer and Multi-layer Structures.	46
Figure 3.5 : Experimental Setup.....	47
Figure 3.6 : Implementation of the Test Sample in the Impedance Tube.	47
Figure 3.7 : Sound Absorption Coefficient Curves Tested (Solid Red Curve: Configuration-0 and Dashed Red Curve: Configuration-1).	48
Figure 3.8 : Sound Absorption Coefficient Curves Calculated with the Analytical Model (Solid Red Curve: Configuration-0, Dashed Red Curve: Configuration-1, Solid Orange Curve: Configuration-2, Solid Blue Curve: Configuration-3, Solid Green Curve: Configuration-4, Solid Black Curve: Configuration-5).	49
Figure 3.9 : Sound Absorption Coefficient Curves Calculated vs. Tested (Black Curve: Test result of Configuration-5, Dashed Black Curve: Calculation Result of Configuration-5).....	50
Figure 3.10 : Sound Absorption Coefficient Curves Calculated vs. Tested (Orange Curve: Test result of Configuration-2, Dashed Orange Curve: Calculation Result of Configuration-2).....	51
Figure 4.1 : Schematic of helical resonator.	55
Figure 4.2 : Circular cross-section helical resonator (left), air cavity of the resonator (right).....	57
Figure 4.3 : Geometrical parameters of circular cross-section helical resonator.....	58
Figure 4.4 : Circular cross-section helical resonator transmission loss (solid curve: analytical model result, dashed curve: virtual analysis result).	59
Figure 4.5 : Pressure drop virtual analysis calculation result (solid curve: circular cross-section helical resonator, dashed curve: rectangular cross-section helical resonator).....	60
Figure 4.6 : Rectangular cross-section helical resonator.	60
Figure 4.7 : Geometrical parameters of rectangular cross-section helical resonator.....	61
Figure 4.8 : Rectangular cross-section helical resonator transmission loss (solid curve: analytical model result, dashed curve: virtual analysis result).	61
Figure 4.9 : Prototype part.	62
Figure 4.10 : Pressure drop test setup.....	62
Figure 4.11 : Pressure drop virtual analysis calculation vs test result (solid curve: test result, dashed curve: numerical analysis result).	63
Figure 4.12 : Rectangular cross-section helical resonator transmission loss test setup.	63
Figure 4.13 : Rectangular cross-section helical resonator transmission loss (solid curve: test result, dashed curve: virtual analysis result).....	64
Figure 4.14 : Vehicle level validation test setup.	65
Figure 4.15 : Ais pipe opening radiated noise, colormap representation.	66
Figure 4.16 : Ais pipe opening radiated noise, overall level and noise level at main engine orders.....	67
Figure 4.17 : Noise level at driver ear, overall level and main engine orders.	68

DEVELOPMENT OF METHODOLOGIES AND THEIR APPLICATIONS ON THE IMPROVEMENT OF VEHICLE NVH PERFORMANCE

SUMMARY

In today's competitive automotive industry, analyzing the noise level inside a passenger compartment and determining the contributors to the interior noise level has become more important due to opportunities for improvement. Finding opportunities for improvement to provide customers with a more refined vehicle in terms of passenger compartment noise level provides an advantage to the automotive manufacturer over its competitors. In the first phase of our study, integration of Acoustic Source Quantification (ASQ) and SEA methodologies is aimed to model the interior noise level inside the passenger compartment. The ASQ Direct Method, briefly explained in theory part of section 2, has been used to perform Panel Contribution Analysis (PACA), in order to investigate regions with panels that contribute primarily to the interior noise level and to determine opportunities for refining the interior noise levels within vehicles. To determine the airborne contributions of engines, the ASQ Indirect Method, briefly explained in theory section, has been applied. Creating a contribution model using MATLAB (PACA and Engine ASQ), the interior noise level of the vehicle has been calculated and correlated with the test results. By performing further analysis on the interior noise contribution model and focusing on the panel contributions, the regions with the most contributing panels have been determined and interior noise refining actions have been applied. By applying interventions, which are the refining outputs of the panel acoustic contribution analysis, an improvement of up to 3 dB(A) for a few engine speed ranges has been obtained for the overall noise level of the vehicle.

In addition to the panel contribution analysis, which is the primary focus of this study, thickness optimization of the inner dash isolator has been performed for a correlated SEA model, which confirms that no performance loss occurred in the acoustic transfer functions from the engine to the passenger compartment. The physical prototype of the optimized inner dash isolator has been assembled in the vehicle during the panel contribution analysis validation tests.

The integration of the ASQ (direct & indirect) and SEA techniques may be offered as a unique method that can be applied in the refinement phase of product development when the physical vehicle is available, to release refined and lower weight vehicles.

In the second phase of our work, we have developed an analytical model of a multilayer porous material based on the transfer matrix method to predict the absorption behavior at plane wave incidence. The aim of this study is to modify/tune the sound absorption coefficient of a felt to obtain an improved absorbing performance in the mid frequency range without increasing its weight. To achieve this target, the developed model has been used to find the best combination of each layer type and thickness. The analytical results were validated by test results.

The second section consists of three parts. First, we describe the analytical model based on the transfer matrix method of a multilayer porous material to predict the sound absorption coefficient subjected to plane waves with a rigid backing boundary condition. Second, the sound absorption coefficient calculation result of the model for a multilayer material has been presented to obtain more absorbing performance in the mid frequency range without increasing its weight, which is the main objective of this study. Generally, the mid-frequency range sound absorption performances of felts are low compared to their performance in the relatively high frequency range. There may be some cases where one may want to increase the mid-frequency absorption performance of a felt without increasing its weight. In such cases, according to the experimental results shown in this section of our study, one can modify the sound absorption curve characteristic of a felt using elastic films and the air gap without increasing or decreasing its weight. Finally, the model results have been validated with the experimental results. There is a good agreement between the analytical and experimental results in terms of the amplitude of the sound absorption coefficient in most of the frequency range and the tendency of the behavior of the curve comparing different configurations. In conclusion, compared to the initial condition, with 12% less weight, one can gain 35% in the absorption performance in the relatively mid-frequency range with a loss (20%) in the relatively high frequency range.

In the third phase of our work, we have developed an analytical model that uses the transfer matrix method to predict the transmission loss (TL) of a resonator system with a helical side branch duct connected to the main duct. The resonator system is tuned to a proper frequency range to be applied on vehicle in order to decrease the air intake pipe radiated noise of the selected passenger car below 1000 Hz. In order to fulfill the packaging requirements, the developed resonator does not require an additional volume. The designed helical resonator is a tunable resonator and can be tuned to the required frequency range by adjusting the dimensions. Resonator in our study is tuned to mainly 300 Hz – 600 Hz frequency range to decrease the noise level of the selected passenger car of which's air intake pipe radiated noise in the specified frequency range is high. Developed helical resonator has been analyzed numerically, the analytical results are first validated with the numerical ones, and the prototype part has been produced with rapid prototyping technique. Finally, the prototype part has been tested on a 1.6 l Gasoline Engine Vehicle. Our numerical calculations show that the 1D analytical approach yields satisfactorily accurate approximations in the 0 to 1000 Hz. The physical verification test results are well correlated with the numerical analysis results for both the pressure drop and the sound transmission loss. The developed tunable resonator shows significant improvement in the noise radiated from the AIS pipe between 300 and 600 Hz. This improvement resulted in a quieter passenger compartment. Considering these results, the designed tunable helical resonator is a solution for high AIS radiated noise in vehicles, especially those vehicles with small volume engine compartments where strict packaging requirements are necessary. The application of these resonators may become widespread with the further development of rapid prototyping techniques.

ARAÇ NVH PERFORMANSININ İYİLEŞTİRİLMESİNİ HEDEFLEYEN YÖNTEMLERİN GELİŞTİRİLMESİ VE UYGULAMALARI

ÖZET

Bugünün rekabetçi otomotiv dünyasında, araç kabini içerisindeki gürültü seviyesinin olan katkıların ayrıştırılması suretiyle kabin içi gürültü seviyelerinin analizi, bu gürültülerin azaltılması için fırsatlar yakalanması açısından oldukça önemlidir. Müşterisine daha rafine ve memnuniyet verici kabin içi gürültü seviyesine sahip araçlar sunabilmek için bu gürültü seviyesini iyileştirici fırsatları yakalayabilmek, bir otomotiv üreticisine rakipleri karşısında önemli bir avantaj sağlar.

Çalışmamızın birinci aşamasında, Acoustic Source Quantification (ASQ) ve İstatistiksel Enerji Analizi (SEA) yöntemlerini kullanarak araç kabini içerisindeki gürültü seviyesinin modellenmesi amaçlanmıştır. İkinci kısmın teori bölümünde açıklanan ASQ Doğrudan Yöntemi, Panel Katkıları Analizi (PACA) gerçekleştirmek için kullanılmıştır. Buradaki amaç, kabin içi gürültü seviyesine olan panel katkılarının ayrıştırılarak gürültü seviyesinin iyileştirilmesi için olası fırsatları elde etmektir. Motordan kabin içerisine olan hava yollu katkıları belirlemek için, ikinci kısmın teori bölümünde açıklanan ASQ Dolaylı Yöntemi kullanılmıştır. MATLAB programı aracılığı ile kurulan katkı modeli ile (PACA ve Motor ASQ) kabin içi gürültü seviyesi hesaplanmış ve test verileri ile olan ilgileşimi incelenmiştir. Katkı modeli ile gerçekleştirilen devam analizleri ile kabin içi gürültü seviyesine olan panel katkılarına odaklanılmış ve gürültüye en çok katkı yapan gövde panel bölgeleri belirlenmiştir. Belirlenen panel bölgelerindeki titreşimlerin azaltılması için karşı önlemler belirlenmiştir. Panel katkıları analizinin iyileştirme çıktıları olan bu karşı önlemler araca uygulanması ile birlikte kabin içi toplam gürültü seviyesinde ilgili motor devri bölgelerinde 3 dB(A)'ya kadar iyileştirme elde edilmiştir.

İlk faz çalışmalarının ana odak noktası olan panel katkıları analizine ek olarak, korele bir araç SEA modeli üzerinde ön göğüs izolatörünün kalınlık optimizasyonuna çalışılmıştır. Burada amaç kalınlık optimizasyonu gerçekleştirirken, motor kompartımanından kabin içerisine olan akustik transfer fonksiyonunda bir performans kaybı oluşmamasıdır. SEA modeli üzerinden gerçekleştirilen kalınlık optimizasyonu çıktısı olan ön göğüs izolatörünün prototipi oluşturulmuş ve araca montajı gerçekleştirilmiştir. Bu ön göğüs izolatörü hem panel katkılarını iyileştirme çalışmalarında araç üzerinde bulunmuş, ondan önce de motor kompartımanından kabin içerisine olan akustik transfer fonksiyonu doğrulaması yapılmıştır. Bu doğrulama ile SEA yöntemi çıktılarına da uygun olarak akustik transfer fonksiyonunda bir kayıp oluşturmadığı doğrulanmıştır.

Ürün geliştirme sırasında, kabin içi gürültü seviyesinin iyileştirmesi ve hafiflik azaltma amacıyla panel katkıları yöntemi ve istatistiksel enerji analizi yöntemi birlikte kullanılabilir yöntemler olarak önerilebilir.

İkinci faz çalışmalarında, düzlem dalgaya maruz kalan çok katmanlı bir gözenekli malzemenin ses yutum davranışının öngörülebilmesi için transfer matrisi yöntemi ile analitik modeli oluşturulmuştur. Bu çalışmalardaki amaç, bu analitik modeli kullanarak, keçe tipi gözenekli yutucu malzemenin ağırlığını arttırmadan ses yutum katsayısını orta frekans bölgesinde daha yüksek performans elde etmek amacıyla değiştirebilmektir. Bu amaçla, analitik model kullanılarak her bir katmanın tipini ve kalınlığının en uygun tipte ve kalınlıkta olacak şekilde seçilmiştir. Analitik model sonuçları daha sonra fiziksel test sonuçları ile doğrulanmıştır.

İkinci faz çalışmaları üç kısımdan oluşmaktadır. Birinci kısım, düzlem dalgaya maruz kalan çok katmanlı bir gözenekli malzemenin ses yutum davranışının öngörülebilmesi için transfer matrisi yöntemi ile analitik modeli oluşturulmasını anlatmaktadır. İkinci kısım, ağırlığını arttırmadan orta frekans bölgesinde daha yüksek ses yutum katsayısı elde edilen çok katmanlı gözenekli malzemenin analitik model sonuçları verilmiştir. Keçe tipi yutucu malzemelerin ses yutum katsayıları genellikle orta frekans bölgesinde yüksek frekans bölgelerine kıyasla daha düşüktür. Poliüretan tipi maliyeti yüksek ve ağır malzemeler orta frekans bölgelerindeki yutum performansları nispeten yüksek olmakla birlikte ağırlık ve maliyet dezavantajı getirmektedir. Maliyet ve ağırlık avantajından dolayı kullanılmak istenilen keçe tipi yutucu malzemelerin bazı durumlarda orta frekans ses yutum performanslarının iyileştirilmesi istenebilir. Bu gibi durumlarda, ikinci faz çalışmalarında da belirtildiği gibi, geliştirilen analitik modelleme ile ve deneysel sonuçlarda da paylaşıldığı gibi toplam ağırlığı değiştirmeden keçe tipi malzemeye ek olarak elastik film ve hava boşluğu ile çok katmanlı bir yapı elde edilerek orta frekans ses yutum performansı yüksek bir yutucu malzeme oluşturulabilir. Üçüncü kısımda, analitik model sonuçları fiziksel test sonuçları ile doğrulanmıştır. Değişik konfigürasyonlar için analitik model sonuçları ile fiziksel test sonuçları arasında ses yutum katsayısı genlikleri ve frekansa bağlı olarak değişim davranışı üzerine yüksek bir uyum elde edilmiştir.

Bahsedilen ikinci faz çalışmalarının çıktısı olarak başlangıç koşulundaki tek katmanlı keçe tipi yutucu malzemeyle karşılaştırıldığında % 12 daha düşük ağırlık ile yüksek frekanslarda ortalama %20 düşüş ile birlikte orta frekans bölgesinde % 35 daha yüksek ses yutum performansı elde edilmiştir.

Üçüncü faz çalışmalarında, transfer matrisi yöntemini kullanarak ana boruya bağlı olan helisel yan dal borularından oluşan bir hava emiş sistem rezonatörünün iletim kaybını hesaplayan bir analitik modeli oluşturulmuştur. Bu rezonatör sistemi, ilgili parametrelerini ayarlayarak, bir araca uygulanmak üzere, aracın hava emiş sisteminden yayılan gürültüyü azaltma amacına uygun olarak 1000 Hz frekans bölgesinden daha düşük frekanslarda çalışacak şekilde tasarlanmıştır. Bu rezonatör sistemi ayrıca sıkı motor bölgesi paketleme ihtiyaçlarını karşılamaya uygun olarak fazladan bir hacme ihtiyaç duymamaktadır. Bu rezonatör sistemi, helisel rezonatör olarak adlandırılmış, geometrik parametreleri değiştirilerek çalışması istenilen frekans bölgesinde çalışması ayarlanabilmektedir. Bu çalışmada tasarlanan helisel rezonatörün geometrik parametreleri, seçilen aracın ihtiyacına uygun olarak 300 Hz – 600 Hz frekans aralığında çalışacak şekilde ayarlanmıştır.

Geliştirilen helisel rezonatörün analitik model sonuçlarını doğrulamak amacıyla bir nümerik modeli oluşturulmuştur. Nümerik model sonuçları ile analitik model sonuçları arasında belirgin bir uyum elde edilmiştir. Ardından hızlı prototipleme yöntemi kullanılarak geliştirilen bu helisel rezonatörün prototipi üretilmiştir. Üretilen fiziksel prototip, parça seviyesi iletim kaybı ve basınç düşüşü fiziksel deneylerinin

ardından araç üzeri gürültü testlerini gerçekleştirmek üzere belirlenen 1.6 litre benzinli test aracı üzerine monte edilmiştir.

Bahsedilen üçüncü faz çalışmalarının çıktıları olarak, geliştirilen 1 boyutlu analitik modelleme yaklaşımı 0-1000 Hz frekans bölgesinde nümerik sonuçlar ile tatminkâr seviyede uyum içerisindedir. Fiziksel iletim kaybı ve basınç düşüşü test sonuçlarının nümerik analiz sonuçları ile uyum içerisinde olduğu da gözlenmiştir. Araç üzeri gürültü test sonuçları yorumlandığında, geliştirilen helisel, çalışma frekansı ayarlanabilir hava emiş rezonatör sisteminin kullanılması, belirlenen test aracının hava emiş sisteminden yayılan gürültüde belirgin bir iyileşme olduğu görülmektedir. Bu iyileşme kabin içi gürültü seviyesine de yansımış ve müşteri kullanım koşullarında, hızlanma manevrasında kabin içerisinde hissedilen hava emiş sistem sesinde belirgin bir azalma oluşmasını sağlamıştır.

Tüm bu sonuçlar ile birlikte, geliştirilen helisel, çalışma frekansı ayarlanabilir hava emiş rezonatörü, hava emiş sisteminden yayılan gürültünün yüksek olduğu, motor kompartımanı küçük dolayısı ile paketleme kıstasları sıkı olan araçlar üzerinde kullanılması önerilebilir. Hızlı prototipleme yöntemlerinin yaygınlaşma, daha hızlı ve ucuzlama eğiliminde olduğu günümüz dünyasında önerilen rezonatör sistemlerinin yaygınlaşması da kaçınılmaz olacaktır.



1. INTRODUCTION

Mainly, structure-borne and airborne sources contribute to the noise level inside the vehicle passenger compartment. The TPA (transfer path analysis) methodology is commonly used for creating a contribution model for structure-borne paths and performing analysis to determine individual contributing paths.

The methodology for modeling the airborne sources starts with determining the individual airborne sources like engine, intake, exhaust, etc. systems. The radiated noise in operational conditions is measured initially to multiply later with the acoustic transfer functions and to finally obtain the contribution of each airborne source to the interior noise.

There are alternative methodologies to TPA for building up a structure-borne contribution model, like panel acoustic contribution analysis (PACA) methodology. In PACA, the contribution of the radiating panels to the interior noise level is analyzed. Grosso et al [1], defines a cavity S which's surface excites the sound field when it is under operating conditions and an infinitesimal small area M inside S for studying how different areas of the cavity 'contribute' to a point at M . p^{TF} and u^{TF} are defined as the pressure and particle velocity during the reciprocal transfer function measurements. On the other hand, p and u are the pressure and particle velocity during the noise measurements [1]. Starting from the acoustic reciprocity relation [2].

$$\int_M (p^{TF} \cdot u - p \cdot u^{TF}) dM + \int_S (p^{TF} \cdot u - p \cdot u^{TF}) dS = 0 \quad (1.1)$$

The integral of particle velocity u across the entire surface M will be zero due to there is no net energy going throughout M during the noise measurements. Furthermore, the pressure p can be integrated over M during the noise measurements obtaining the reference pressure p_r . Besides, integrating the particle velocity over M during the transfer function measurement will lead to obtain the volume velocity of the monopole source Q . This leads to present the base equation of many velocity based panel noise contribution methods as [1]

$$Pr = \int_S \left(\frac{p^{TF}}{Q} \cdot u - p \cdot \frac{u^{TF}}{Q} \right) dS \quad (1.2)$$

The statistical energy analysis is not a new methodology and being used in automotive industry by the help of the commercial programs over decades. These programs are well adapted to the optimization methodologies and nowadays these optimization processes are being used more commonly on acoustic treatments of the vehicles.

The aim of the first phase studies is to offer a methodology to determine the acoustic pack of a vehicle and refine the interior noise which may even be applicable from the early stages of vehicle development process.

In the first phase studies, the thickness optimization of the inner dash isolator of the test vehicle is performed using the available SEA model of the vehicle. To achieve this, first the SEA model is validated using the engine to passenger compartment noise reduction (NR) test results.

ASQ (air-borne source quantification) methodology consists of two methods, Direct Method and Indirect or Matrix Inversion Method.

Engine air-borne noise contribution analysis in this study is performed with ASQ-Matrix Inversion Methodology (Shortly ASQ is used for air-borne contribution model instead of ASQ-Matrix inversion methodology), and panel acoustic contribution analysis is performed with ASQ-Direct Method. PACA is the specific application of ASQ-Direct Method to determine the panel contributions. In this study, to prevent a confusion, PACA is used as a name of the methodology for determining contributions of body panels to interior noise level. (It can also be named as ASQ Direct Method in the literature).

A matlab script has been developed for calculation of the interior noise level in 3rd Gear WOT (wide open throttle) maneuver with all the sub-panel contributions and engine airborne contribution.

The thickness optimization of the acoustic pack is performed and validated over a SEA model. The initial panel acoustic contribution analysis showed contribution of some sub-panels to interior noise level and after the refinement of this individual paths, new panel excitations are implemented again into the matlab script to obtain the new and refined interior noise level curve of the test vehicle.

For final validation, the interventions that are the refining outputs of the panel acoustic contribution analysis has been tested on the vehicle with the optimized inner dash isolator and the improvements are shown and discussed in related section.

There exist various studies and applications of SEA methodology in aerospace and automotive industry in the literature. Additional to SEA methodology applications, ASQ methodology has been applied many times individually (not integrated with the SEA methodology) in automotive industry.

Pass-by-noise is being validated in late phases of the product development period, once the representative test vehicles has been produced, i.e.. A. R. Fleszar *et al* [3], studied on the application of the ASQ methodology, measuring the noise level of the individual components, engine, exhaust, transmission, etc., in the early stage of the product development and superposing each individual source to obtain the final pass-by-noise of the test vehicle. It has been stated that inserting these individual source noise levels to the ASQ model, the PBN can be well predicted before the physical vehicles has been produced.

J. A. Steel *et al* [4] studied on a vehicle which has an exhaust noise sensitivity problem at 5700 rpm engine speed. Using the SEA methodology, the contribution of the exhaust noise to the passenger compartment has been calculated and the contribution is divided into two sub contributions, structural and airborne contributions. It has been concluded that the result of tested and calculated passenger compartment noise level is well correlated over 250 Hz.

The noise contribution from engine compartment to passenger compartment has been modelled in another study carried out by Xin Chen, Dengfeng Wang, Xue Yu and Zheng-Dong Ma [5]. In this study an SEA model of the vehicle has been built up and the vehicle in the model has been divided into subsystems; vehicle body, windshield, air cavity, etc. The inputs to the SEA model are noise and vibration of the engine and these quantities has been gathered during physical road tests. For validation of the virtual model, the SEA analysis and test results are compared using the SPL at the driver ear position. It has been observed that in high frequencies the SEA model has a good ability to model to model the engine noise contribution. Further analysis has been carried out by making a ranking of the noise contributions of various subsystems like dash, fender, front door, rear door, windshield, etc. to the interior noise level at 50 kph

and it has been stated that at this certain condition the vehicle front-end (dash) has been found to be the main contributor.

Shuming CHEN *et al* [6], have studied aiming to obtain a minimum weighted vehicle acoustic pack with improved vehicle idle noise level. A vehicle SEA model has been built-up and vehicle interior noise level at idle has been calculated. The calculated and tested noise level has been compared to set an optimization target. The ranking of the contributing regions has been performed and dash region has been found to be the most contributing region at idle noise. The sound absorption coefficient of the initial inner dash isolator has been tested additionally and a new multi-layered acoustic pack has been developed for the dash region. The performance of this new multi-layered acoustic pack with 0.8 kg less weight compared to the initial pack's performance and it has been validated that the noise level at idle condition with this new pack is similar to the the initial test results. It has been stated that with multi-layered acoustic packs, the isolation performance could be improved by improving the sound absorbing performances. Finally, it has been concluded that with the optimized acoustic pack, the noise level inside passenger compartment when the vehicle is running in idle condition has been decreased from 40.61 dB(A) to 37.47 dB(A) and the weight of the acoustic pack has been decreased 0.8 kg.

Hans-Peter Keller and Liangyu Huang [7] have studied to improve the transmission loss performance of vehicle doors. For this purpose, the SEA model of the vehicle door has been developed. The TL performance has been analysed in SEA environment in three different conditions; base door, optimized door and optimized door with additional glass. And the correlation of SEA TL results has been studied by comparing them with the physical test results of these three conditions and the SEA model has been validated. It has been concluded that the air leakage of the doors has an important effect on the TL performance of the doors and the TL performance can be improved by eliminating these air leaking regions.

Ennes Sarradj [8] has used the SEA methodology to calculate the structure-borne contribution of engine mounts to vehicle interior noise level and concluded with a good correlation between the SEA model and physical test results.

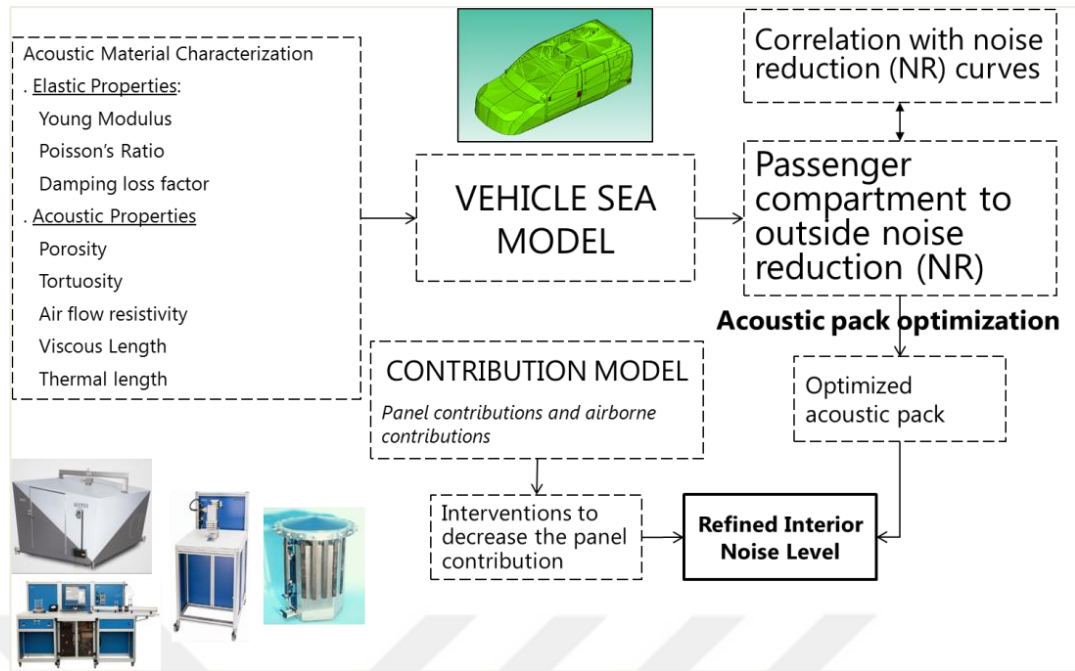


Figure 1.1 : Integration of PACA, ASQ and SEA methodologies.

For the airborne contribution, many types of sound absorbing materials are used in noise-control applications. These materials include glass fiber, polymeric fibrous materials, and various types of foams¹. Acoustical material plays a number of roles that are important in acoustic engineering, such as the control of room acoustics, industrial noise control, studio acoustics and automotive acoustics [9]. Low weight with higher or equal acoustic performance is the main goal of the automotive industry in recent years.

Materials that reduce the acoustic energy of a sound wave as the wave passes through it by the phenomenon of absorption are called sound absorptive materials [9]. They are commonly used to soften the acoustic environment of a closed volume by reducing the amplitude of the reflected waves [9]. Felt type materials generally have a sound absorption coefficient that increases quasi-linearly from lower to higher frequencies. There may be cases where one may want to increase the mid-frequency absorption performance of a felt. In the near future, by the presence of electric vehicles, tonal noises will become more important than today because of the lack of a broadband background noise generated by today's internal combustion engines. In these cases, tunable sound absorbing materials, with similar weights of today's acoustic packs, may have more importance. Designing a multilayer absorber needs some pre-work to forecast its acoustic properties, such as the absorption coefficient and transmission

loss. There are various studies in the literature that develop analytical models to predict the acoustic performances. Guofeng Bai et al [10] investigated the sound insulation performance of a multiple-layer structure, which consists of elastic solid, fluid and porous material. They calculated the sound insulation performance of composite materials based on the transfer matrix method. They showed using simulation and experimental results that the sound insulation performance is greatly improved after the air layer is used. M. Abid and M. S. Abbas et al [11] developed a method to predict the acoustic parameters of viscoelastic materials to improve the acoustic insulation of multilayer panels, and different layer arrangements were also tested to find the best configuration of a multilayer panel in terms of the acoustic insulation.

In the second phase studies, first we describe the analytical model based on the transfer matrix method of a multilayer porous material to predict the sound absorption coefficient subjected to plane waves with a rigid backing boundary condition. Second, the sound absorption coefficient calculation result of the model for a multilayer material has been presented to obtain more absorbing performance in the mid frequency range without increasing its weight which is the main objective of this study. Finally, the model results have been validated with the experimental results.

In the third phase studies, we focused on the air intake system noises and developed a novel air intake system resonator. As recently quietness has become an important quality parameter for automotive vehicles and as a result various improvements have been brought to reduce noise at system level and vehicle level [12]. Due to stringent noise emission norms on automotive vehicles and increasing desire of quieter in-cab performance by users, reduction of air intake noise tends to be an area of explanation [12]. The air induction system of an automobile engine contributes to the noise level generated by a passenger car. The contribution is significant in the perception of vehicle noise quality. There is a great value in reducing and controlling passenger car air induction noise [13]. Researches on noise control applied to the air intake systems have not received much attention when compared research on exhaust systems [12]. One way of attenuating broad band noise that propagates through ducts or pipe systems is to use one or more reactive-type acoustic components, each of which is specifically designed for optimal performance at a particular frequency range [14]. The operational principles of intake and exhaust silencers can be divided into two types, dissipative and reactive type, that dissipative silencers contain absorptive materials which

physically absorbs acoustic energy from the gas flow where reactive silencers operate on the principle that when the sound in a pipe or duct encounters a discontinuity in the cross-section, some of the acoustic energy is reflected back towards the sound source thereby creating destructive interface [15]. Many types of sound absorbing materials are used in noise-control applications. These materials include glass fiber, polymeric fibrous materials, and various types of foams [16]. As reactive type resonators, expansion chambers, Helmholtz resonators and quarter wave tubes are commonly being used in today's vehicles where the need for the size of such resonators increase with the decrease in working frequency range. Actively controlled Helmholtz resonator has been developed by Tanaka and Nishio by placing a speaker inside the cavity of the resonator located at a branch of the fresh air duct [17,18]. According to the literature available so far on the intake noise reduction, the techniques currently used to reduce air induction noise include usage of expansion chambers, absorption or cancellation principle [12,19,20,21].

Design constraints for noise attenuation devices employed in automotive induction systems are continuously being challenged to provide optimum performance for the least cost and packaging space [22]. Packaging space in particular is becoming increasingly difficult, especially for four cylinder vehicles where large reactive elements such as Helmholtz resonators are needed to attenuate low frequency "boom" [15]. Due to these resonators requiring extra volume in vehicle engine compartment and creating packaging problems, means interference and/or not enough space with the neighbor system elements, mostly new design of these neighbor elements may be necessary which means extra time and cost for the vehicle. In order to prevent this problem alternative designs for the air intake system resonators may be mandatory in some cases. In the third phase studies, we propose a small size air intake system resonator with a helical side branch duct connected to the main duct, being the same size with the main pipe thus not requiring an additional volume, which is very suitable for the packaging requirements. The designed helical resonator is a tunable resonator and can be tuned to the required frequency range by adjusting its dimensions. The analytical model is initially developed of the resonator and it is tuned to the desired frequency range. Then the analytical model is initially correlated with the numerical model and then with component level transmission loss and pressure drop test result.

Finally the vehicle level performance of the resonator is tested on a 1.6 liter gasoline passenger car.



2. NOISE CONTRIBUTION ANALYSIS OF A VEHICLE PASSENGER COMPARTMENT¹

2.1 Abstract

In today's competitive automotive industry, analyzing the noise level inside a passenger compartment and determining the contributors to the interior noise level has become more important due to opportunities for improvement. Finding opportunities for improvement to provide customers with a more refined vehicle in terms of passenger compartment noise level provides an advantage to the automotive manufacturer over its competitors. In this study, integration of Acoustic Source Quantification (ASQ) and SEA methodologies is aimed to model the interior noise level inside the passenger compartment. The ASQ Direct Method, briefly explained in theory section, has been used to perform Panel Contribution Analysis (PACA), in order to investigate regions with panels that contribute primarily to the interior noise level and to determine opportunities for refining the interior noise levels within vehicles. To determine the airborne contributions of engines, the ASQ Indirect Method, briefly explained in theory section, has been applied. Creating a contribution model using MATLAB (PACA and Engine ASQ), the interior noise level of the vehicle has been calculated and correlated with the test results. By performing further analysis on the interior noise contribution model and focusing on the panel contributions, the regions with the most contributing panels have been determined and interior noise refining actions have been applied. By applying interventions, which are the refining outputs of the panel acoustic contribution analysis, an improvement of up to 3 dB(A) for a few engine speed ranges has been obtained for the overall noise level of the vehicle.

In addition to the panel contribution analysis, which is the primary focus of this study, thickness optimization of the inner dash isolator has been performed for a correlated

¹ This chapter is based on the paper “C. Meriç, H. Erol and A. Özkan (2016). Noise contribution analysis of a vehicle passenger compartment. *Noise Control Engineering Journal*, 64(5), 646-657. Doi: <https://doi.org/10.3397/1/376409>.”

SEA model, which confirms that no performance loss occurred in the acoustic transfer functions from the engine to the passenger compartment. The physical prototype of the optimized inner dash isolator has been assembled in the vehicle during the panel contribution analysis validation tests.

The integration of the ASQ (direct & indirect) and SEA techniques may be offered as a unique method that can be applied in the refinement phase of product development when the physical vehicle is available, to release refined and lower weight vehicles.

2.2 Introduction

Noise legislation and subjective customer demands have set future standards for noise and vibration control in all types of vehicles, from small passenger cars to heavy trucks [1]. Recently, interior noise quality has developed into a decisive aspect that is used to evaluate the overall vehicle quality [23]. For most operating points, the dominating interior noise is generated by the powertrain. Interior noise simulation is a new tool that is used for upgrading the interior noise. Based on measurements of air- and structure-borne noise excitations caused by the powertrain, the interior noise shares are determined by applying the properties of the transfer paths [23]. By superimposing the individual interior noise shares, the overall interior noise can be predicted [23]. Manuel Sánchez Castillo and Andreas Schuhmacher [24] stated that microphone array-based Panel Acoustic Contribution Analysis (PACA) is a new technique that can be used for the sound package design optimization for commercial vehicles. This technique allows for noise control performance and cost optimization. Furthermore, this technique ranks the contributions of fully trimmed structural panels (e.g., floor, roof, etc.) and leaks in a vehicle cabin to the noise levels experienced by the driver while the vehicle is operating at cruising speed. Often, the noise and vibration sources (engine, transmission, exhaust, aerodynamic noise, tires, etc.) cannot be easily modified, thus the only practical solution to solve noise problems is to design noise control treatments that can be applied to the vehicle panels. It has been concluded that studying the contour maps of sound field parameters on the panel surfaces allows engineers to investigate which panels radiate sound energy into the cabin.

A systematic approach, i.e., the Panel Acoustic Contribution Analysis (PACA), has been developed by Y. Kevin Zhang et al [25] to determine the contributions of the body panels to the vehicle interior sound pressure, pinpoint the local areas of the panel

that require modification and provide the most effective solutions. The developed PACA technique has been applied to both production and prototype vehicles [25]. In one of the applications, the identified noise concern was reduced by applying appropriate treatments to the panel identified as a major positive contributor.

The goal of this study is to offer a methodology integrating ASQ (direct & indirect) and SEA techniques that determines the acoustic pack of a vehicle and refines the interior noise, which may be applicable in the refinement phase of product development when the physical vehicle is available. The process is summarized in Figure 2.1.

The ASQ (air-borne source quantification) methodology consists of two methods: the Direct Method and Indirect or Matrix Inversion Method. The engine air-borne noise contribution analysis in this study is performed using the ASQ-Matrix Inversion Methodology (ASQ is used for the air-borne contribution model instead of the ASQ-Matrix inversion methodology) whereas the panel acoustic contribution analysis is performed using the ASQ-Direct Method. The PACA is a specific application of the ASQ-Direct Method that is used to determine the panel contributions. In this study, to prevent confusion, the PACA is used as the name of the methodology used for determining the contributions of body panels to the interior noise level. (It can also be known as the ASQ Direct Method in the literature).

A MATLAB script has been developed to calculate the interior noise level during the 3rd Gear WOT (wide-open throttle) maneuver including all the sub-panel contributions and the engine airborne contributions. An initial panel acoustic contribution analysis indicated which sub-panels contributed to the interior noise level, and after the individual paths were refined, new panel excitations were implemented again into the MATLAB script to obtain a new and refined interior noise level curve of the test vehicle.

In this study, the thickness optimization of the inner dash isolator of the test vehicle is performed using the correlated SEA model of the vehicle. To achieve this optimization, the SEA model is first validated using the engine to passenger compartment noise reduction (NR) test results.

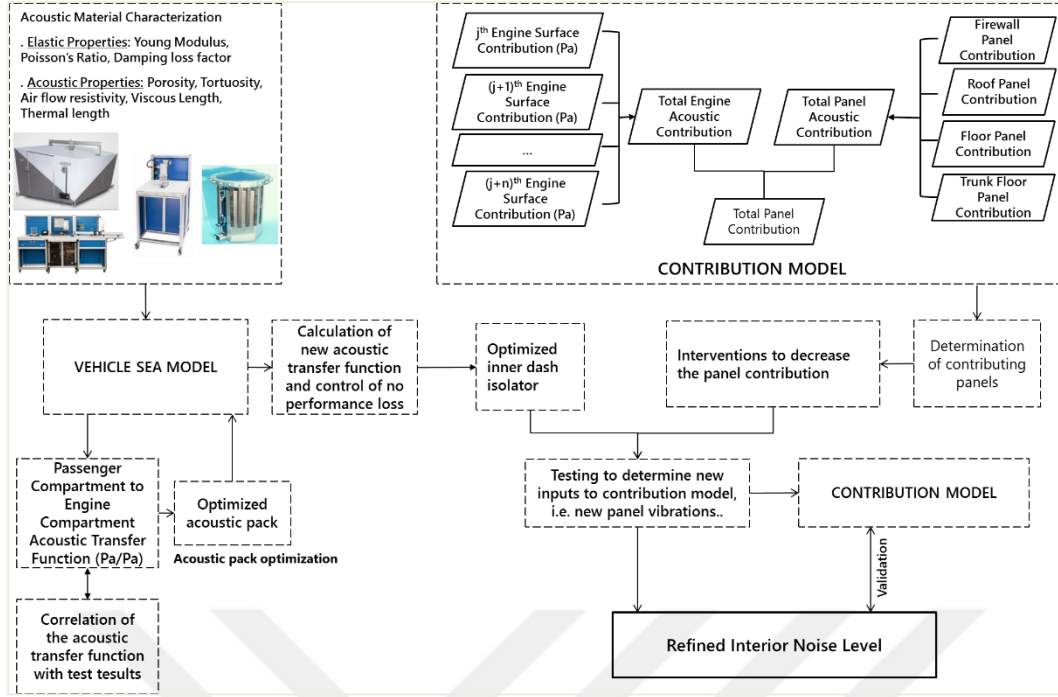


Figure 2.1 : Integration of the PACA, ASQ and SEA methodologies.

2.3 Theory

In the PACA, the contribution of the radiating panels to the interior noise level is analyzed. Grosso et al [1] defined a cavity S whose surface excites the sound field when it is under operating conditions as well as an infinitesimal small area M inside S for studying how different areas of the cavity ‘contribute’ to a point at M . p^{TF} and u^{TF} are defined as the pressure and the particle velocity during the reciprocal transfer function measurements, respectively. However, p and u are the pressure and the particle velocity during the noise measurements [26], respectively. From the acoustic reciprocity relation [2], we can obtain the following expression.

$$\int_M (p^{TF} \cdot u - p \cdot u^{TF}) dM + \int_S (p^{TF} \cdot u - p \cdot u^{TF}) dS = 0 \quad (2.1)$$

The integral of the particle velocity u across the entire surface M will be zero because there is no net energy going throughout M during the noise measurements. Furthermore, the pressure p can be integrated over M during the noise measurements, which results in the reference pressure p_r . Moreover, integrating the particle velocity M during the transfer function measurement will lead to the volume velocity of the monopole source Q , which results in the base equation of several velocity-based panel noise contribution methods as follows [1]:

$$Pr = \int_S \left(\frac{p^{TF}}{Q} \cdot u - p \cdot \frac{u^{TF}}{Q} \right) dS \quad (2.2)$$

The statistical energy analysis is not a new methodology and has been used in the automotive industry by commercial programs for decades. These programs are well adapted to the optimization methodologies, and these optimization processes are currently being used more commonly for the acoustic treatments of vehicles.

The integration of three methodologies is investigated in this study. The PACA (*for panel contribution*) & ASQ (*for engine airborne contribution*) techniques are generally experimental methods, and a MATLAB script has been created to integrate the outputs of these two methodologies to create an interior noise contribution analysis (structure-borne and engine air-borne) model. The third methodology is a numerical method known as SEA (*statistical energy analysis*). These methodologies are explained briefly in this section. The ASQ (air-borne source quantification) methodology consists of two methods: the *Direct Method* and the *Indirect or Matrix Inversion Method*. The PACA methodology is a specific case of the ASQ methodology, the *ASQ Direct Method*, which has been used to determine the noise radiating from the panels, i.e., the body panel of the vehicle and inside the passenger compartment. To explain the panel contribution (*PACA or ASQ-Direct Method*) briefly, the operational loads occurring on the panels are determined first, and then the acoustic transfer function from the corresponding panel to the target position is measured. The contribution of the panel is calculated by multiplying the two quantities in the frequency band.

The ASQ Direct Methodology can be expressed mathematically as follows:

If

P_{target} [Pa]: total calculated sound pressure level at the target position

P_i [Pa]: contribution of each panel to the total noise level at the target position

Then, the total sound pressure at the target position, P_{target} , can be calculated as the sum of each sub-contribution of the panels as follows:

$$P_{target} = \sum P_i \quad (2.3)$$

If

\dot{Q}_i [m³/s²]: operational loads of panel i

H_i [Pa/(m³/s²)]: acoustic transfer function from the panel i to the target position

Then, the contribution of the panel i , P_i , to the total sound pressure level at the target position, P_{target} , can be expressed as follows:

$$P_i = \dot{Q}_i \cdot H_i \quad (2.4)$$

The operational loads can be calculated as follows:

\ddot{x}_i [m/s²]: acceleration of i^{th} panel

A_i [m²]: area of the panel i

Thus, the operational load on the panel i can be obtained as follows:

$$\dot{Q}_i = \ddot{x}_i \cdot A_i \quad (2.5)$$

The methodology is summarized in Figure 2.22.

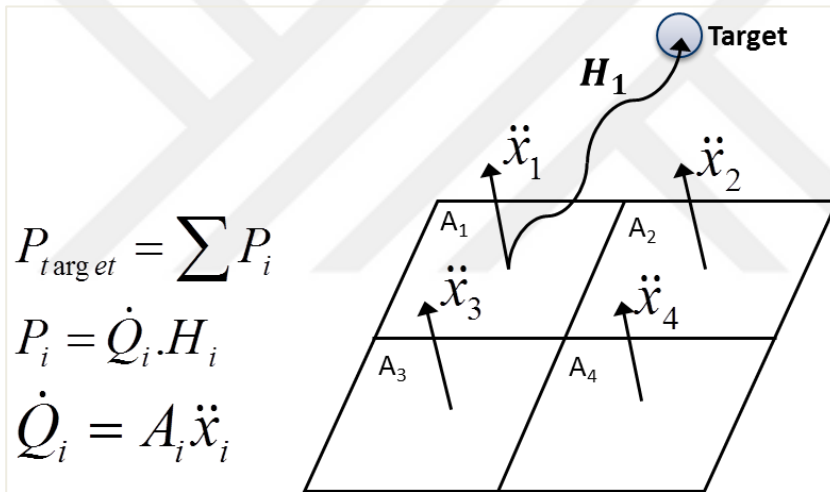


Figure 2.2 : Panel contribution systematic.

Similar to the ASQ-Direct Method, the operational loads around the noise source can be determined during the ASQ-Matrix Inversion Method. In this specific case, the noise radiated from the engine during the operation (3rd gear WOT) has been obtained using a series of indicator microphones (T1, T2, F5..., Ti etc.) located inside the engine compartment around the engine. Then, the acoustic transfer function measurements from the source to the target position (e.g., passenger compartment, driver's ear position) are needed to perform under stationary conditions, as described in Figure 2.3. The VVSS is placed in 6 engine surfaces one-by-one during the ATF measurements to obtain two ATFs: NATF (Near Field Acoustic Transfer Function) and FATF (Far Field Acoustic Transfer Function).

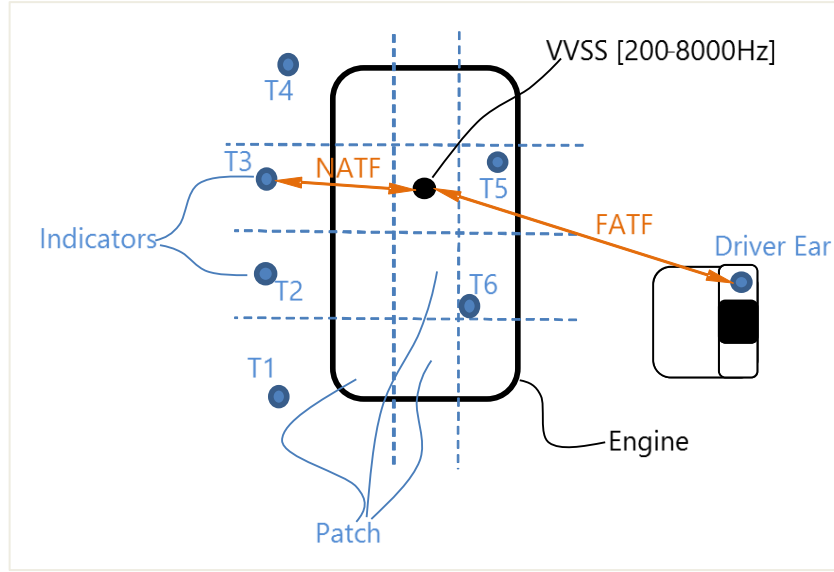


Figure 2.3 : ASQ-Inverse matrix method for determining the engine acoustic contribution (indicator microphones, volume velocity sound source, target position (driver ear)).

Once the operational SPLs (Pa) at the indicator microphone locations and the ATFs (Pa/(m³/s²)) have been obtained, these two quantities in the frequency range are multiplied to obtain the contribution of each source location at the target position.

The methodology can be expressed mathematically as follows:

If

P_{Ti}^{OP} [Pa]: the sound pressure level at each indicator microphones in operational conditions (i:1,2...,12)

\dot{Q}_{VVSS}^j [m³/s²]: the volume acceleration at VVSS on each engine surface during the ATF measurements (j:1,2...,6)

P_{Ti}^{TF} [Pa]: the sound pressure level at each indicator microphone in the stationary ATF measurements

P_{TARGET}^{TF} [Pa]: the sound pressure level at the target microphone (DRE: Driver Ear) in the stationary ATF measurements

$$NATF_j = P_{Ti}^{TF} / \dot{Q}_{VVSS}^j \quad [Pa/(m^3/s^2)] \quad (2.6)$$

$$FATF = P_{TARGET}^{TF} / \dot{Q}_{VVSS}^j \quad [Pa/(m^3/s^2)] \quad (2.7)$$

\dot{Q}_i^{OP} [m³/s²]: the operational loads at indicator i

Then, the operational loads at each indicator microphone locations can be calculated as follows:

$$\dot{Q}_i^{OP} = P_{Ti}^{OP} \cdot NATF_j^{-1} \quad [m^3/s^2] \quad (2.8)$$

P_i [Pa]: the contribution of each indicator location

$$P_i = \dot{Q}_i^{OP} \cdot FATF_j \quad [Pa] \quad (2.9)$$

P_{target} [Pa]: the total calculated sound pressure level at the target position

Then, the total sound pressure at the target position, P_{target} , can be calculated as the sum of each sub-contribution of the indicator locations as follows:

$$P_{target} = \sum P_i \quad (2.10)$$

The statistical energy analysis methodology is being worked over for decades and it is well adapted to automotive industry with the help of the developed commercial programs. With the development of the optimization algorithms, these commercial programs developed in such a way as including optimization modules. Today with the help of this development, the optimization process of vehicle acoustic pack treatments of are currently being performed more commonly for the acoustic treatments of vehicles.

The acoustic and vibration behavior of the system in SEA is characterized in terms of energy quantities [8]. The energy is the kinetic and potential energy in the resonant modes of the system [27]. The primary idea in the SEA is that a structure is partitioned into coupled “subsystems”, and the stored and exchanged energies are analyzed [1].

The SEA methodology is formed using the solution of the power-balance equations [27]. The inputs required for the power balance equations are the damping and the coupling loss factors, subsystem masses, input powers and modal densities [28]. The average vibration and sound pressures are then computed from the predictions of the subsystem energies [28].

The modes within a subsystem receive, store and transfer energy [27]. The modal density n_i of a subsystem i is defined as the number of the natural frequencies or modes per unit frequency as follows:

$$n_i = \frac{\Delta N_i}{\Delta f} \quad (2.11)$$

Energy losses inside a subsystem as well as the energy flow from that subsystem to other subsystems are described by parameters related to energy, i.e., damping loss factors and coupling loss factors [27]. The coupling loss factor values for the different junction types are available in the literature [27]. The final parameter is the power inputs, which are specified by the user of the SEA power balance equations or computed for the simple force or displacement inputs [27].

The power balance equations for a system formed of two subsystems can be written for the system shown in Figure 2.4 as follows:

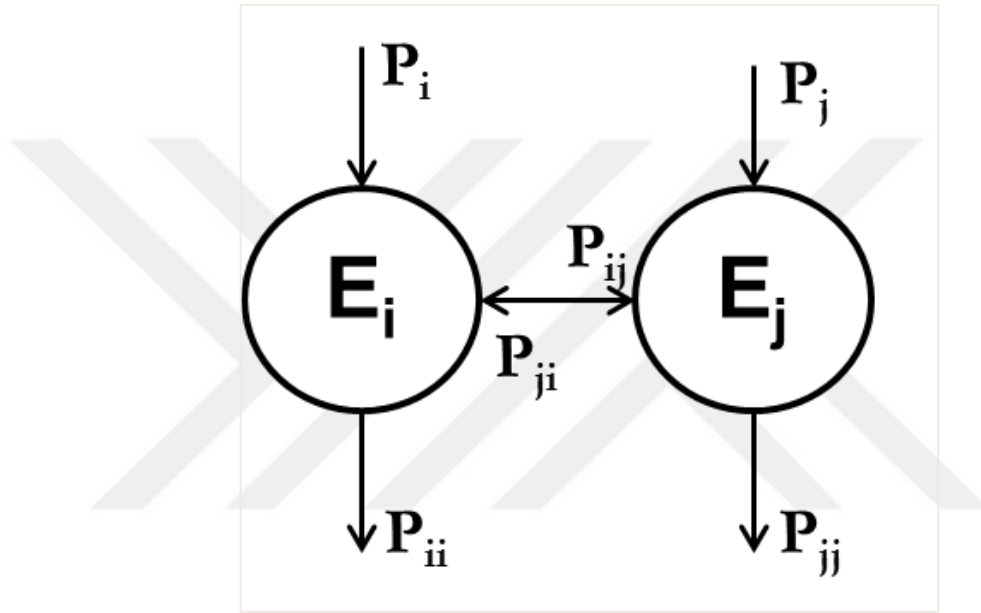


Figure 2.4 : Power balance equations for a sample system.

The dissipated power inside the system can be written as follows:

$$P_{ii} = \omega \eta_{11} E_1 \quad (2.12)$$

The dissipated power between the subsystems can be written as follows:

$$P_{ij} = \omega \eta_{ij} E_i \quad (2.13)$$

The power balance equations can be expressed as follows:

$$\begin{Bmatrix} P_i \\ P_j \end{Bmatrix} = 2\pi f \begin{bmatrix} (\eta_{11} + \eta_{12}) \cdot n_1 & -\eta_{21} \cdot n_2 \\ -\eta_{12} \cdot n_1 & (\eta_{22} + \eta_{21}) \cdot n_2 \end{bmatrix} \cdot \begin{Bmatrix} E_1/n_1 \\ E_2/n_2 \end{Bmatrix}$$

where $E_{i,j}$ and $P_{i,j}$ are the energy and power inputs of the subsystems i and j , respectively; $P_{ii,jj}$ is energy dissipated inside the subsystems i and j , $P_{ij,ji}$ is the energy dissipation between the subsystem i and j . Here, $(\eta_{11} + \eta_{12})$ represents the total loss

factor (damping loss + coupling loss) of the subsystem i , and $(\eta_{22}+\eta_{21})$ represents the total loss factor (damping loss + coupling loss) of the subsystem j .

The vehicle acoustic pack typically consists of porous materials, such as foams, felts, fibers, etc., structural damping materials and plate and solid layers [29]. The porous materials consist of two phases, solid and fluid. They transform the acoustic energy into heat, and this energy is dissipated by the viscous and thermal effects as well as structural damping [29]. The primary performance indicators for the acoustic treatments are sound absorption and transmission loss. The propagation of the acoustic waves in porous media was studied for low frequency [30] and high frequency ranges [31] by Biot in the 1950s. The Biot theory was later extended to the modeling of elastic porous acoustic materials, as presented by Allard [32]. The transfer matrix method is adapted for modeling the sound propagation in layered media in various studies, such as B. Brouard et al [33].

2.4 Experimental Studies

The SEA model of the vehicle is built-up using one of the sophisticated programs, VA One. In VA One, four different models are available to represent the foam and fibrous materials: elastic porous (foam), limp porous (fiber), rigid (fiber) porous and Delany-Bazley [34] (fiber) [35]. Building up the SEA model of a vehicle requires detailed information on the poro-elastic properties of the acoustic treatment materials. The BIOT parameters, such as tortuosity, porosity, airflow resistivity, viscous length, and thermal length, of the acoustic materials are necessary to be tested or determined from the literature. For the application of this methodology, a material library of the vehicle acoustic package has been developed by testing the BIOT parameters of the existing acoustic pack, including porosity, tortuosity, damping loss factor, air flow resistivity, viscous length, and thermal length.



Figure 2.5 : Acoustic material characterization test setups.

The Acoustic Material Characterization Laboratory, as depicted in Figure 2.5, has been used for the characterization of the materials. The laboratory consists of a porosity test bench, a test bench for the elastic properties of porous materials, e.g., damping loss factor, Young's modulus, Poisson's ratio, another test bench for the acoustical properties of porous materials, e.g., AFR, tortuosity, viscous length, thermal length, pore shape factor, and sound absorption coefficient, and an Alfa Cabin for testing the sound absorption coefficient in a reverberant environment.

After building up the SEA model of the vehicle, the model has been correlated with the tested acoustic transfer function measurements from the engine to the passenger compartment, as indicated in Figure 2.6. For this purpose, 20 microphones have been placed inside the engine compartment around the engine, and another 20 microphones have been placed in the passenger compartment inside the driver cavity, as modeled in the SEA method. The primary purpose of the amount of microphones used is to obtain the average sound pressure levels in these cavities to compare with the ATF output of the SEA model calculated in the same manner, i.e., dividing the average sound pressure levels of the two cavities, passenger and engine. The sound source has been placed at the driver's ear position, and the ATF has been measured reciprocally.

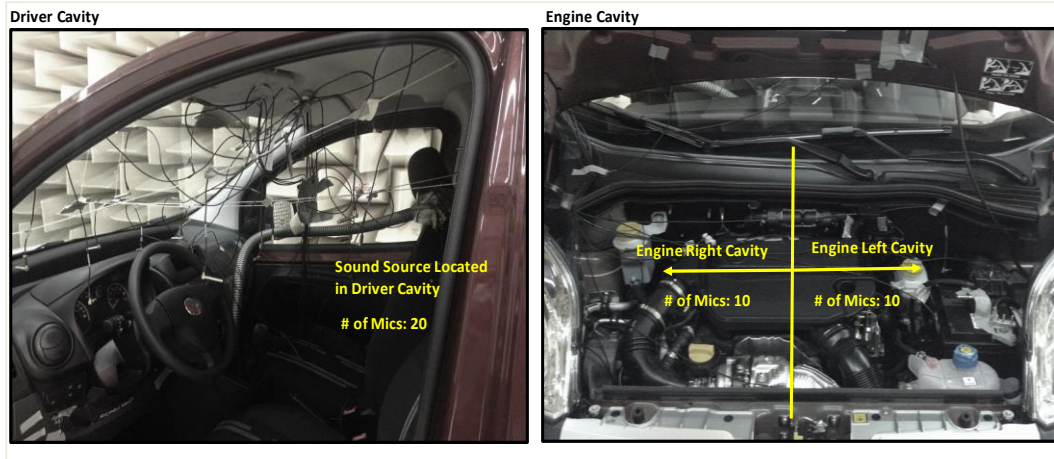


Figure 2.6 : ATF measurement for the SEA model correlation (left: vehicle cavity, right: engine cavity).

The ATF between the passenger cavity and the engine cavity has been calculated using the average of each of the 20 microphones. The comparison of the SEA model and the tested ATFs after certain modifications in the SEA model, i.e., adjusting the leakage, is depicted in Figure 2.7. The microphones used in the acoustic transfer function measurements for the SEA model correlation are Bruel&Kjaer 4958 1/4" microphones with a sensitivity of 12.5 mV/Pa, frequency range of 10-20000 Hz, and dynamic range of 28-140 dB.

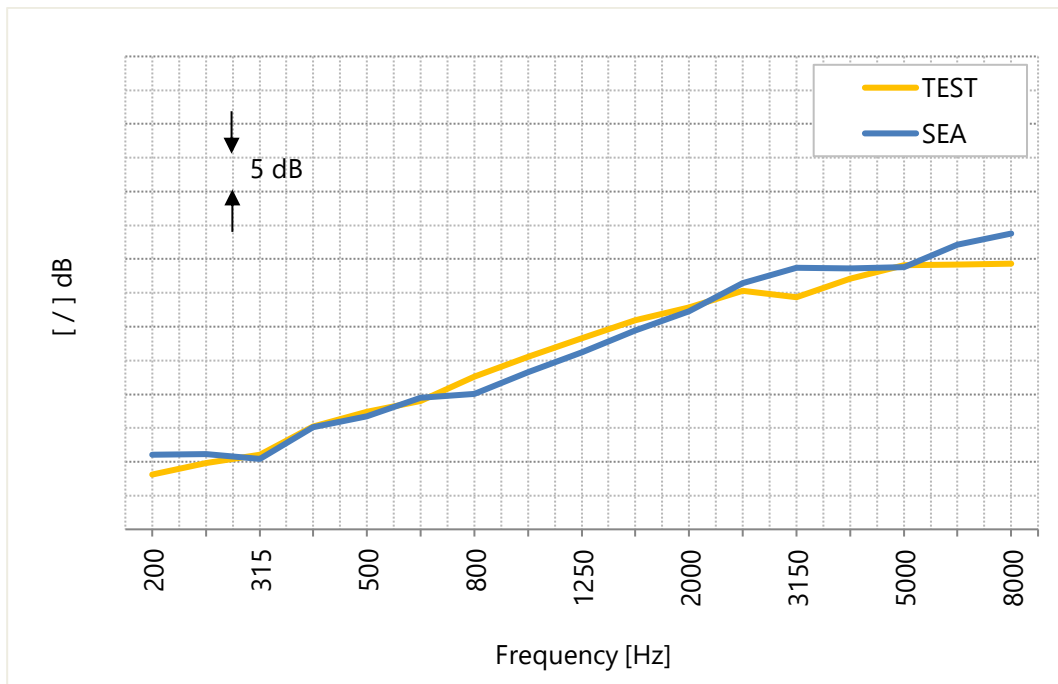


Figure 2.7 : ATF measurement for the SEA model correlation (calculated vs. tested).

Once the initial model has been established and the major contributors are determined, the thickness optimization of the acoustic pack is performed on the correlated SEA model presented in Figure 2.8. The inner dash isolator is divided into 4 areas based on the manufacturability, and the constraints for the thickness optimization are set according to the packaging requirements of the vehicle. These 4 regions have the same materials with different average thicknesses.

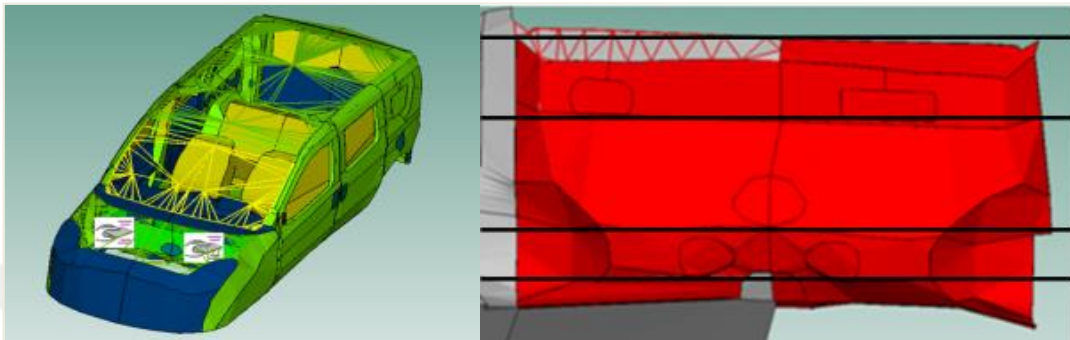


Figure 2.8 : Vehicle SEA (left) and inner-dash isolator optimization model (right).

After the optimization process, the SEA model has been updated with the new thickness values, and the new ATF has been obtained in the graph below compared with the initial ATF curve. The improvement in the engine-passenger compartment ATF can be observed in Figure 2.9.

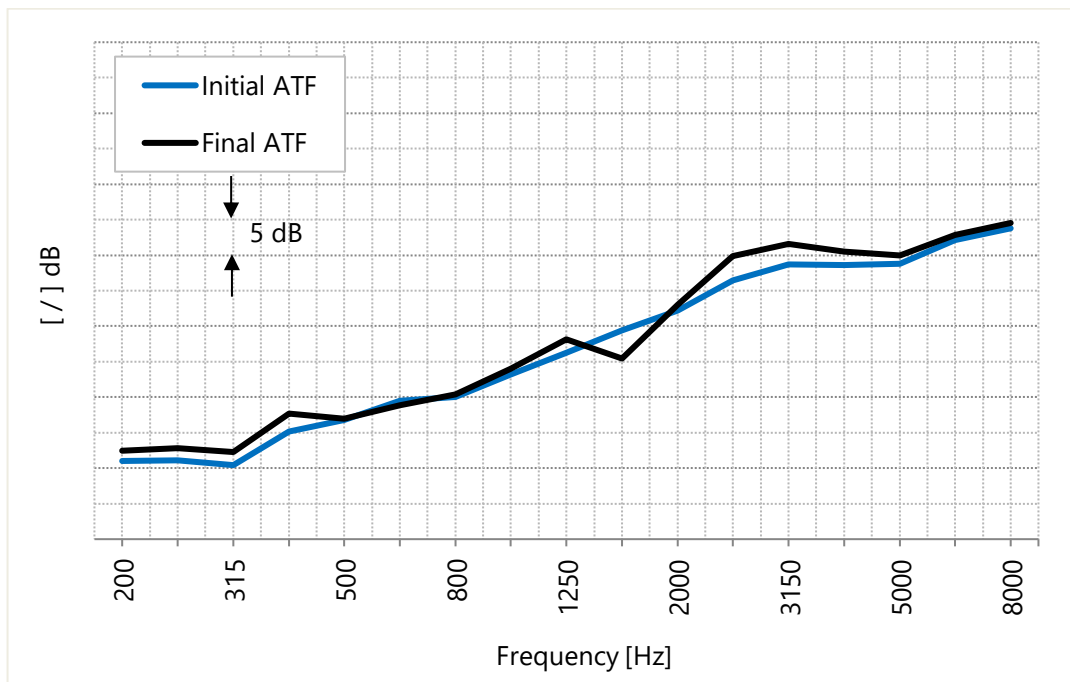


Figure 2.9 : Initial vs. final SEA calculated ATFs.

After the initial validation of the optimization results in the SEA environment, the prototype of the new acoustic pack is produced with new thickness values and implemented later in the vehicle to test the interior noise level with the improvements gained from the panel contribution study explained in the current section.

There are generally two different measurements for both the engine airborne and panel contribution models: operational and transfer function measurements.

The required data have been obtained during the operational measurements in the 3rd gear WOT acceleration for both of the models. During the operational measurement of the engine acoustic contribution model, microphones are located around the engine to obtain the engine emitted noise as well as the sound pressure level distribution around the mentioned areas, i.e., at least 2 microphones for each of the 6 surfaces of the engine.

The rpm-based frequency spectrum is the output of these measurements. The acoustic transfer functions for each of these microphone locations are then measured as described in the ASQ title in the theory section. The mid/high frequency volume source, as indicated in Figure 2.10, covers a 200 to 8000 Hz frequency band that is placed in several locations on each of the engine surfaces.



Figure 2.10 : Mid/high frequency volume source.

The indicator microphones are in the same positions around the engine and inside the passenger compartment. The outputs of the acoustic transfer function measurement,

presented in Figure 2.11, are the Nearfield Acoustic Transfer Function (NATF) and Farfield Acoustic Transfer Function (FATF).



Figure 2.11 : Application of engine ASQ, (Left: operational, 2 microphones for each engine face. Right: Positioning of volume source, at least 2 places on each engine face).

The microphones used in this study, in the ATF and operational measurements for the engine acoustic contribution, are 1/2" microphones with a sensitivity of 50 mV/Pa, frequency range of 6.3-20000 Hz, and dynamic range of 14.6-146 dB.

In the operational measurement of the *panel acoustic contribution analysis*, the normal acceleration of the panel surfaces is measured under the 3rd gear WOT using 1D accelerometers with a sensitivity of 100 mV/Pa, frequency range of 0.3 - 6000 Hz and maximum operational level of 1 g (peak).

The panels are divided into subpanels, the areas of which are known and small enough to create a model up to an 8th engine order, i.e., for a 4800 engine rpm, the maximum frequency of interest is 640 Hz while the maximum mesh size is approximately 27 cm.

$$(F_{\max} = c/2.d_{\max} = 340/2.0,27 = 640 \text{ Hz})$$

The output of the panel contribution operational measurement is the rpm-based operational load, $\dot{Q}_i [m^3/s^2]$ vs. rpm, for each order of interest, 2nd, 4th, 6th, and 8th, which is obtained using the multiplication of the subpanel normal acceleration [m/s^2] and the area of the subpanel [m^2].

For the transfer function measurement of the panel contribution model, the microphones, P [Pa], are located on each subpanel, and the low/mid frequency volume source [m^3/s^2], depicted in Figure 2.12, is located at the reference position, i.e., the driver's ear.

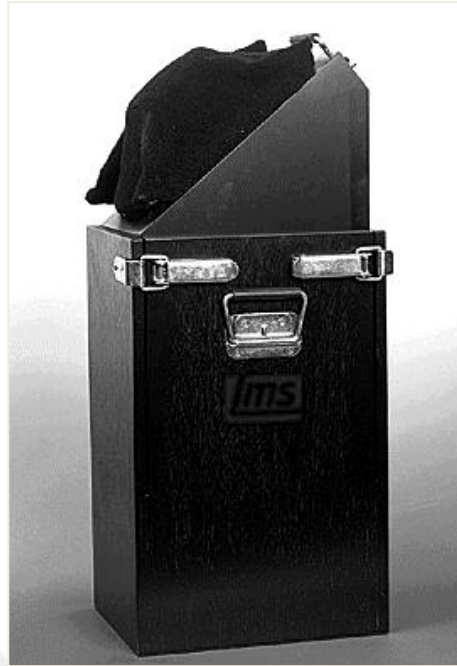


Figure 2.12 : Low/mid frequency volume source.

The low/mid frequency volume source covers a 10 to 1000 Hz frequency band. The output of the transfer function measurement is P_i/\dot{Q}_i , thus the output is again multiplied with the output of the operational measurement to create a contribution analysis.

The flowchart of the MATLAB script is presented in Figure 2.13. The airborne contribution is imported and the panel contribution is calculated. Furthermore, 2D graphs are drawn to analyze each contribution, and the contribution of the subpanels result in a more thorough analysis.

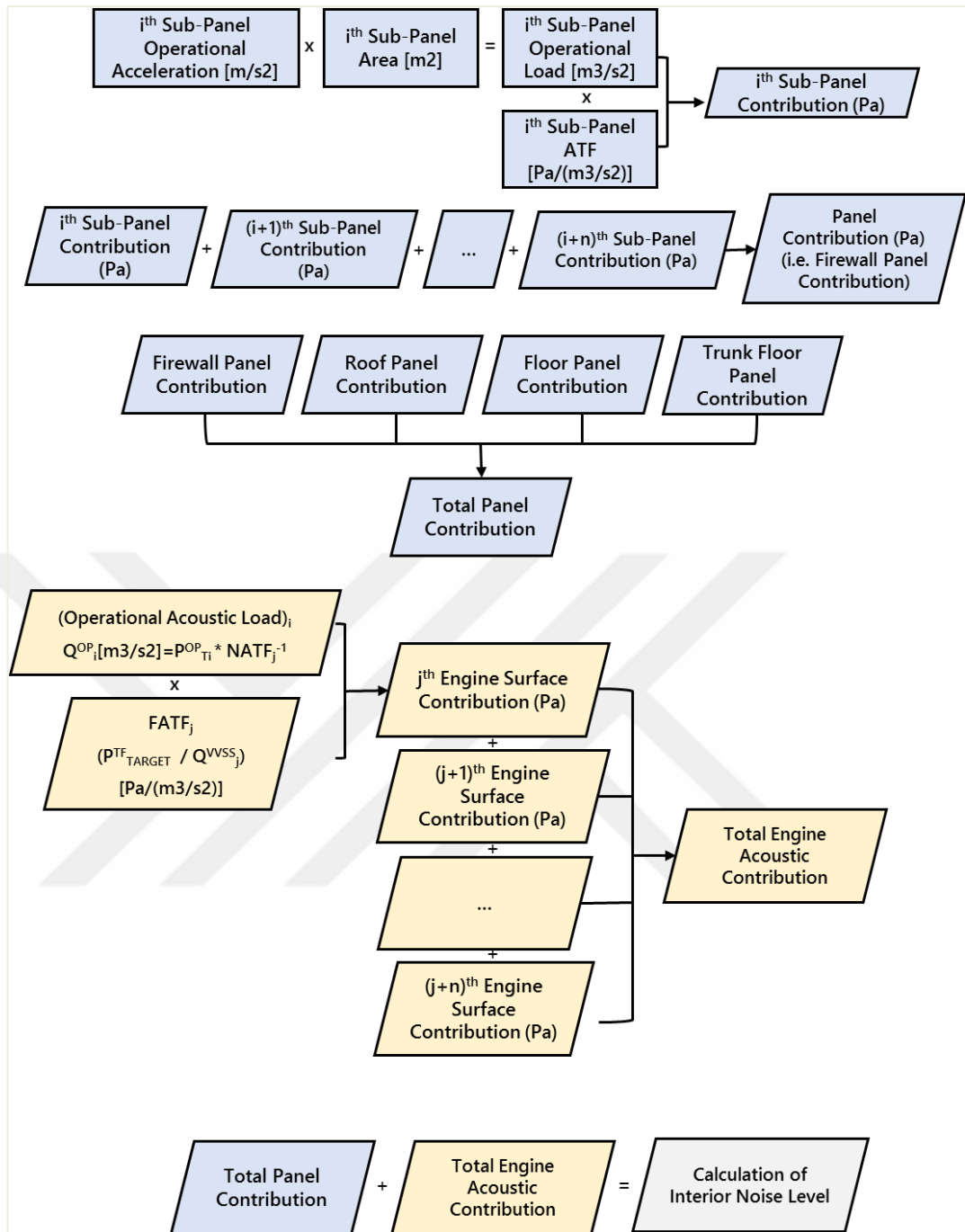


Figure 2.13 : MATLAB model flowchart.

A panel contribution analysis has been performed for the firewall, front floor, trunk floor and the roof panels. Each panel is divided into subpanels such that the total number of subpanels analyzed is 100.



Figure 2.14 : Application of panel contribution (accelerometers on each subpanel), roof (left) and trunk floor (right).

Figure 2.14 depicts the positions of the accelerometers in the operational measurements. The operational measurements are performed in the 3rd gear WOT acceleration from 1000 rpm to 4800 rpm, and the transfer function measurements are conducted to measure the acoustic transfer function from each subpanel to the driver's ear position. Once all of the data are obtained, the results are imported into the MATLAB model to visualize the contributions and perform a more detailed contribution analysis.

This methodology is applied in the TOFAŞ (Turkish Automotive Factory A.Ş.) on a Doblo Combi Panorama with a 1.3 lt Mjet 95PS engine.

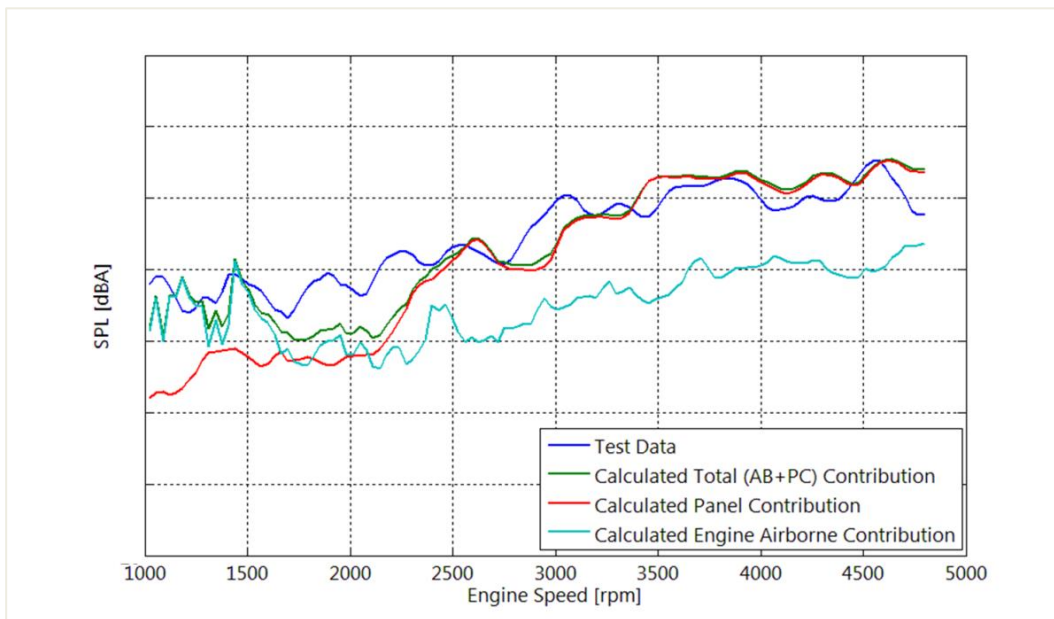


Figure 2.15 : Result of the evaluation.

The result of the application is provided in Figure 2.15. The blue curve denotes the test result of the sound pressure level at the driver's ear position while the green curve is the calculated sum of the panel contributions (red curve) and the engine airborne (turquoise curve). The correlation of the measured and the calculated results appears to be sufficient for most of the rpm range.

To refine the interior noise level, the panel contributions can be analyzed. The major panel contributions to the interior noise level have been determined via the MATLAB model. The order content of each subpanel can be analyzed such that the frequency information of any contribution is available. A panel contribution is formed from the operational load times the acoustic transfer function, and a contribution may occur because of the high operational loads or the high acoustic transfer functions.

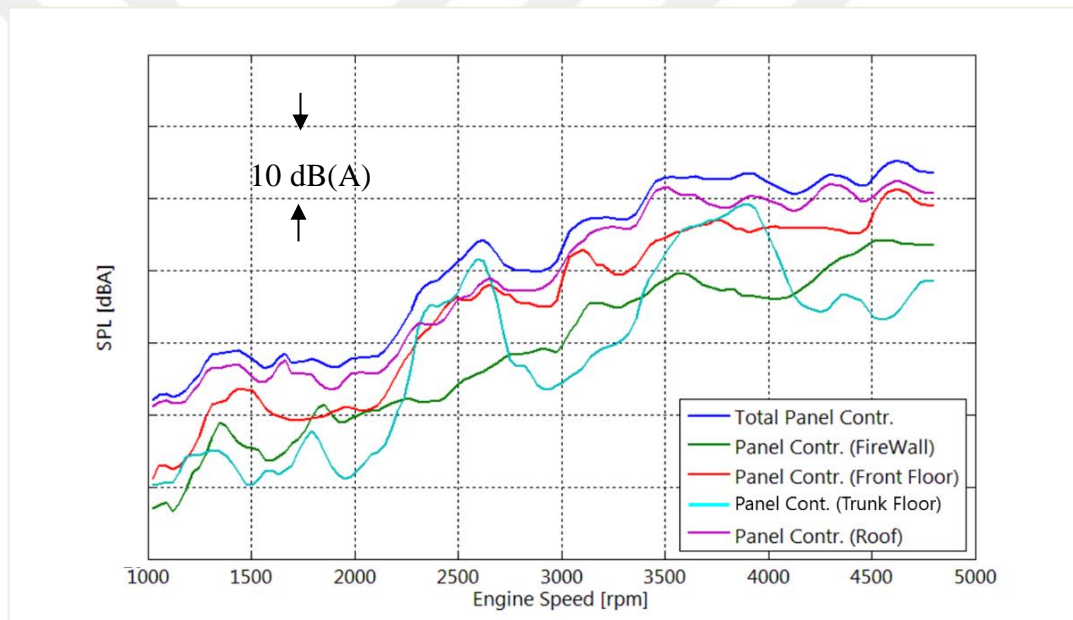


Figure 2.16 : Calculation Result: Major contributors.

The detailed panel contribution results are provided in Figure 2.16. The blue curve represents the total calculated panel contribution while the green, red, turquoise and purple curves represent the firewall, front floor, trunk floor and roof panels' contributions, respectively. The firewall has the lowest contribution whereas the roof has the highest contribution in the 1000-2000 rpm range and 3000-4800 rpm range, respectively. The trunk floor contribution has two peaks at approximately 2600 and 3800 rpms, which is more critical in terms of the sound quality and subjective evaluation. Especially at 2600 rpm, due to the quick increase in the noise level, it is perceived as an unpleasant noise inside the passenger compartment during an

acceleration maneuver. Lastly, the front floor has high contributions of approximately 2500 and 3200 rpms.

The major subpanel contributions are highlighted in orange in Figure 2.17.

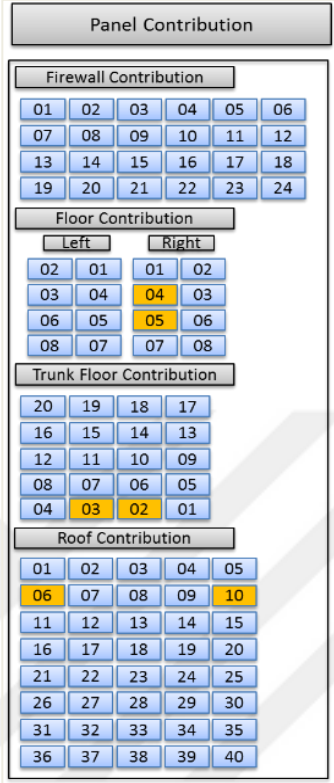


Figure 2.17 : Subpanels and main contributor subpanels (highlighted in orange).

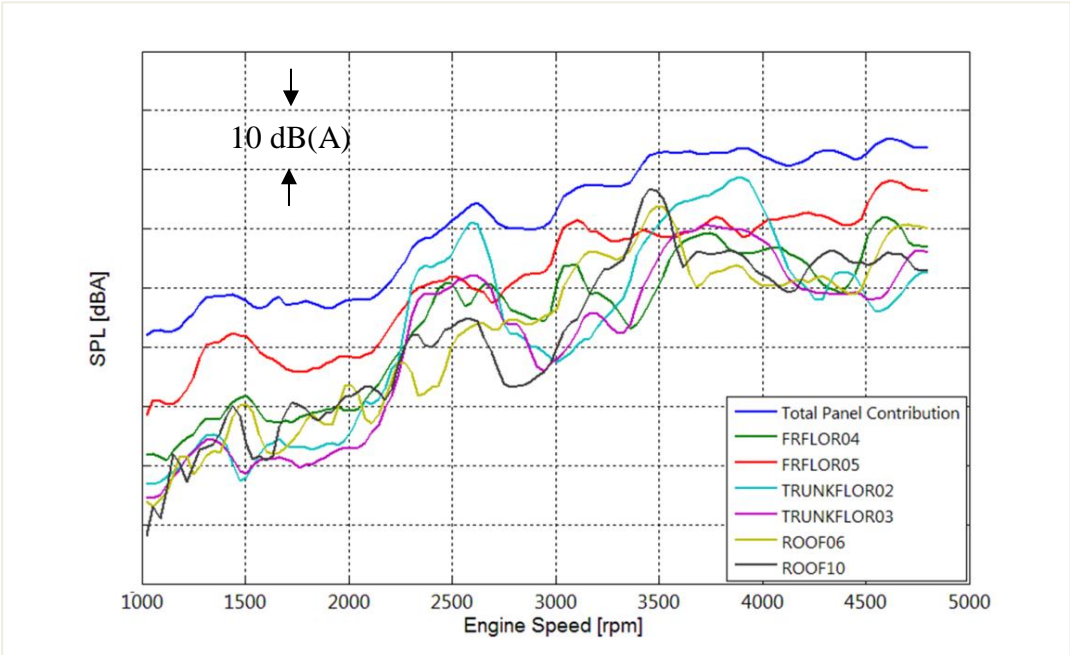


Figure 2.18 : Calculation result: Detailed subpanel contribution.

The contribution of the primary contributing sub-panels can be observed in Figure 2.18. The high contribution is determined to be caused by the high operational load on the sub-panels FRFL04 & FRFL05 (4th and 5th sub-panels of front right floor), TRUNKFLOR02 & TRUNKFLOR03 (2nd and 3rd sub-panels of trunk floor) and ROOF06 & ROOF10 (6th and 10th sub-panels of the roof).

Furthermore, the acoustic transfer function has been analyzed around the corresponding frequency, and the ATF is reasonably low. A structural dampening material, similar to the current ones being used on the other areas of the vehicle with the damping loss factor around 0.2, has been applied, as indicated in Figure 2.19, to the highlighted subpanels to decrease the vibrations level and thus the operational loads.

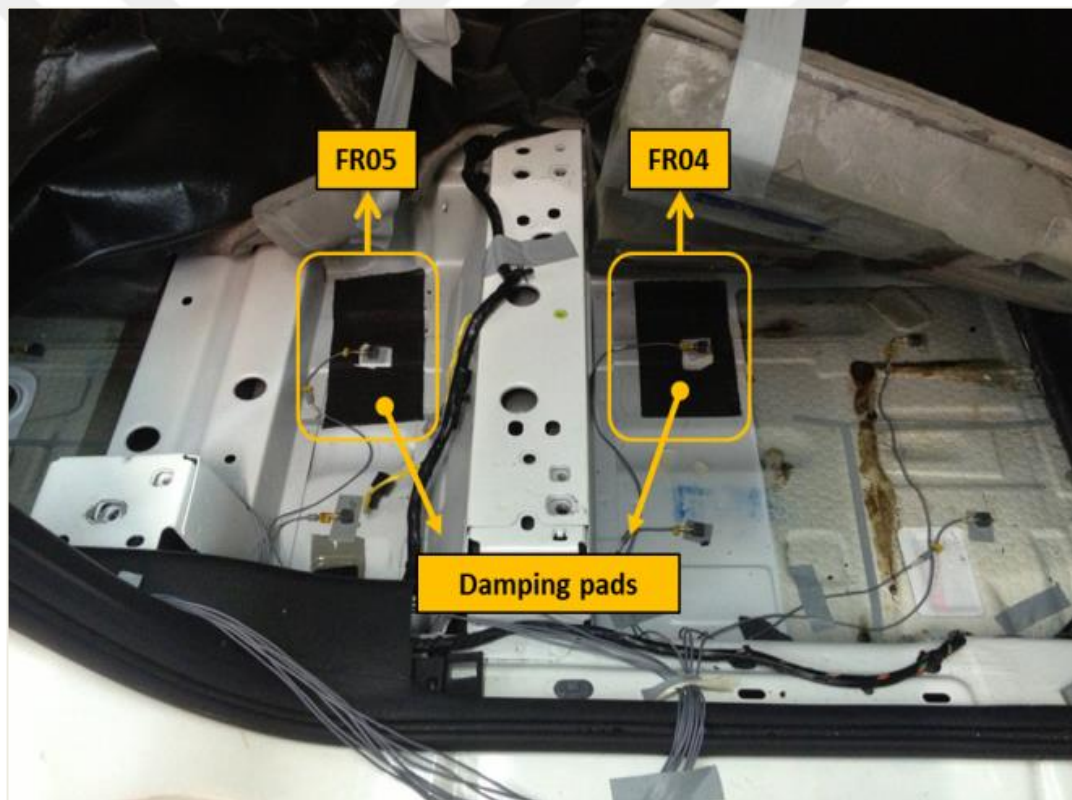


Figure 2.19 : Front right floor contributing subpanels-Adding damping pads.

The operational measurements have been performed to obtain the new sub-panel vibrations with damping pads on front floor and roof, and the new vibrations have been implemented into the MATLAB model to calculate the new contributions. An improvement in the front floor and the roof contributions can be observed in Figure 2.20 and Figure 2.21, respectively.

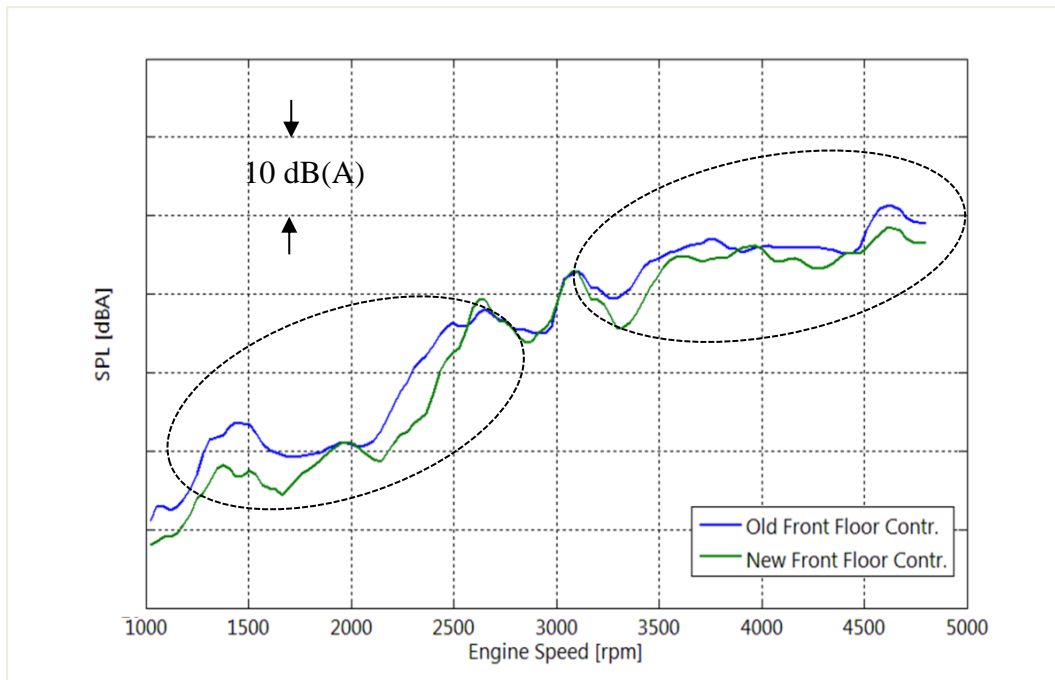


Figure 2.20 : Improvement in the front floor contribution (before and after the application of damping pads).

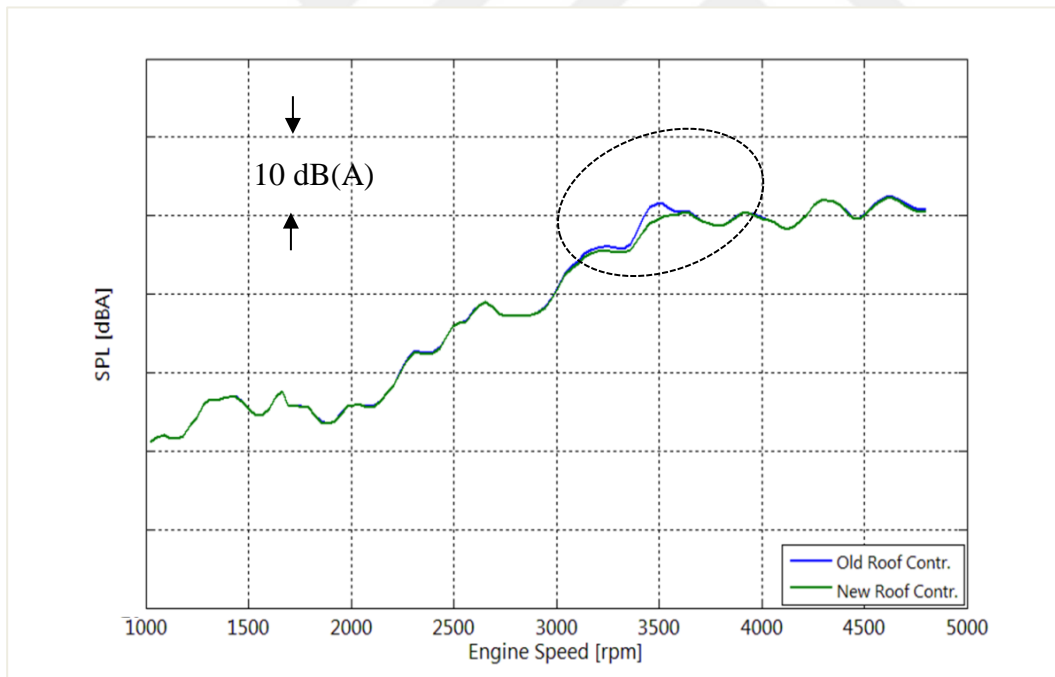


Figure 2.21 : Improvement in the roof contribution (before and after the application of damping pads).

The trunk floor contribution is further analyzed in the following two figures to provide additional information on the analyzing methodology. The two graphs depict the operational acceleration on sub-panel #2 of the trunk floor.

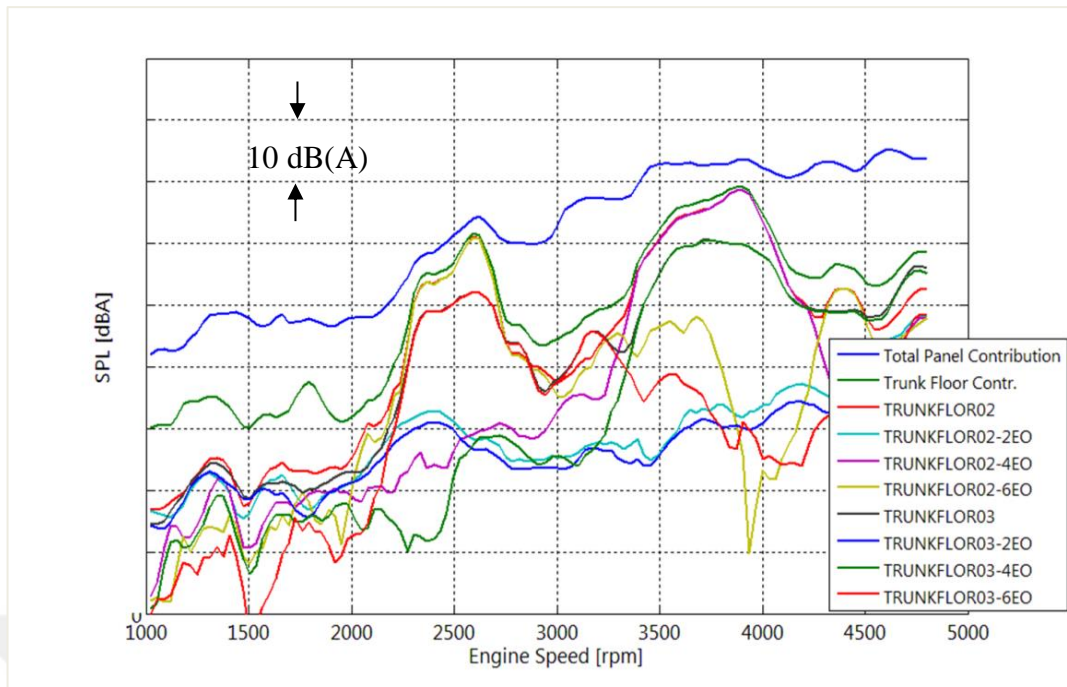


Figure 2.22 : Trunk floor - detailed contribution analysis.

As indicated in Figure 2.22, the 6th and 4th order contributions of trunk floor sub-panel #2 is dominant at approximately 2600 and 3800 rpms, respectively, and it can be calculated that both contributions correspond to 260 Hz.

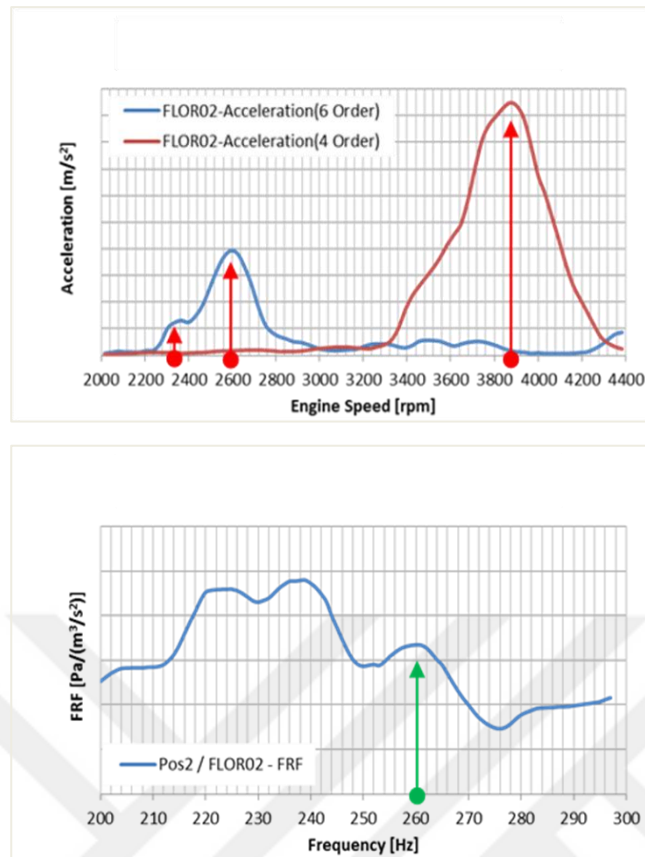


Figure 2.23 : Trunk floor sub-panel #2 operational load and ATF analysis.

The peaks in the operational loads can be observed on the left side, and the ATF from trunk floor sub-panel #2 to the driver’s ear position can be observed on the right side in Figure 2.23. The high total contribution of sub-panel #2 results from the peaks in the operational loads rather than the ATF. Although there is a small peak in the ATF at approximately 260 Hz, the level is lower compared to that of the other frequency regions, and the character of the total contribution curve is similar to the operational loads, which is a hint for the detailed analyses.

The high contribution of sub-panels #2 and #3 is caused by the high excitation coming from the exhaust hanger located extremely close to the mentioned panels. Additionally, the vibration insulation test has been performed on the exhaust hanger to determine the level of vibration filtration from the active side (on exhaust) to the passive side (on the body attachment point, close to the mentioned sub-panels). The results indicated that the hanger has a weak insulation performance at approximately 260 Hz. A new exhaust hanger with a different material is assembled on the vehicle, and new operational measurements have been performed to obtain the new vibrations from the trunk panels.

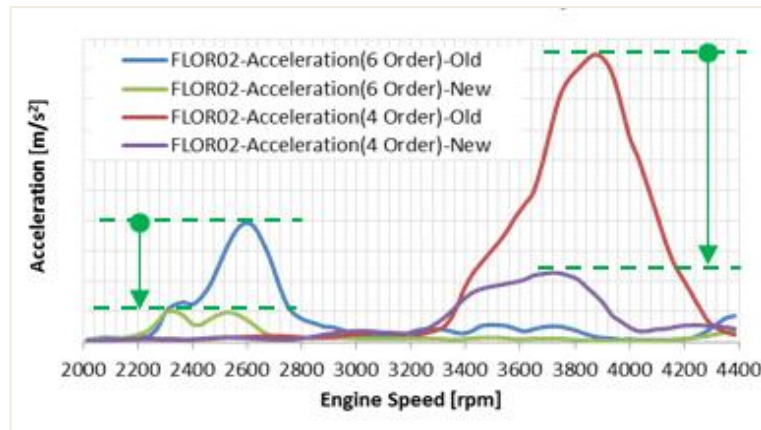


Figure 2.24 : The decrease in panel vibrations around 260 Hz (old: old exhaust hanger, new: new exhaust hanger with more vibration insulation performance).

The new data are imported into the model, and the calculation of the improvement in the trunk panel contribution is provided in Figure 2.25.

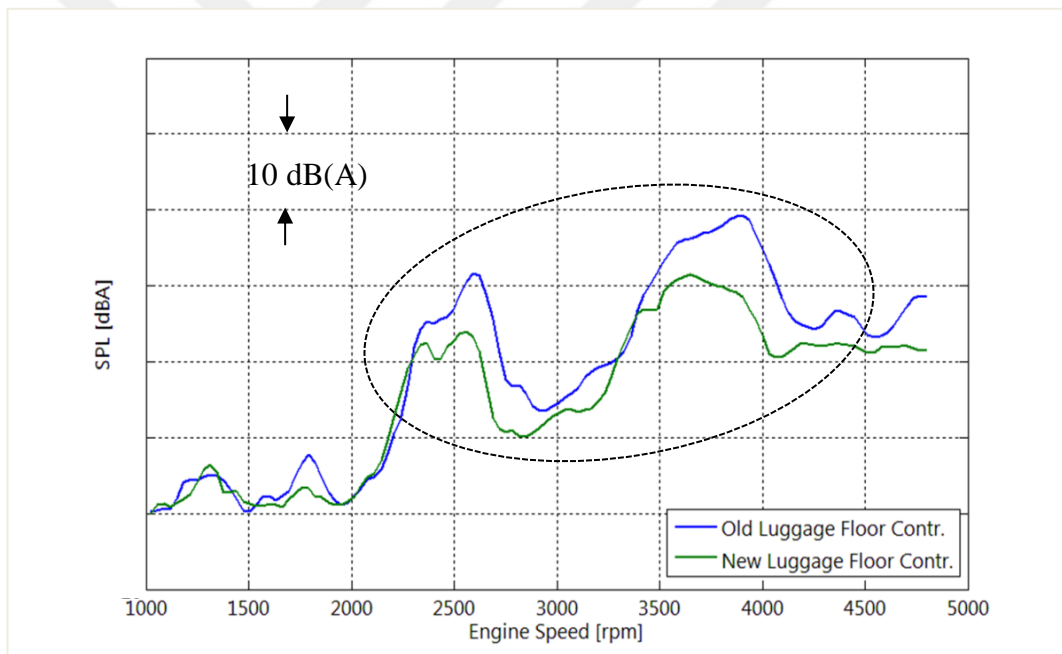


Figure 2.25 : Improvement in the trunk floor contribution.

According to Figure 2.25, an approximately 10 dB improvement for the approximately 2600 and 3800 rpm regions has been gained.

By implementing all of the new subpanel operational loads data in the model, a new refined interior noise level has been calculated and can be observed in Figure 2.26.

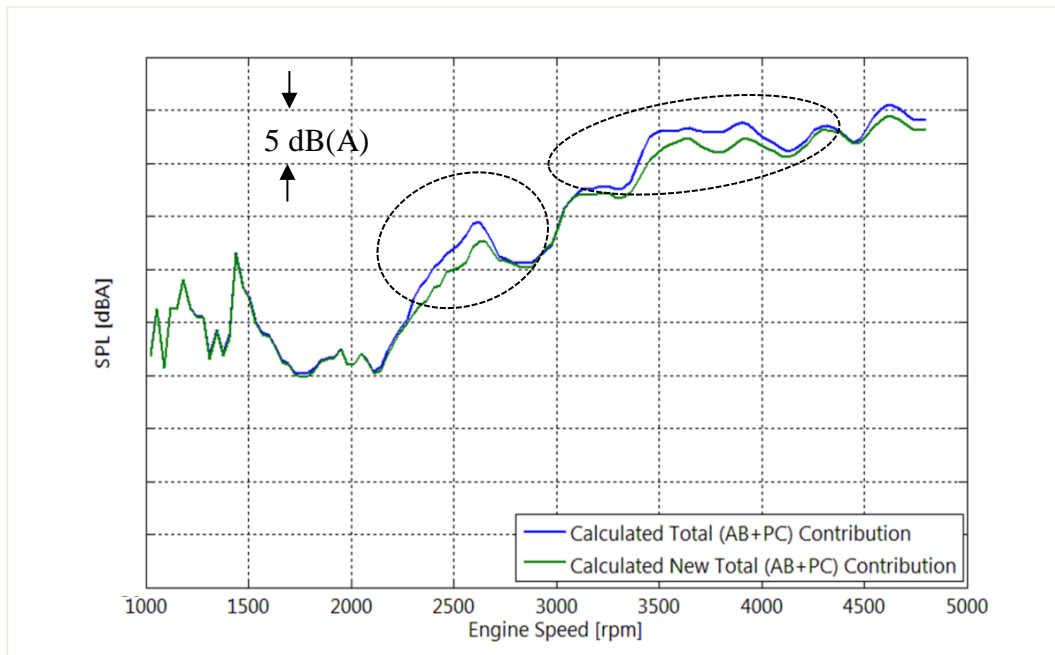


Figure 2.26 : Calculated initial and final interior noise level.

The blue and green curves represent the initial and final calculated interior noise level, respectively. The improvements in the overall sound pressure level are primarily between 2250-2750 rpm and 3000-4100 rpms with a level of approximately 3 dB(A).

To verify the final correlation and the final status of the interior noise level of the vehicle with the interventions on the subpanels (the new inner dash isolator was also implemented on the vehicle), the interior noise level of the vehicle has been tested, and the result can be observed in Figure 2.27.

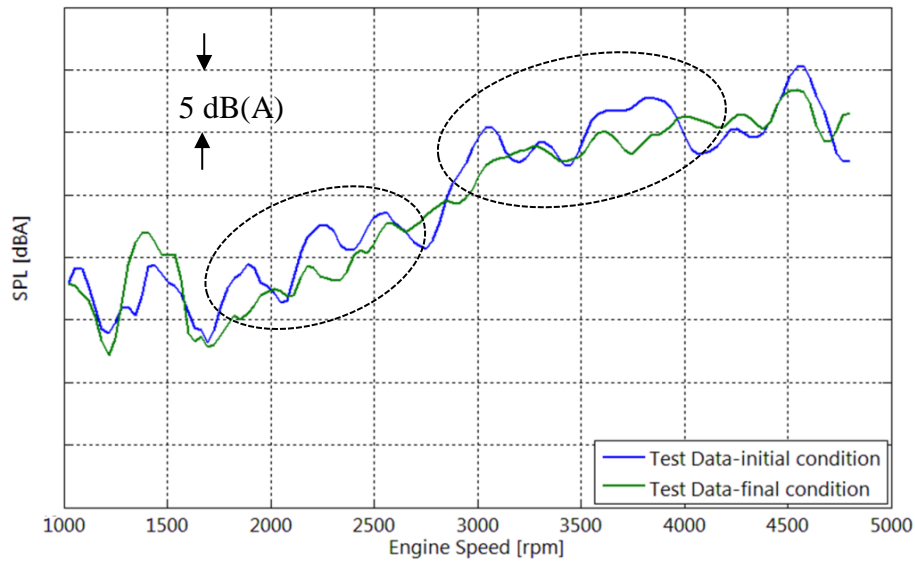


Figure 2.27 : Tested final interior noise level.

According to the test result, the interior noise levels indicate improvements in the overall noise level on 1750-2750 rpm and the 3000-4100 rpm ranges with the elimination of some peaks in the overall noise curve getting a more linearly increasing trend. Most of this range is correlated to the improvements observed in the contribution model.

2.5 Conclusion

To summarize, using the developed methodology combining the optimization process performed on an SEA model and the airborne and panel acoustic contribution analysis performed on a vehicle, a lighter acoustic pack and a vehicle with a more refined interior noise level with decreased panel contributions can be developed.

The calculated results indicated a good correlation in most of the rpm ranges whereas less correlation was obtained in a few regions (1250-2250 rpm). This result may be due to the panel dimensions that determine the frequency range of the analysis. In this study, the body panels that have a direct interaction with the passenger cavity have been analyzed. The lack of correlation in the mentioned region may be due to the absence of the windscreen and the door panels. This topic should be investigated further.

The final test result of the vehicle interior noise level indicated improvement (Figure 2.27), and the improved regions are similar to what is calculated with the contribution model. The integration of the ASQ and SEA methodologies may be offered as a unique methodology that can be applied in the product development stage to release refined and lower weight vehicles.



3. ON THE SOUND ABSORPTION PERFORMANCE OF A FELT SOUND ABSORBER²

3.1 Abstract

In this work, we have developed an analytical model of a multilayer porous material based on the transfer matrix method to predict the absorption behavior at plane wave incidence. The aim of this study is to modify/tune the sound absorption coefficient of a felt to obtain an improved absorbing performance in the mid frequency range without increasing its weight. To achieve this target, the developed model has been used to find the best combination of each layer type and thickness. The analytical results were validated by test results.

3.2 Introduction

Many types of sound absorbing materials are used in noise-control applications. These materials include glass fiber, polymeric fibrous materials, and various types of foams¹. Acoustical material plays a number of roles that are important in acoustic engineering, such as the control of room acoustics, industrial noise control, studio acoustics and automotive acoustics [9]. Low weight with higher or equal acoustic performance is the main goal of the automotive industry in recent years.

Materials that reduce the acoustic energy of a sound wave as the wave passes through it by the phenomenon of absorption are called sound absorptive materials [9]. They are commonly used to soften the acoustic environment of a closed volume by reducing the amplitude of the reflected waves [9]. Felt type materials generally have a sound absorption coefficient that increases quasi-linearly from lower to higher frequencies. There may be cases where one may want to increase the mid-frequency absorption performance of a felt. In the near future, by the presence of electric vehicles, tonal

² This chapter is based on the paper “C. Meriç, H. Erol and A. Özkan (2016). On the sound absorption performance of a felt sound absorber. *Applied Acoustics*, 114, 275–280. Doi: <http://dx.doi.org/10.1016/j.apacoust.2016.08.003>.”

noises will become more important than today because of the lack of a broadband background noise generated by today's internal combustion engines. In these cases, tunable sound absorbing materials, with similar weights of today's acoustic packs, may have more importance. Designing a multilayer absorber needs some pre-work to forecast its acoustic properties, such as the absorption coefficient and transmission loss. There are various studies in the literature that develop analytical models to predict the acoustic performances. Guofeng Bai et al [10] investigated the sound insulation performance of a multiple-layer structure, which consists of elastic solid, fluid and porous material. They calculated the sound insulation performance of composite materials based on the transfer matrix method. They showed using simulation and experimental results that the sound insulation performance is greatly improved after the air layer is used. M. Abid and M. S. Abbes et al [11] developed a method to predict the acoustic parameters of viscoelastic materials to improve the acoustic insulation of multilayer panels, and different layer arrangements were also tested to find the best configuration of a multilayer panel in terms of the acoustic insulation.

This paper consists of three parts. First, we describe the analytical model based on the transfer matrix method of a multilayer porous material to predict the sound absorption coefficient subjected to plane waves with a rigid backing boundary condition. Second, the sound absorption coefficient calculation result of the model for a multilayer material has been presented to obtain more absorbing performance in the mid frequency range without increasing its weight which is the main objective of this study. Finally, the model results have been validated with the experimental results.

3.3 Theoretical Background

Two main categories can be found in the literature for modeling the sound propagation in porous materials. The first one considers the porous media as an equivalent fluid with an effective density and bulk modulus, and this class of modeling applies to materials having either a rigid skeleton or a limp skeleton. In these materials, wave propagation can be described by a unique compression wave. The second category considers the elasticity of the frame. Biot theory is based on this consideration. The porous medium is modeled as two superimposed phases that are fluid and solid and describes wave propagation in terms of three waves propagating simultaneously in the solid and fluid phases, two compression waves and one shear wave [36].

Two approaches are found to be the most useful in modeling the propagation of sound within a porous absorbent. The first is a completely empirical approach as exemplified by Delany and Bazley⁶. A second approach to modeling porous absorbent is to formulate the problem using a semi-analytical approach. For instance, the propagation within the pores can be modeled semi-analytically by working on a microscopic scale⁶.

One widely used model from the first category is the Johnson-Champoux-Allard model. This model considers the rigid foam frame as solid and the air saturated in the porous medium as fluid, having an effective density (ρ) and an effective bulk modulus (K). The values of these two quantities are found from Equations (1) and (2) by five macroscopic quantities, the open porosity (ϕ), the static airflow resistivity (σ), the tortuosity (α_∞), the viscous characteristic length (Λ) and the thermal characteristic length (Λ') [32,36,37].

$$\rho = \alpha_\infty \rho_0 \left[1 + \frac{\sigma \phi}{j \omega \rho_0 \alpha_\infty} G_J(\omega) \right] \quad (3.1)$$

$$K = \gamma P_0 / \left[\gamma - (\gamma - 1) \left[1 + \frac{\sigma' \phi}{j B^2 \omega \rho_0 \alpha_\infty} G'_J(B^2 \omega) \right] \right] \quad (3.2)$$

where P_0 is the atmospheric pressure, ρ_0 is the density of air, ω is the angular frequency, γ is the adiabatic constant, B is the Prandtl number, and $\sigma' \approx c' \sigma$, where c' is a coefficient. $G_J(\omega)$ and $G'_J(\omega)$ are the functions of the angular frequency and defined by Equations (3) and (4) [32,36,37].

$$G_J(\omega) = \left(1 + \frac{4j \alpha_\infty^2 \eta \rho_0 \omega}{\sigma^2 \Lambda^2 \phi^2} \right)^{1/2} \quad (3.3)$$

$$G'_J(B^2 \omega) = \left(1 + \frac{4j \alpha_\infty^2 \eta \rho_0 \omega B^2}{\sigma'^2 \Lambda'^2 \phi^2} \right)^{1/2} \quad (3.4)$$

The values of Λ and Λ' are given by Equations (5) and (6) [32,36,37].

$$\Lambda' = \sqrt{\frac{8 \alpha_\infty \eta}{\phi \sigma'}} \quad (3.5)$$

$$\Lambda = \frac{1}{c} \sqrt{\frac{8 \alpha_\infty \eta}{\phi \sigma}} \quad (3.6)$$

where c is a constant that defines the cell structure shape and η is the dynamic viscosity of air. The viscous characteristic length (Λ) corresponds to the dimension of the

narrow sections (small pores) in the pore network, where viscous loss is dominant because of the boundary layer effect. The thermal characteristic length (Λ') indicates the dimension of the sections with larger surface areas within the pore network, where thermal loss is dominant. As per this definition, Λ' will be larger than or equal to Λ depending upon the value of the constant c , which depends on the geometry of the pore structure [32,36,37].

Once the characteristic impedance (Z_C) and wave number (k) for the material are known, it is necessary to convert these to the surface impedance and absorption coefficient for a particular thickness of the porous material with known boundary conditions. In this case, the most flexible way of predicting the surface properties of the porous material is to use the transfer matrix method [32].

$$Z_S = -j \cdot \frac{Z_C}{\phi} \cdot \cot g(K \cdot d) \quad (3.7)$$

where $Z_C = \sqrt{k \cdot \rho}$, $k = \omega \cdot \sqrt{\frac{\rho}{K}}$ and d is thickness of the porous material.

The reflection coefficient (R) and the absorption coefficient (α) of the material can be estimated by Equations (8) and (9), respectively [32,36,37].

$$R = \frac{Z_S - \rho_0 c_0}{Z_S + \rho_0 c_0} \quad (3.8)$$

$$\alpha = 1 - |R|^2 \quad (3.9)$$

For a multilayer porous material, at each interface between the layers, the continuity of the pressure and particle velocity is assumed. This allows a relationship between the pressure and the particle velocity at the top and bottom of a layer to be produced, which is compactly given in matrix format [38].

$$\begin{Bmatrix} p_{li} \\ u_{li} \end{Bmatrix} = \begin{Bmatrix} p_{xi+1} \\ u_{xi+1} \end{Bmatrix} = \begin{bmatrix} \cos(k_{xi} d_i) & j \frac{\omega \rho_i}{k_{xi}} \sin(k_{xi} d_i) \\ j \frac{k_{xi}}{\omega \rho_i} \sin(k_{xi} d_i) & \cos(k_{xi} d_i) \end{bmatrix} \begin{Bmatrix} p_{xi} \\ u_{xi} \end{Bmatrix} \quad (3.10)$$

where p_{xi} and u_{xi} are the pressure and particle velocity at the bottom of the i^{th} layer, respectively; p_{xi+1} and u_{xi+1} are the pressure and particle velocity at the bottom of the $(i + 1)^{\text{th}}$ layer, respectively; p_{li} and u_{li} are the pressure and particle velocity at the top of the i^{th} layer, respectively; d_i is the thickness of the layer; ρ_i the density of the i^{th} layer; and k_{xi} is the wavenumber for the i^{th} layer [38]. Figure 3.1 shows the structure of a multilayer porous material.

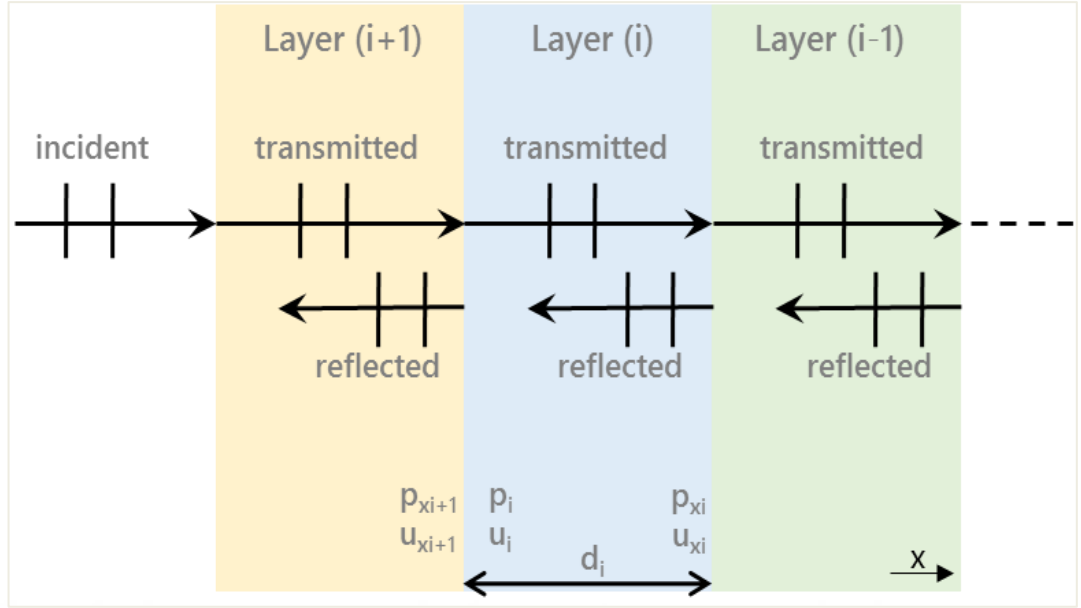


Figure 3.1 : Representation of the Multilayer Porous Material Structure.

If the bottom of layer i has an impedance of z_{si} and layer i has a characteristic impedance z_i , then the impedance at the bottom of the $(i + 1)^{\text{th}}$ layer is [38]:

$$z_{si+1} = \frac{-jz_{si}z_i \cot(k_{xi}d_i) + z_i^2}{z_{si} - jz_i \cot(k_{xi}d_i)} \quad (3.11)$$

To measure the normal sound absorption coefficients in an impedance tube, the transfer function method (ISO 10534-2:1998) is used. This method uses two microphone positions at points x_1 and x_2 . The sound pressures at these points are expressed as $p_1 = p_i \cdot e^{jkx_1} + r \cdot p_i \cdot e^{-jkx_1}$ and $p_2 = p_i \cdot e^{jkx_2} + r \cdot p_i \cdot e^{-jkx_2}$, where the time variation factor is omitted. The complex acoustic transfer function between these two microphones is then $H_{21} = \frac{p_2}{p_1}$, which can be solved for $R = \frac{H_{21} - H_I}{H_R - H_{21}} \cdot e^{2jx_1}$, where $H_I = e^{-jks}$ and $H_R = e^{jks}$, where $s = x_1 - x_2$ is the distance between measurement points [39]. The normal sound absorption coefficient is calculated from $\alpha = 1 - |R|^2$, and the specific acoustic impedance ratio is obtained as [39] $\frac{Z}{\rho c} = \frac{1+R}{1-R}$.

The schematic of the impedance tube can be seen in Figure 3.2.

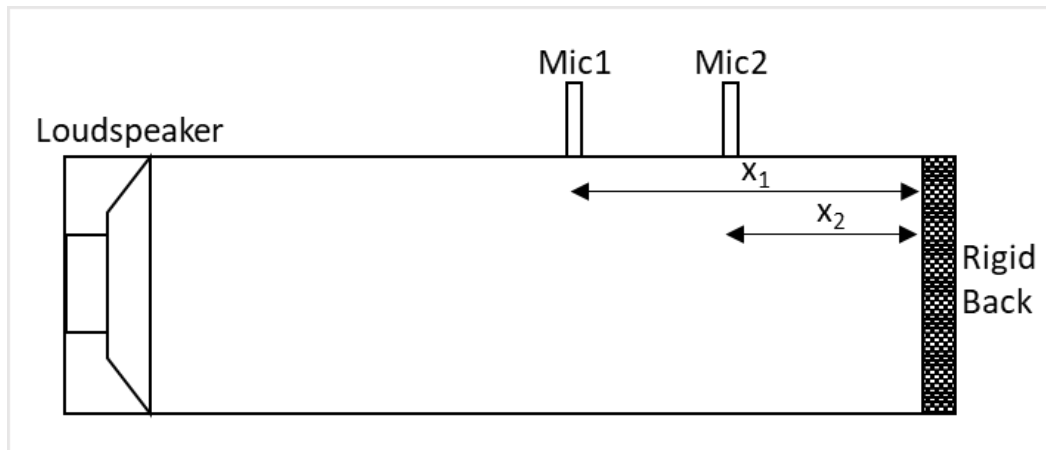


Figure 3.2 : Schematic of the Impedance Tube.

3.4 Analytical Studies

The main objective of the analytical studies is to calculate the absorption coefficient of a felt with the transfer matrix method and obtain a multilayer material to increase its absorption coefficient in the mid-frequency range. For the one-layer felt, the Johnson-Champoux-Allard model is used, and for the multilayer material, the developed code based on the transfer matrix method is used.

To summarize the approach in the analytical studies, first, the sound absorption coefficient of the initial one-layer felt is calculated using the Biot parameters shown in Table 1. Second, a *felt-air layer-felt* structure, which satisfies the sound absorption coefficient of the initial *one-layer felt*, has been developed. The proper felt layers are selected with a lower weight per unit area, and their Biot parameters are obtained from the previously developed material characterization library. The total thickness is kept constant. In the second step, it is observed that the air layer behaves like a felt layer, and one can obtain similar absorption performance with the *felt-air-felt* system to that of the *one-layer felt* system. Third, a film layer is inserted in the system, and a *felt-air-film-felt* system is developed. In order to add the film layer in the transfer matrix model, mechanical impedance of the film is calculated by considering it as a thin elastic plate as stated by J.F.Allard and N.Atalla [32] in section 11.3.5. The behavior of the sound absorption coefficient with increasing density of the film layer is investigated. In the third step, it is observed that with increasing density of the film layer, the mid-frequency absorption coefficient increases, whereas the high frequency absorption coefficient decreases. Finally, the layout of the multi-layer absorber is changed to the

felt-film-air-film-felt configuration. In the final step, it is observed that the mid-frequency absorption coefficient increases significantly, whereas the loss in the high frequency absorption performance is negligible. The sound absorption coefficient calculation result of all four steps of the *multi-layer absorber* compared to the initial *one-layer felt* is shown in Figure 3.3. All the configurations is listed in Table 3.2.



Table 3.1 : Material acoustical parameters.

	Material	Density [gr/m2]	Thickness [mm]	Porosity [-]	AFR [N.s.m- 4]	Tortuosity [-]	Viscous Length [m]	Thermal Length [m]	Shape Factor [-]
1. Felt	Felt-0	1600	24	0.985	24000	1.1	0.000055	0.000142	1.4
2.	Felt-1	800	11	0.945	42000	1.3	0.000041	0.000137	1.7
Felt+Air+Felt	Air		8						
	Felt-2	500	7	0.96	20000	1.2	0.000080	0.000134	1.2

Table 3.2 : Tested configurations.

Configuration #	Description(from loudspeaker to rigid back)	Material	Density (gr/m2)	Thickness (mm)
Configuration-0	One-layer Felt	Felt-0	1600	24
Configuration-1	Felt + Air + Felt	Felt-1	800	11
		Air		8
		Felt-2	500	7
Configuration-2	Felt + Air + Film + Felt	Felt-1	800	11
		Air		8
		Film	100	0.1
		Felt-2	500	7
Configuration-3	Felt + Air + Film + Felt	Felt-1	800	11
		Air		8
		Film	200	0.2
		Felt-2	500	7
Configuration-4	Felt + Air + Film + Felt	Felt-1	800	11
		Air		8
		Film	300	0.3
		Felt-2	500	7
Configuration-5	Felt + Film + Air + Film + Felt	Felt-1	800	11
		Film	100	0.1
		Air		8
		Film	100	0.1
		Felt-2	500	7

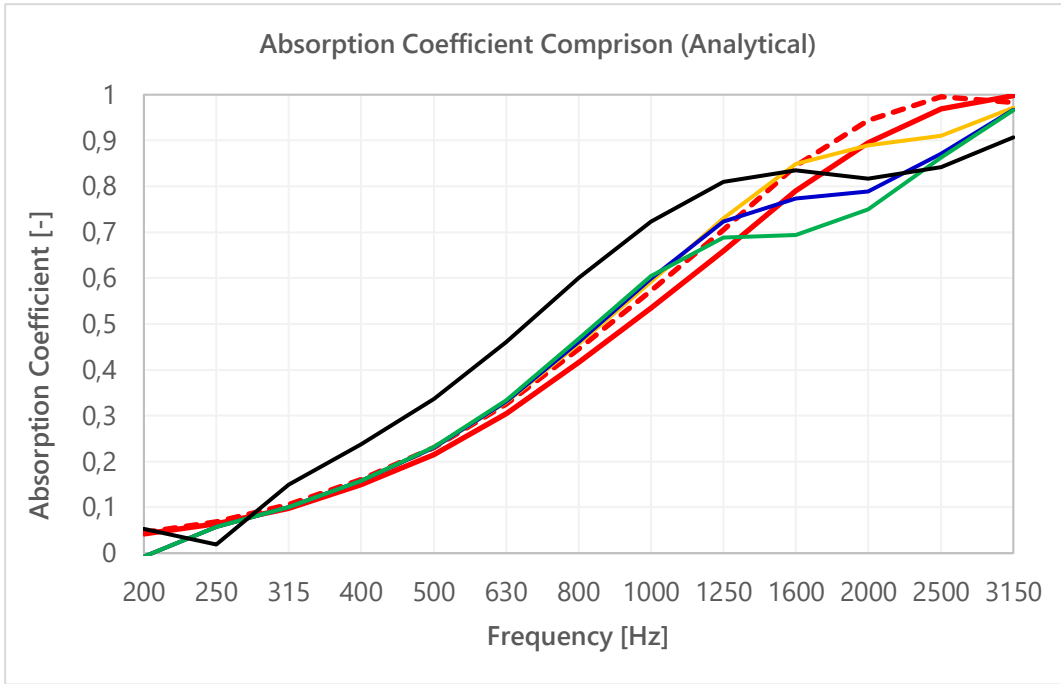


Figure 3.3 : Sound Absorption Coefficient Curves Calculated with the Analytical Model (Solid Red Curve: Configuration-0, Dashed Red Curve: Configuration-1, Solid Orange Curve: Configuration-2, Solid Blue Curve: Configuration-3, Solid Green Curve: Configuration-4, Solid Black Curve: Configuration-5).

The schematic of the initial one-layer and multi-layer structures explained above is shown in Figure 3.4.

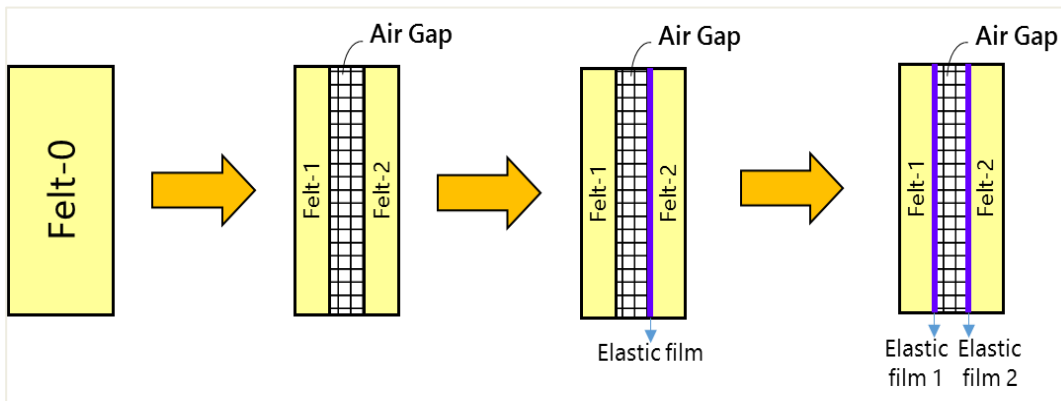


Figure 3.4 : Schematic of the Initial One-layer and Multi-layer Structures.

A table comparing the sound absorption and weight of the analytical studies section is listed in the conclusion section to compare these values with the output of experimental studies section

3.5 Experimental Studies

In experimental studies, first, to verify the output of the analytical modeling results, a non-compressed non-phenolic felt with a density of 1600 g/m² and a thickness of 24 mm is used. The sound absorption coefficient tests are performed using the impedance tube method.

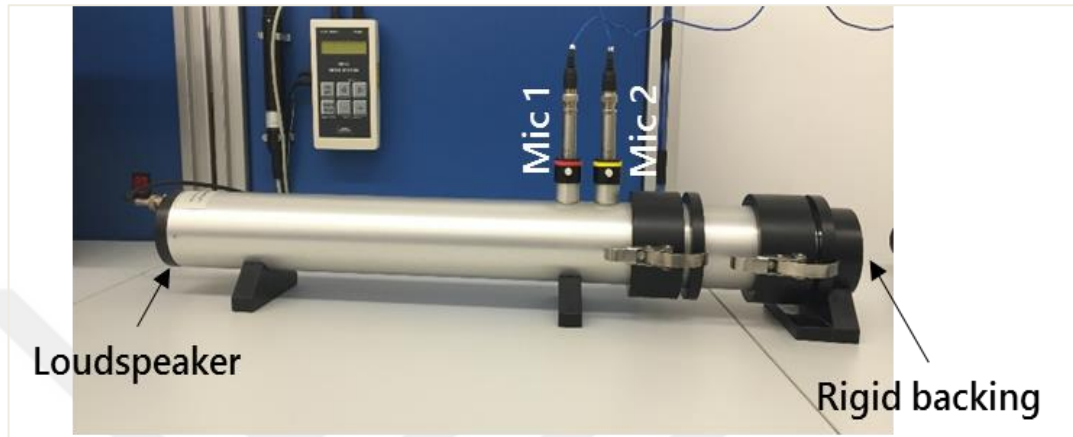


Figure 3.5 : Experimental Setup.

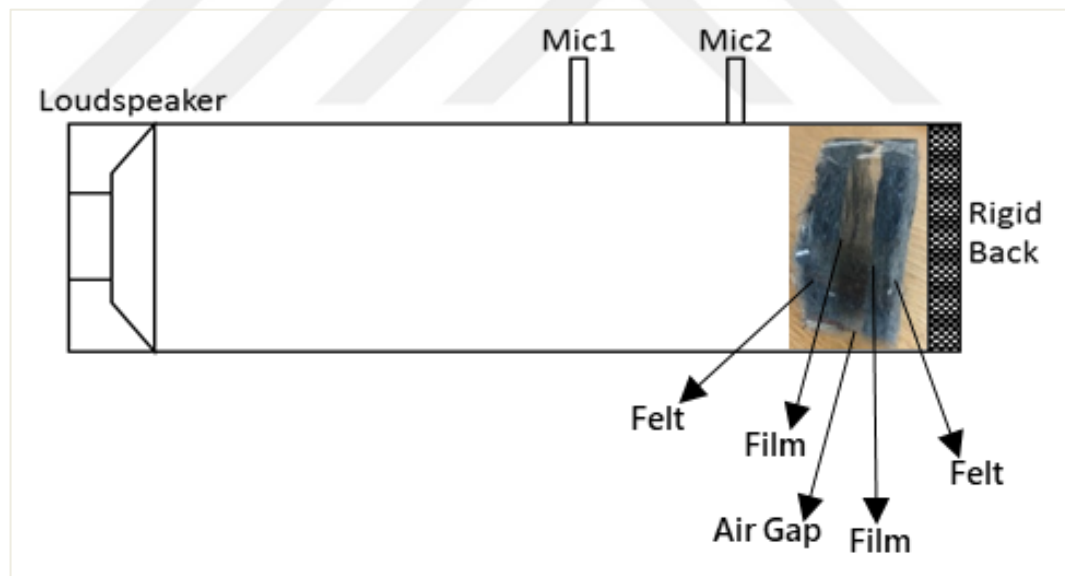


Figure 3.6 : Implementation of the Test Sample in the Impedance Tube.

Second, the sound absorption coefficient of Configuration-1 is tested. In Figure 3.7, the sound absorption coefficient test result is shown. As in the output of the analytical model, the sound absorption performance of these two systems is very close to each other. One may refer to Figure 3.3 also to better compare the analytical and test results.

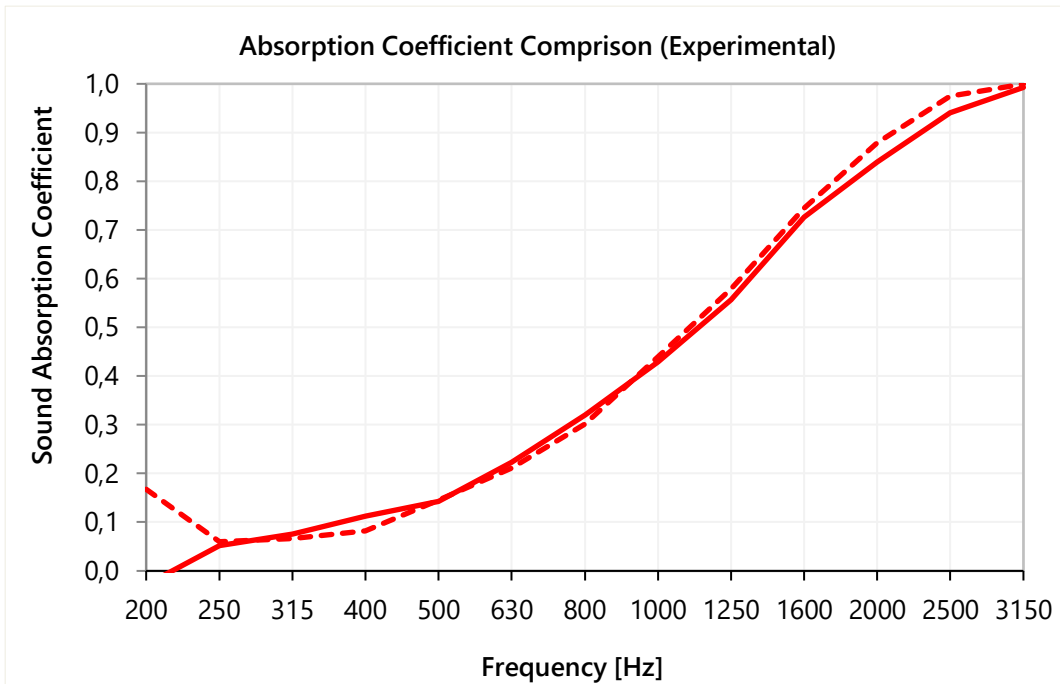


Figure 3.7 : Sound Absorption Coefficient Curves Tested (Solid Red Curve: Configuration-0 and Dashed Red Curve: Configuration-1).

Figure 3.8 shows the experimental results of all the configurations shown in Table 3.2. In order to realize the listed configurations 2- 5, a self-adhesive film is used in the experiments and the samples are located from loudspeaker to the rigid-back in the sequence shown the description in Table 3.2 from left to right. An example of test position is shown in Figure 3.6. The experimental results show good agreement with the analytical modeling results.

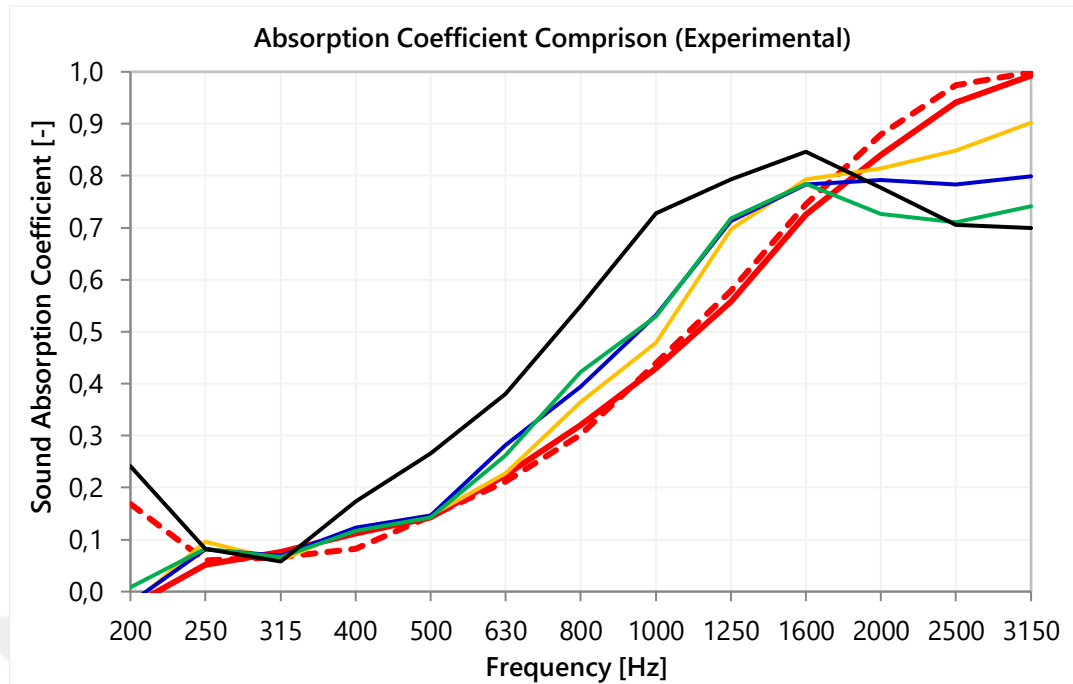


Figure 3.8 : Sound Absorption Coefficient Curves Calculated with the Analytical Model (Solid Red Curve: Configuration-0, Dashed Red Curve: Configuration-1, Solid Orange Curve: Configuration-2, Solid Blue Curve: Configuration-3, Solid Green Curve: Configuration-4, Solid Black Curve: Configuration-5).

3.6 Conclusion

Generally, the mid-frequency range sound absorption performances of felts are low compared to their performance in the relatively high frequency range. There may be some cases where one may want to increase the mid-frequency absorption performance of a felt without increasing its weight. In such cases, according to the experimental results shown in this study, one can modify the sound absorption curve characteristic of a felt using elastic films and the air gap without increasing or decreasing its weight. The weight and sound absorption performance is compared in Table 3.3 for the analytical model and in Table 3.4 for the experimental verification studies. There is a good agreement between the analytical and experimental results in terms of the amplitude of the sound absorption coefficient in most of the frequency range and the tendency of the behavior of the curve comparing different configurations listed in summary tables and in Figures 3.9 and Figure 3.10.

In conclusion, compared to the initial condition, with 12% less weight, one can gain 35% in the absorption performance in the relatively mid-frequency range with a loss (20%) in the relatively high frequency range.

Table 3.3 : Weight and Sound Absorption Performance Comparison (Analytical Studies).

	Weight [g]	Average Absorption Coefficient [-]		
		Average (250-3150hz)	Average (250-2000hz)	Average (2000-3150hz)
Configuration-0	☆ 4,52	0,51	0,41	0,95
Configuration-1	★ 3,68	0,53	0,44	0,97
Configuration-2	★ 3,83	0,52	0,44	0,92
Configuration-3	★ 3,98	0,51	0,42	0,88
Configuration-4	★ 4,13	0,49	0,41	0,86
Configuration-5	★ 3,98	0,56	0,50	0,86

Table 3.4 : Weight and Sound Absorption Performance Comparison (Experimental Studies).

	Weight [g]	Average Absorption Coefficient [-]		
		Average (250-3150hz)	Average (250-2000hz)	Average (2000-3150hz)
Configuration-0	☆ 4,52	0,45	0,35	0,92
Configuration-1	★ 3,68	0,46	0,35	0,95
Configuration-2	★ 3,83	0,46	0,38	0,85
Configuration-3	★ 3,98	0,46	0,39	0,79
Configuration-4	★ 4,13	0,44	0,39	0,73
Configuration-5	★ 3,98	0,50	0,47	0,73

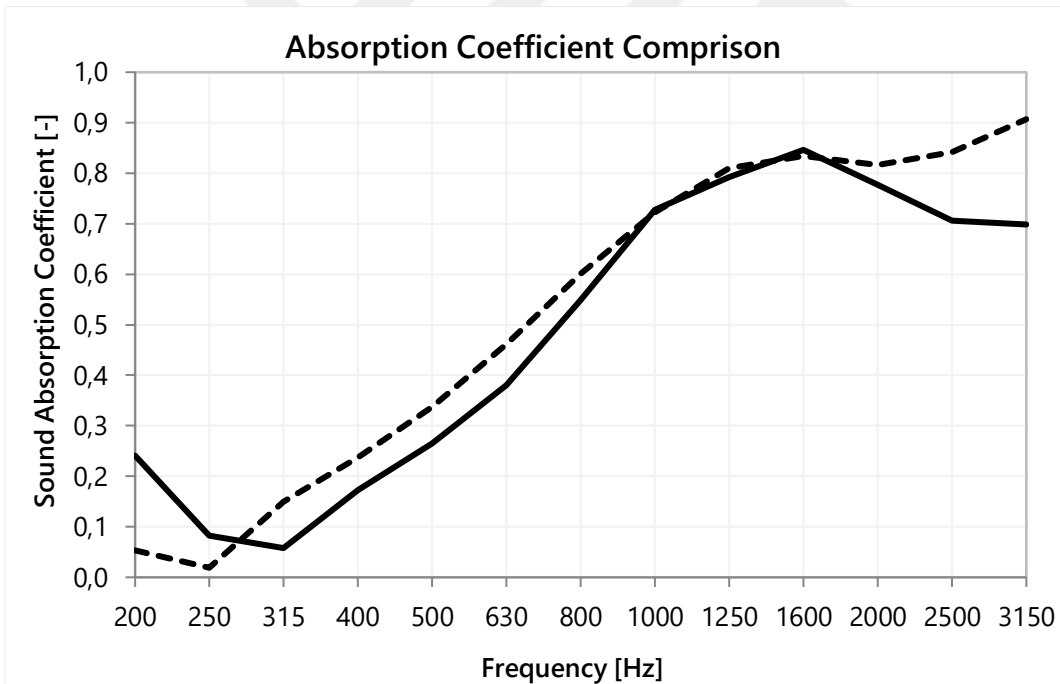


Figure 3.9 : Sound Absorption Coefficient Curves Calculated vs. Tested (Black Curve: Test result of Configuration-5, Dashed Black Curve: Calculation Result of Configuration-5).

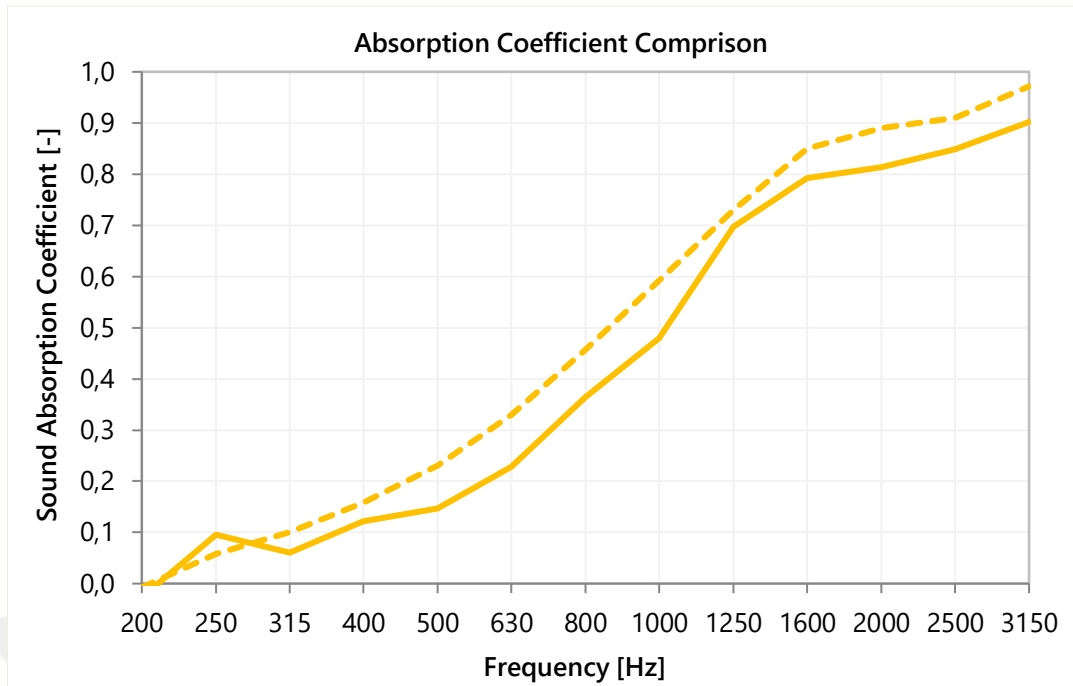


Figure 3.10 : Sound Absorption Coefficient Curves Calculated vs. Tested (Orange Curve: Test result of Configuration-2, Dashed Orange Curve: Calculation Result of Configuration-2).



4. DESIGN AND APPLICATION OF A COMPACT HELICAL AIR INTAKE SYSTEM RESONATOR FOR BROADBAND NOISE CONTROL³

4.1 Abstract

In this work, we have developed an analytical model that uses the transfer matrix method to predict the transmission loss (TL) of a resonator system with a helical side branch duct connected to the main duct. The resonator system is tuned to a proper frequency range to be applied on vehicle in order to decrease the air intake pipe radiated noise of the selected passenger car below 1000 Hz. In order to fulfill the packaging requirements, the developed resonator does not require an additional volume. Developed helical resonator has been analyzed numerically and the analytical results are first validated with the numerical ones and the prototype part has been produced with rapid prototyping technique. Finally, the prototype part has been tested on a 1.6 l Gasoline Engine Vehicle.

Keywords: resonator, air intake system (AIS), helical resonator

4.2 Introduction

Recently quietness has become an important quality parameter for automotive vehicles and as a result various improvements have been brought to reduce noise at system and vehicle level [12]. Due to stringent noise emission norms on automotive vehicles and increasing desire of quieter in-cab performance by users, reduction of air intake noise tends to be an area of explanation [12]. The air induction system of an automobile engine contributes to the noise level generated by a passenger car. The contribution is significant in the perception of vehicle noise quality. There is a great value in reducing and controlling passenger car air induction noise [13]. Researches on noise control applied to the air intake systems have not received much attention when compared

³ This chapter is based on the paper “C. Meriç, H. Erol and A. Özkan (2018). Design and application of a compact helical air intake system resonator for broadband noise control. *Applied Acoustics*, 131, 103-111. Doi: <http://dx.doi.org/10.1016/j.apacoust.2017.10.022>.

research on exhaust systems [12]. One way of attenuating broad band noise that propagates through ducts or pipe systems is to use one or more reactive-type acoustic components, each of which is specifically designed for optimal performance at a particular frequency range [14]. The operational principles of intake and exhaust silencers can be divided into two types, dissipative and reactive type, that dissipative silencers contain absorptive materials which physically absorbs acoustic energy from the gas flow where reactive silencers operate on the principle that when the sound in a pipe or duct encounters a discontinuity in the cross-section, some of the acoustic energy is reflected back towards the sound source thereby creating destructive interface [15]. Many types of sound absorbing materials are used in noise-control applications. These materials include glass fiber, polymeric fibrous materials, and various types of foams [16]. As reactive type resonators, expansion chambers, Helmholtz resonators and quarter wave tubes are commonly being used in today's vehicles where the need for the size of such resonators increase with the decrease in working frequency range. Actively controlled Helmholtz resonator has been developed by Tanaka and Nishio by placing a speaker inside the cavity of the resonator located at a branch of the fresh air duct [17,18]. According to the literature available so far on the intake noise reduction, the techniques currently used to reduce air induction noise include usage of expansion chambers, absorption or cancellation principle [12,19,20,21].

Design constraints for noise attenuation devices employed in automotive induction systems are continuously being challenged to provide optimum performance for the least cost and packaging space [22]. Packaging space in particular is becoming increasingly difficult, especially for four cylinder vehicles where large reactive elements such as Helmholtz resonators are needed to attenuate low frequency "boom" [15]. Due to these resonators requiring extra volume in vehicle engine compartment and creating packaging problems, means interference and/or not enough space with the neighbor system elements, mostly new design of these neighbor elements may be necessary which means extra time and cost for the vehicle. In order to prevent this problem alternative designs for the air intake system resonators may be mandatory in some cases. This paper proposes a small size air intake system resonator with a helical side branch duct connected to the main duct, being the same size with the main pipe thus not requiring an additional volume, which is very suitable for the packaging

requirements. The designed helical resonator in this paper is a tunable resonator and can be tuned to the required frequency range by adjusting the dimensions that are shown in Figure 4.2 and Figure 4.6. Resonator in this paper is tuned to mainly 300 Hz – 600 Hz frequency range to decrease the noise level of the selected passenger car of which's air intake pipe radiated noise in the specified frequency range is high.

4.3 Theory

Figure 4.1 shows a system diagram. The rigid straight main duct has a constant cross section, and its diameter is d_a . The length of the main duct is l_a . The rigid straight inner duct has a constant cross section, and its diameter is d_b . The length of the inner duct is l_b . The helical side branch ducts connected to the main duct have constant cross sections with diameters d_c and d_d and lengths l_c and l_d . This study deals with the transfer matrix method for predicting, with zero mean flow, the TL of the system.

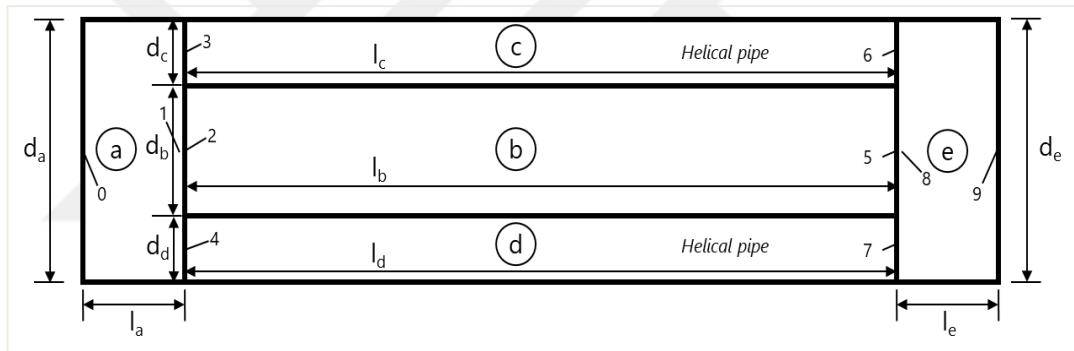


Figure 4.1 : Schematic of helical resonator.

Plane wave propagation in a rigid straight pipe with length L can be described by its transmission (or four-pole) matrix, as follows:

$$\begin{bmatrix} p(0, t) \\ v(0, t) \end{bmatrix} = \begin{bmatrix} A & B \\ C & D \end{bmatrix} \begin{bmatrix} p(L, t) \\ v(L, t) \end{bmatrix} \quad (4.1)$$

where $p(0, t)$, $p(L, t)$, $v(0, t)$ and $v(L, t)$ are the sound pressures and volume velocities at the input and the output; and A, B, C and D are four-pole parameters.

The sound pressure field inside the tube is

$$p(x, t) = p^+ e^{i(\omega t - kx)} + p^- e^{i(\omega t + kx)} \quad (4.2)$$

where $i = \sqrt{-1}$, ω is the angular frequency in radians per second, t is the time, k is the wave number or propagation constant, and x is the plane wave propagation axis. Then the inlet pressure and volume velocity are

$$p(0, t) = (p^+ + p^-)e^{i\omega t} \quad (4.3)$$

$$v(0, t) = \frac{(p^+ - p^-)e^{i\omega t}}{\rho c} \quad (4.4)$$

and the output pressure and volume velocity are

$$p(L, t) = (p^+ e^{-ikL} + p^- e^{ikL})e^{i\omega t} \quad (4.5)$$

$$v(L, t) = \frac{(p^+ e^{-ikL} - p^- e^{ikL})e^{i\omega t}}{\rho c} \quad (4.6)$$

where ρ is the density, and c is the speed of sound.

Thus, from Eqns. (3)–(6)

$$\begin{bmatrix} p(L) \\ v(L) \end{bmatrix} = \begin{bmatrix} \cos(kL) & -i \frac{\rho c}{S} \sin(kL) \\ -i \frac{S}{\rho c} \sin(kL) & -\cos(kL) \end{bmatrix} \begin{bmatrix} p(0) \\ v(0) \end{bmatrix} \quad (4.7)$$

Equation (7) can be rearranged as

$$\begin{bmatrix} p(0) \\ v(0) \end{bmatrix} = \begin{bmatrix} \cos(kL) & i \frac{\rho c}{S} \sin(kL) \\ i \frac{S}{\rho c} \sin(kL) & \cos(kL) \end{bmatrix} \begin{bmatrix} p(L) \\ v(L) \end{bmatrix} \quad (4.8)$$

and then

$$T = \begin{bmatrix} A & B \\ C & D \end{bmatrix} = \begin{bmatrix} \cos(kL) & i \frac{\rho c}{S} \sin(kL) \\ i \frac{S}{\rho c} \sin(kL) & \cos(kL) \end{bmatrix} \quad (4.9)$$

is the transfer matrix of the rigid straight pipe. Here, S is the cross sectional area of the acoustic domains [14].

The description of the subsystems in terms of their four-pole parameters is very convenient, because the output of one system is the input of the next, from which it follows that the transmission matrix of the system which is shown in Figure 4.1 that features multiple cascaded subsystems can be formulated in matrix form as [14]

$$\begin{bmatrix} p_0 \\ v_0 \end{bmatrix} = T_a T_b T_c T_d T_e \begin{bmatrix} p_7 \\ v_7 \end{bmatrix} \quad (4.10)$$

On the other hand, in this study, the characteristic impedances are assumed to be equal at the inlet and the outlet: $Z_a = Z_e = Z$. The transfer matrix of the system shown in Figure 4.1 is obtained as T_{17} .

$$T_{17} = \begin{bmatrix} T_1 & T_2 \\ T_3 & T_4 \end{bmatrix} = T_a T_b T_c T_d T_e \quad (4.11)$$

Transmission loss involves neither the source nor the radiation impedance. It is an invariant property of the element. Since it is independent of the terminations, TL finds favor with researchers who are interested in finding the acoustic transmission behavior of an element or set of elements in the context of isolated terminations [14,16].

Finally, the TL of the system can be expressed as

$$TL = 20 \text{Log}_{10} \left| \frac{1}{2} \left(T_1 + \frac{T_2}{Z} + Z T_3 + T_4 \right) \right| \quad (4.12)$$

4.4 Design And Virtual Verification

The analytical modelling of a helical resonator has been performed using transfer matrix method and all calculations assume that a 1D model is valid [14].

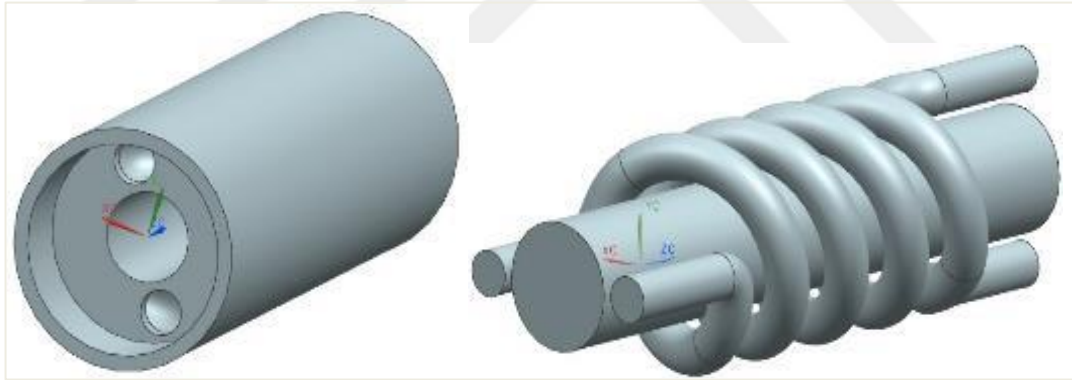


Figure 4.2 : Circular cross-section helical resonator (left), air cavity of the resonator (right).

For the numerical analysis, we first built a solid model of the system using a 3D CAD program, Unigraphics Nx. Then, the solid model was exported to MSc.Patran in parasolid format. This solid model consists of the air in the pipe system, which is called the cavity in this paper. The cavity is meshed using first order tetrahedral solid elements. In numerical acoustic analysis, the mesh size must be smaller than one sixth of the wavelength (mesh size $< \lambda/6$). The frequency range examined in this work is 0–1000 Hz. The minimum wavelength is $\lambda=0.34$ m, and the mesh size used in our

numerical analysis is 0.056 m. After meshing the cavity using solid elements, the input and output faces of the cavity were meshed with first order triangular elements. Two local coordinates with the same x-direction were assigned to these new faces, to give the input and output. Our goal was to be able to read the input and output sound power values after the analysis. A sound pressure value of 1 Pa was set for the nodes on the input face of the cavity. Then, we created a material with the default values of air. The density was 1.225 kg/m³, and the sound speed was 340 m/s. Using the default values in the software, the damping effect of air was not taken into account and was also not considered in our analytical model. We processed the output data in order to obtain the transmission loss of the system. The transmission loss comparison of virtual and analytical calculation results were then compared and is shown in Figure 4.4 for the resonator that is shown in Figure 4.3. There is a good agreement between analytical and numerical analysis results.

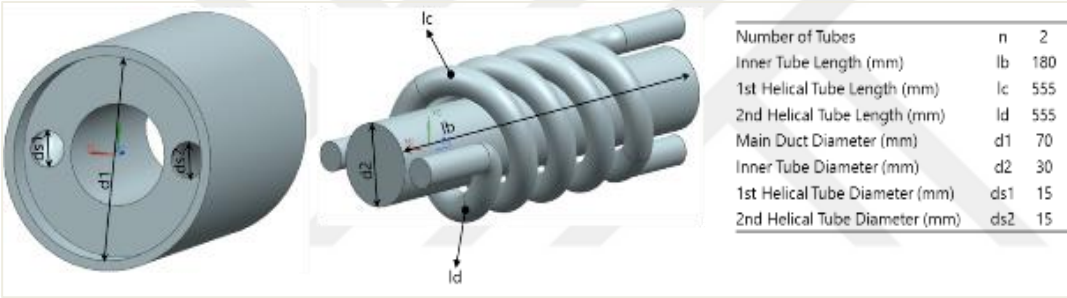


Figure 4.3 : Geometrical parameters of circular cross-section helical resonator.

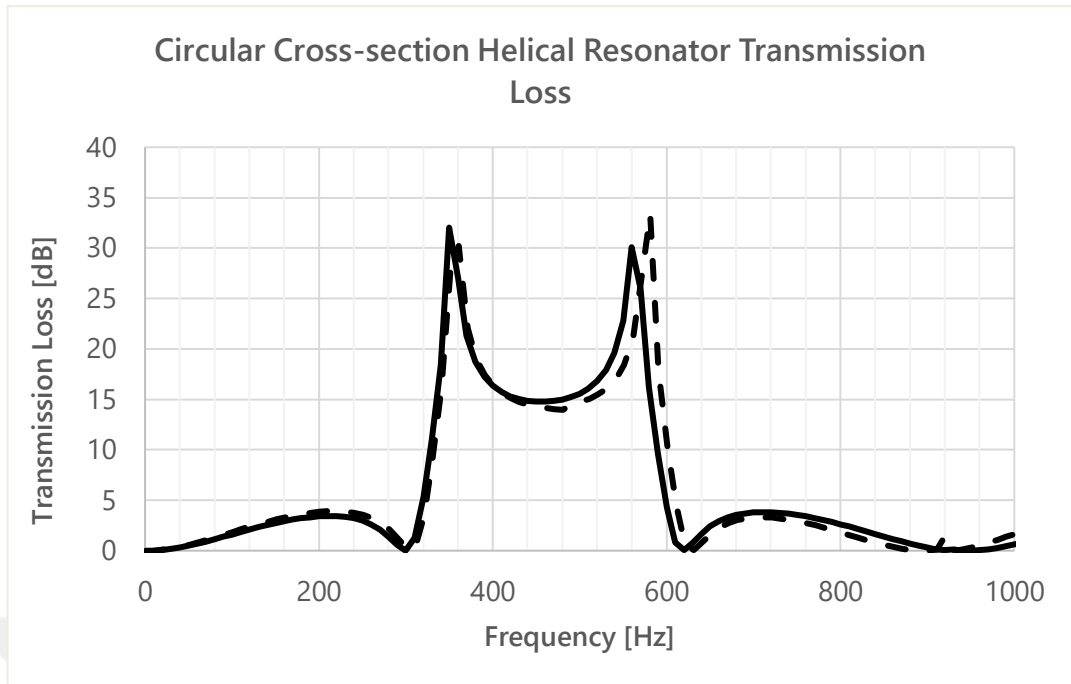


Figure 4.4 : Circular cross-section helical resonator transmission loss (solid curve: analytical model result, dashed curve: virtual analysis result).

In order to decrease the pressure drop of the circular cross-section helical resonator, a new design was created as shown in Figure 4.6. The pressure drop virtual analysis calculation results of both designs is shown in Figure 4.5. The pressure drop of the rectangular cross-section helical resonator is less than the half of the circular cross-section resonator over 200 kg/h flow rate.

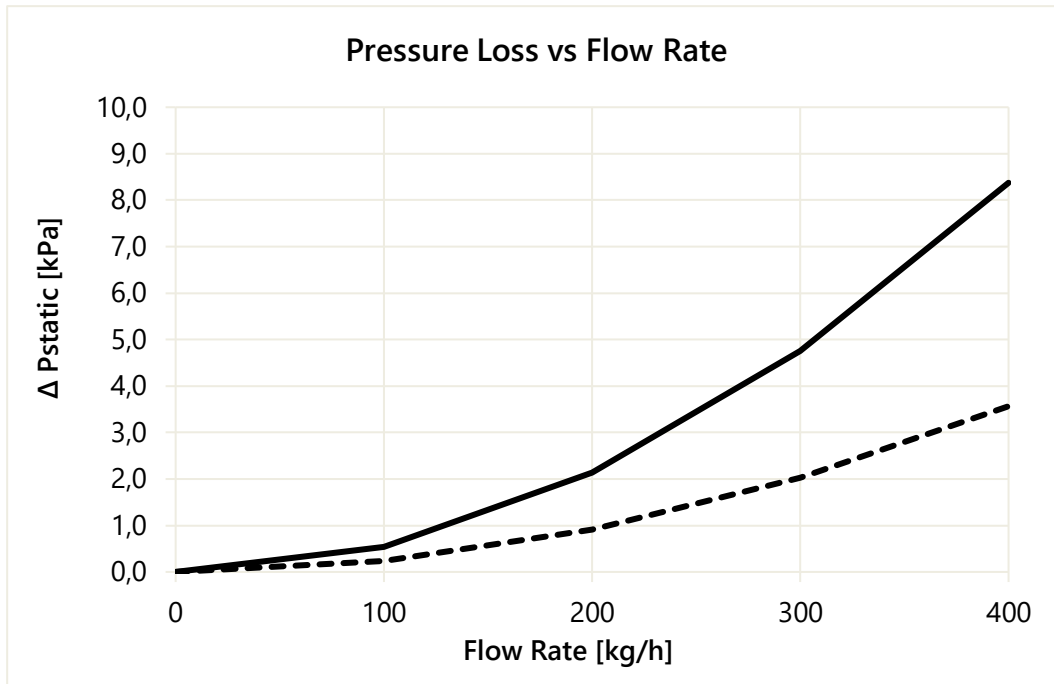


Figure 4.5 : Pressure drop virtual analysis calculation result (solid curve: circular cross-section helical resonator, dashed curve: rectangular cross-section helical resonator).

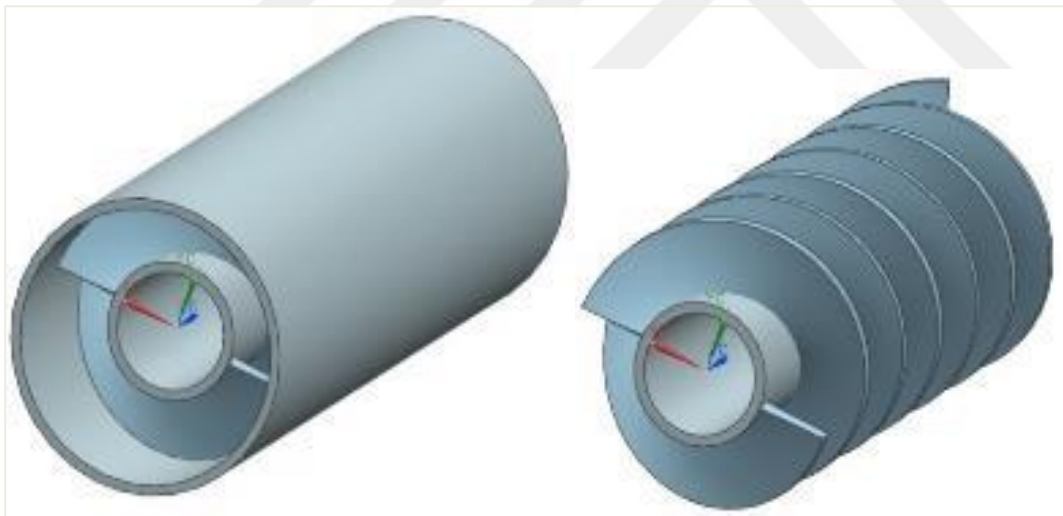


Figure 4.6 : Rectangular cross-section helical resonator.

The transmission loss of the rectangular cross-sections of helical resonator which is shown in Figure 4.7 is calculated with the analytical model and also numerically. The comparison of both is shown in Figure 4.8.

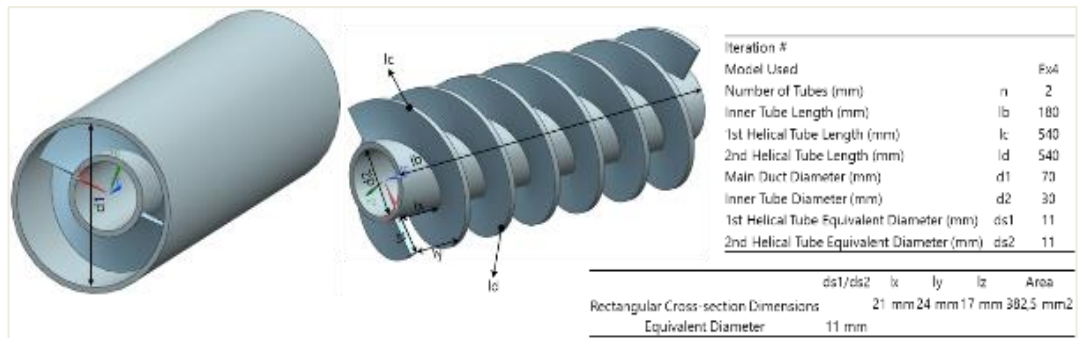


Figure 4.7 : Geometrical parameters of rectangular cross-section helical resonator.

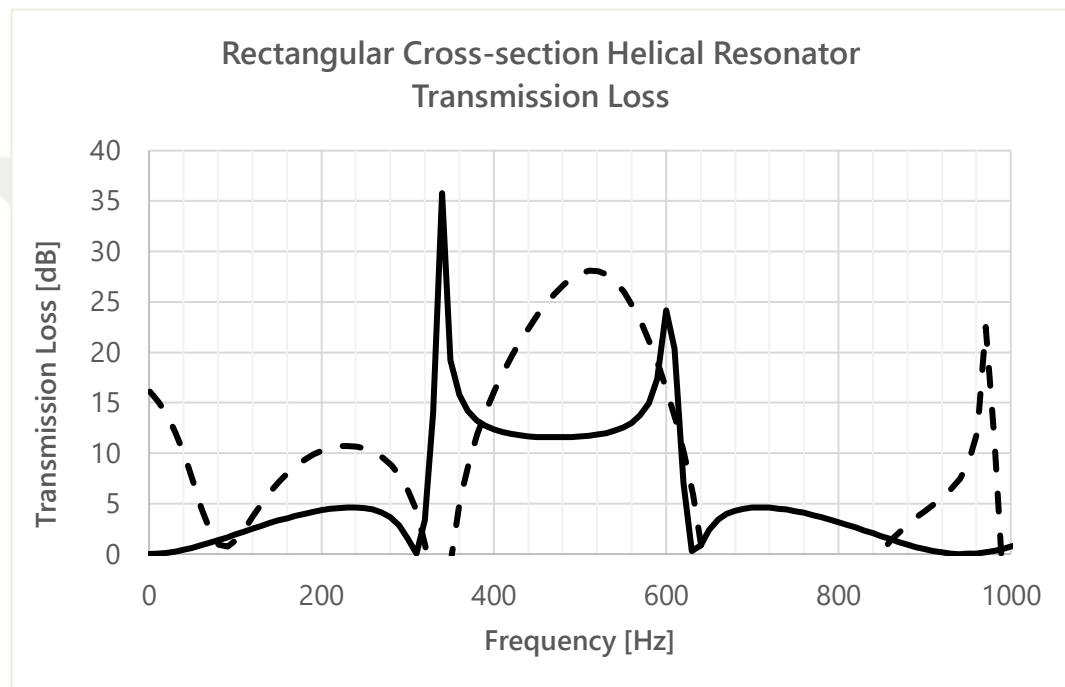


Figure 4.8 : Rectangular cross-section helical resonator transmission loss (solid curve: analytical model result, dashed curve: virtual analysis result).

Since the theory in analytical modelling is only valid for circular cross-section tubes, the area of rectangular cross-section tubes is converted to the equivalent area of the circular cross-section and analytical calculations has been performed with this assumption. The comparison of both models are not so good but considering numerical analysis results, the design in Figure 4.7 has a maximum of 10 dB of transmission loss between 100-300 Hz and 28 dB transmission loss between 340-640 Hz frequency regions. 1D analytical model can be used to estimate roughly the working frequency range and the amplitude of the transmission loss of the designed rectangular cross-section resonator.

4.5 Experimental Studies

In order to verify the output of the numerical model, first the prototype of the rectangular cross-section helical resonator has been produced with rapid prototyping technique which is shown in Figure 4.9.



Figure 4.9 : Prototype part.

First, the pressure drop test of the physical prototype is performed with the experiment setup that is shown in Figure 4.10.

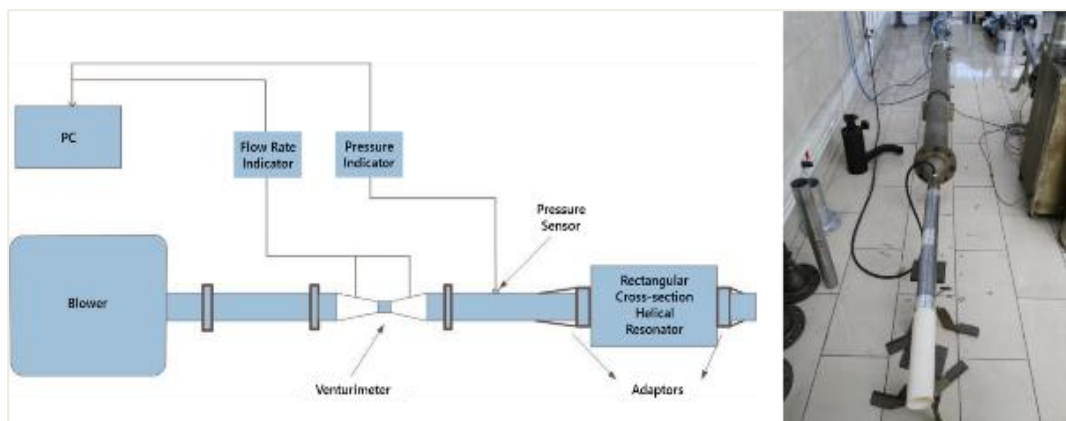


Figure 4.10 : Pressure drop test setup.

Comparison of pressure drop virtual analysis and test results is shown in Figure 4.11. There is a good agreement between numerical and test results.

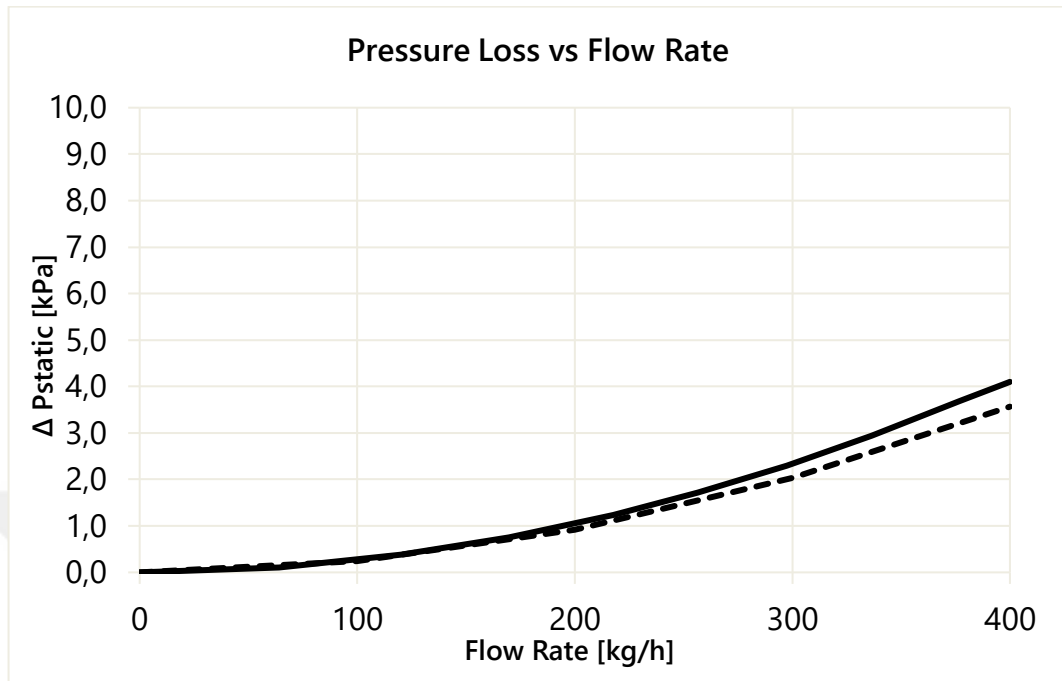


Figure 4.11 : Pressure drop virtual analysis calculation vs test result (solid curve: test result, dashed curve: numerical analysis result).

Second, the sound transmission loss test of the physical prototype is performed with the experiment setup that is shown in Figure 4.12. It consists of a 4 channel FFT analyser (dBFA Suite – NET dB), an amplifier, a loudspeaker and 4 GRAS 46BD type 1/4” microphones with sensitivity of 1.45 mV/Pa, frequency range of 4-70000 Hz and dynamic range of 44-166 dB.

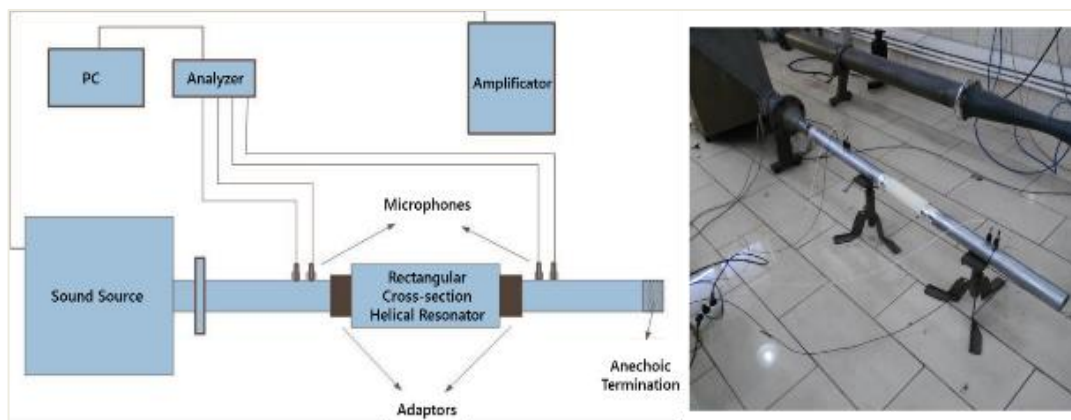


Figure 4.12 : Rectangular cross-section helical resonator transmission loss test setup.

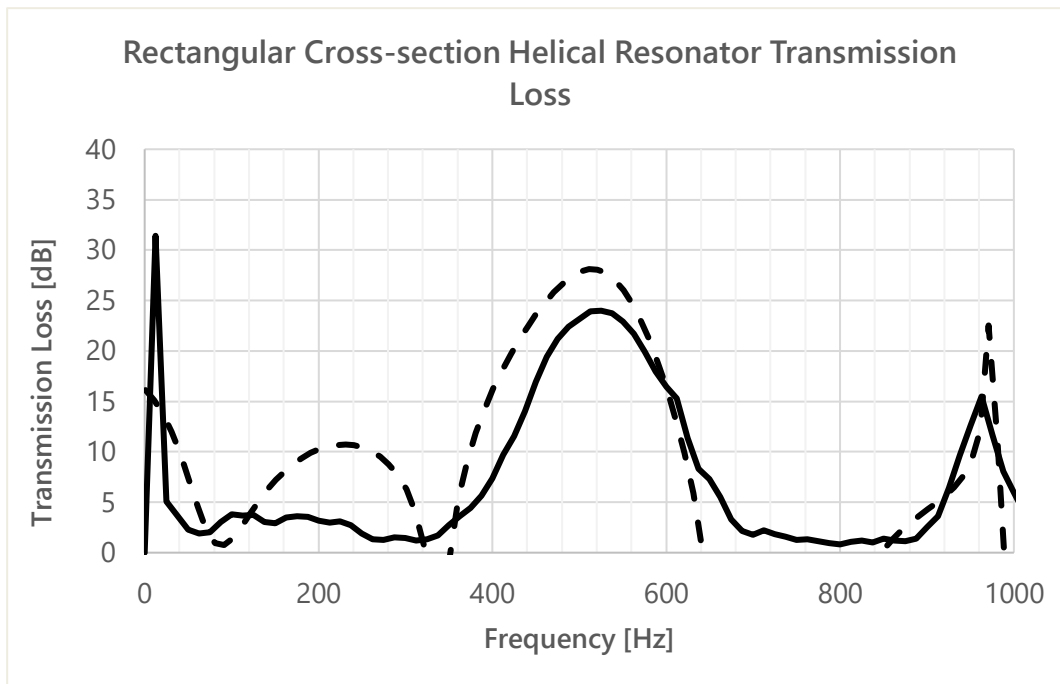


Figure 4.13 : Rectangular cross-section helical resonator transmission loss (solid curve: test result, dashed curve: virtual analysis result).

Transmission loss comparison of virtual analysis and test results is shown in Figure 4.13. Both transmission loss curves seem to show same trend below 1000 Hz. Virtual analysis result seems to have an over estimation around 7dB around 200 Hz and 5 dB around 500 Hz. Considering the TL test result, the rectangular cross-section helical resonator seem to work below 1000 Hz. It shows around 4 dB transmission loss below 300 Hz, maximum 24 dB transmission loss between 400 Hz – 600 Hz and 15 dB transmission loss around 950 Hz.

In order to verify the vehicle level performance of the resonator, a passenger car with a 1.6 liter gasoline atmospheric engine is selected. The reason of this selection is that vehicle air intake pipe radiated noise show high level of noise between 100 Hz – 200 Hz and 300 Hz – 600 Hz regions which is shown as initial condition in Figure 4.15.

The vehicle is equipped with a microphone located at driver ear position and one other at 5cm away from the duct opening. The test maneuver is the 3rd Gear wide open throttle. Microphones used in the physical verification are Bruel&Kjaer 4189 1/2” microphones with a sensitivity of 50 mV/Pa, frequency range of 6.3-20000 Hz, and dynamic range of 14.6-146 dB.

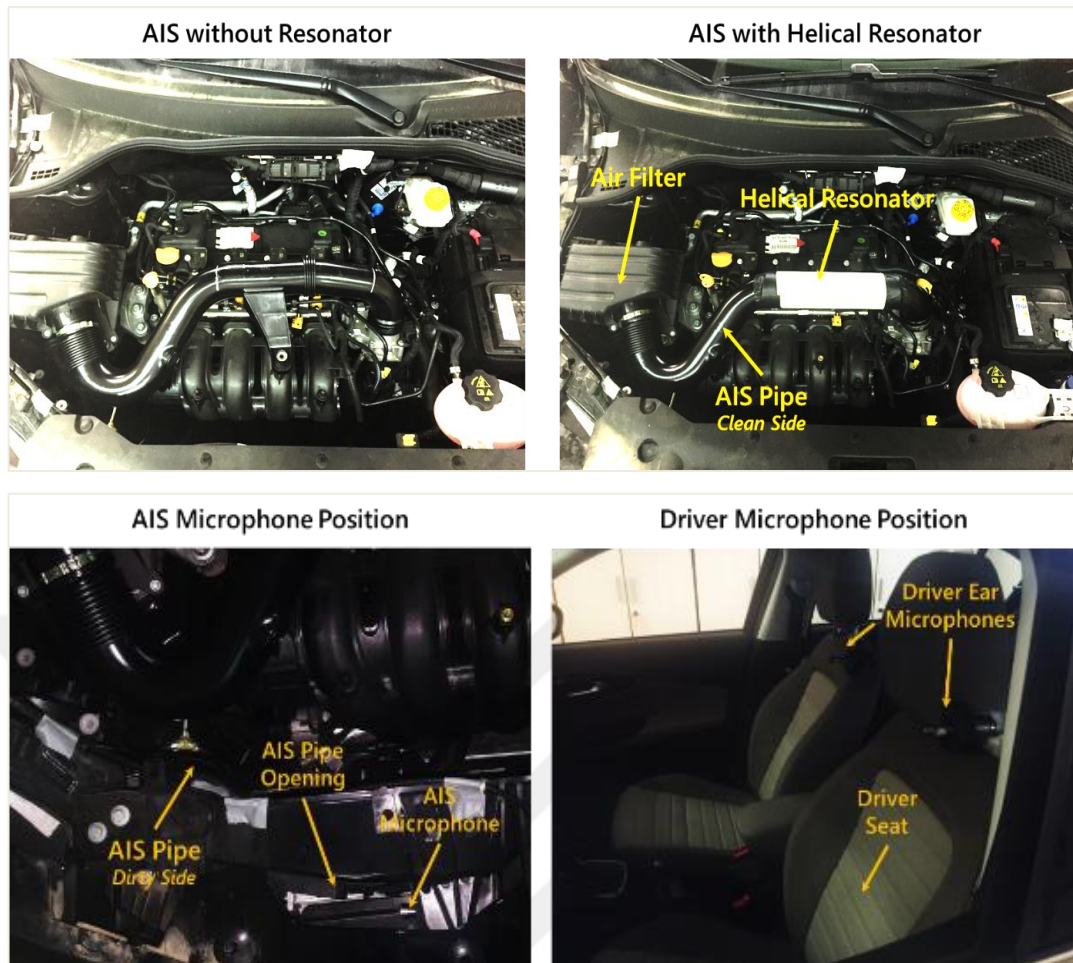


Figure 4.14 : Vehicle level validation test setup.

In the initial condition, without any resonator in the air intake system, resonant zones between 100-200 Hz and 300-600 Hz can be observed at the air intake system microphone (AIS Microphone) located at 5cm away from the intake pipe opening. These resonant zones are highlighted in Figure 4.15. In Figure 4.15, x-axis represents frequency (Hz) and the y-axis represents engine speed (rpm). The noise level at each frequency and engine speed is represented with a color scale from blue to red which is shown at the right side of the graph. After performing the test on the vehicle without AIS resonator, vehicle is equipped with the helical resonator and tested as in the initial condition. The improvement in the resonant zones at AIS microphone can be observed in the lower graph in Figure 4.15.

Physical Verification / Vehicle Level Test Results

Noise Level @ AIS Microphone (Colormap Representation)

AIS: Air Intake System
EO: Engine Order

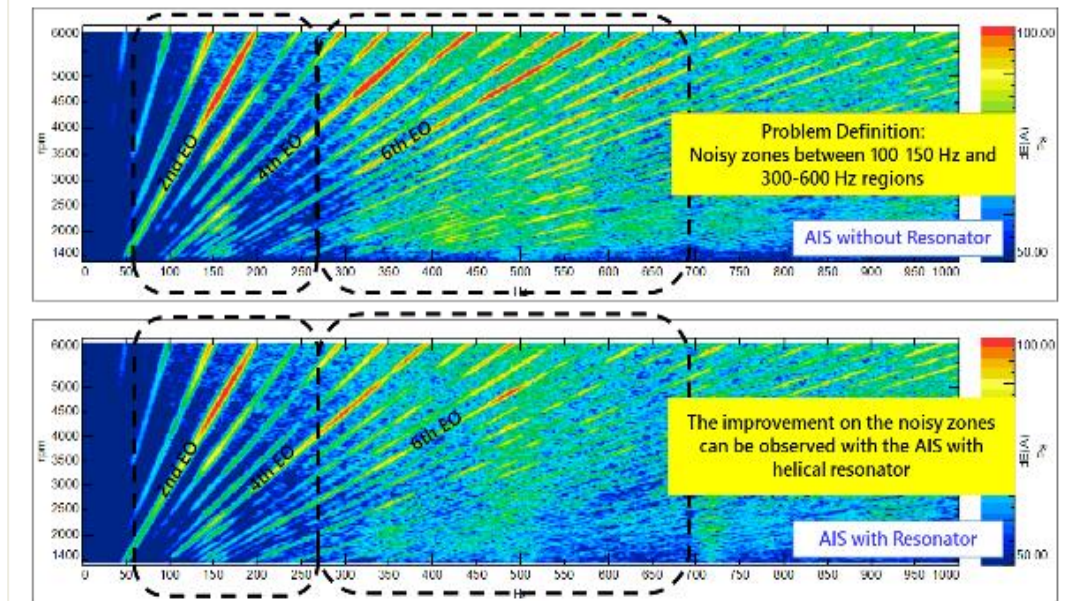


Figure 4.15 : Ais pipe opening radiated noise, colormap representation.

Figure 4.16 shows the 2D representation of the overall noise level radiated from the AIS pipe opening and the noise levels of the main engine orders. In Figure 4.16, lower x-axis represents engine speed (rpm), upper x-axis represents frequency (Hz) and y-axis represents noise level (dB). Red curve is for the vehicle without AIS resonator (initial condition) and blue curve is for the same vehicle with AIS helical resonator.

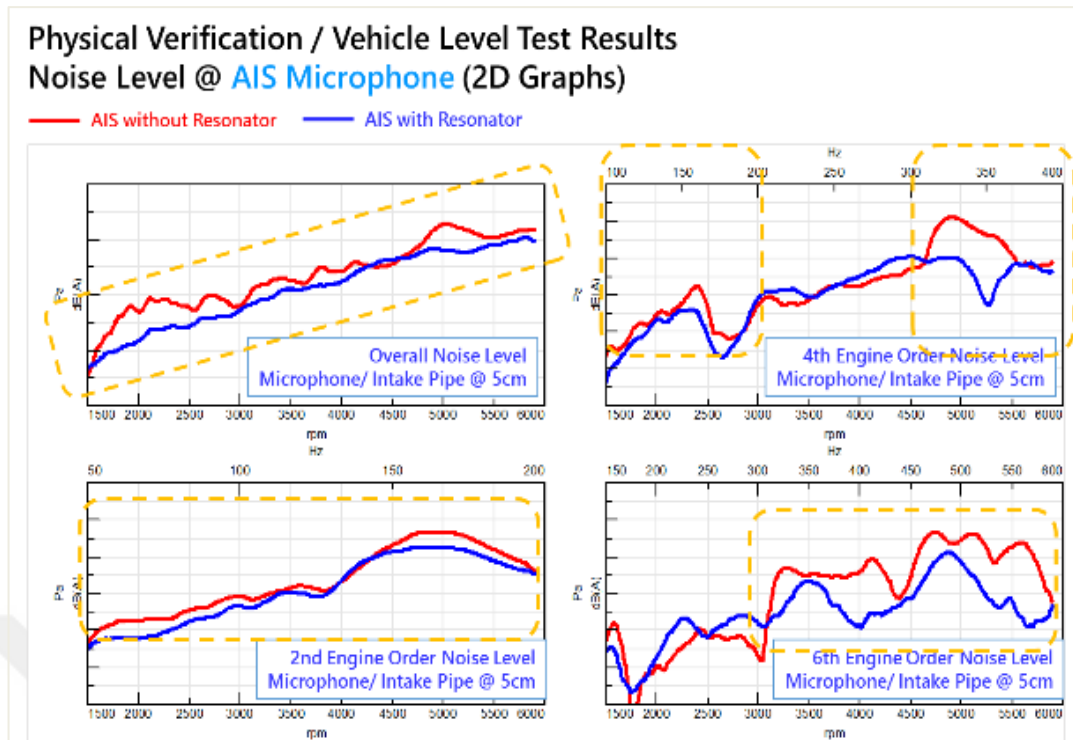


Figure 4.16 : Ais pipe opening radiated noise, overall level and noise level at main engine orders.

According to Figure 4.16, the rectangular cross-section helical AIS resonator improves the noise radiated from the AIS pipe mainly between 300 – 600 Hz and additional improvement can be observed between 100-200 Hz region. This result confirms the transmission loss test results as well as the analytical and numerical outputs. The overall radiated noise and 2nd engine order radiated noise improves nearly in all engine speed range from 1500 to 6000 rpm. The 4th engine order noise level improves mainly between 4500-5500 rpm around 10 dB from peak to peak. The 6th engine order noise level improves between 3000-6000 rpm corresponding to 300 Hz – 600 Hz frequency range.

Considering the improved frequency ranges on the AIS pipe radiated noise, the vehicle level performance of the designed resonator is in line with the virtual and physical transmission loss results are shown in Figure 4.13.

The effect of the improvement in the AIS pipe opening radiated noise to the noise level at driver ear position is shown in Figure 4.17.

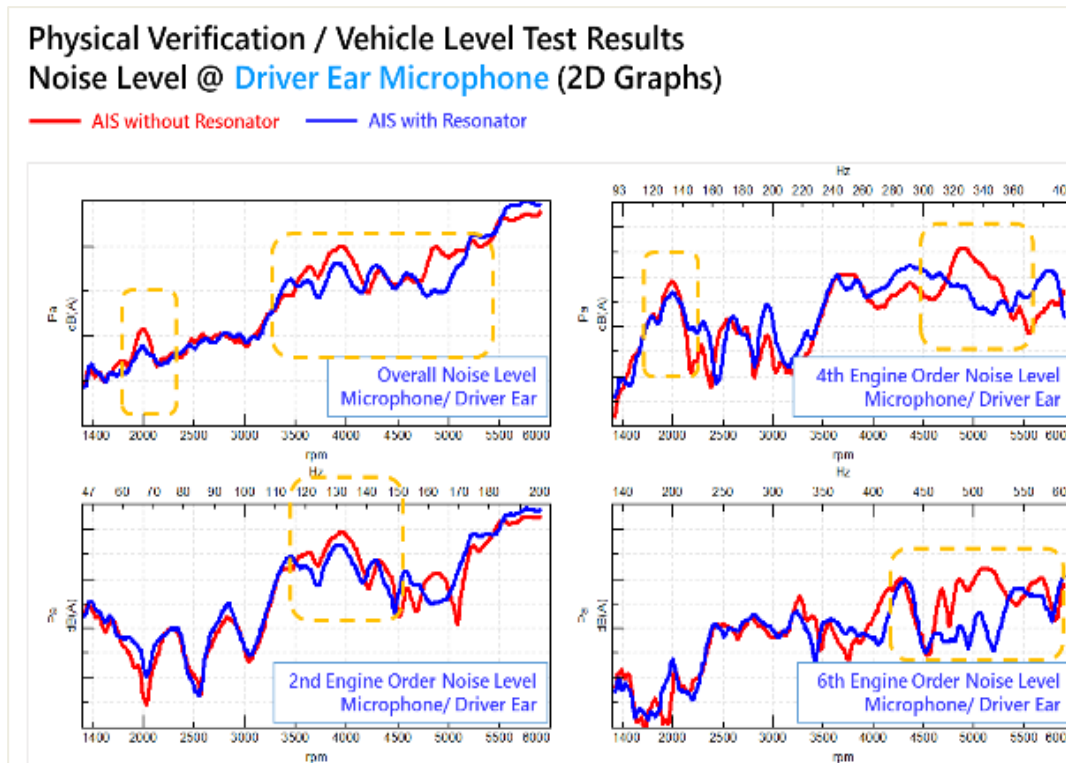


Figure 4.17 : Noise level at driver ear, overall level and main engine orders.

According to Figure 4.17, the overall noise level at driver ear is effected by the improvement in the AIS pipe radiated noise around 2000 rpm, 4000 rpm and 4750 rpm with maximum level of 5 dB(A). Maximum improvement is observed at the noise level of 4th engine order around 4750 rpm (300 Hz – 350 Hz) around 7 dB(A) peak-to-peak and between 4500 rpm – 5500 rpm (450 Hz – 550 Hz) at the 6th engine order around 10 dB(A).

4.6 Conclusion

Numerical applications show that the 1D analytical approach yields satisfactorily accurate approximations in the 0–1000 Hz frequency range for circular cross-section pipes. 1D analytical model can be used to estimate roughly the working frequency range and the amplitude of the transmission loss of the designed rectangular cross-section resonator. The physical verification results are well correlated with the numerical analysis results for both pressure drop and sound transmission loss. The developed tunable resonator show significant improvement on the noise radiated from the AIS pipe mainly between 300 – 600 Hz and additional improvement can be observed between 100-200 Hz region and this improvement resulted in quitter

passenger compartment. Considering this results, the designed tunable rectangular cross-section can be offered as a solution for AIS radiated noise for vehicles especially with small volume engine compartment. The application of these kind of resonators may become widespread with the development of rapid prototyping technique.





5. CONCLUSION

To summarize, using the developed methodology combining the optimization process performed on an SEA model and the airborne and panel acoustic contribution analysis performed on a vehicle, a lighter acoustic pack and a vehicle with a more refined interior noise level with decreased panel contributions can be developed.

The calculated results indicated a good correlation in most of the rpm ranges whereas less correlation was obtained in a few regions (1250-2250 rpm). This result may be due to the panel dimensions that determine the frequency range of the analysis. In this study, the body panels that have a direct interaction with the passenger cavity have been analyzed. The lack of correlation in the mentioned region may be due to the absence of the windscreen and the door panels. This topic should be investigated further.

The final test result of the vehicle interior noise level indicated improvement (Figure 2.27), and the improved regions are similar to what is calculated with the contribution model. The integration of the ASQ and SEA methodologies may be offered as a unique methodology that can be applied in the product development stage to release refined and lower weight vehicles.

Focusing on the acoustic pack materials that are being used on the vehicles, the mid-frequency range sound absorption performances of felts are low compared to their performance in the relatively high frequency range. There may be some cases where one may want to increase the mid-frequency absorption performance of a felt without increasing its weight. In such cases, according to the experimental results shown in this study, one can modify the sound absorption curve characteristic of a felt using elastic films and the air gap without increasing or decreasing its weight. The weight and sound absorption performance is compared in Table 3.3 for the analytical model and in Table 3.4 for the experimental verification studies. There is a good agreement between the analytical and experimental results in terms of the amplitude of the sound absorption coefficient in most of the frequency range and the tendency of the behavior

of the curve comparing different configurations listed in summary tables and in Figures 3.9 and Figure 3.10.

In conclusion, compared to the initial condition, with 12% less weight, one can gain 35% in the absorption performance in the relatively mid-frequency range with a loss (20%) in the relatively high frequency range.

Regarding to the studies focusing on the air intake system noises, numerical applications show that the 1D analytical approach yields satisfactorily accurate approximations in the 0–1000 Hz frequency range for circular cross-section pipes. 1D analytical model can be used to estimate roughly the working frequency range and the amplitude of the transmission loss of the designed rectangular cross-section resonator. The physical verification results are well correlated with the numerical analysis results for both pressure drop and sound transmission loss. The developed tunable resonator show significant improvement on the noise radiated from the AIS pipe mainly between 300 – 600 Hz and additional improvement can be observed between 100-200 Hz region and this improvement resulted in quieter passenger compartment. Considering this results, the designed tunable rectangular cross-section can be offered as a solution for AIS radiated noise for vehicles especially with small volume engine compartment. The application of these kind of resonators may become widespread with the development of rapid prototyping technique.

5.1 Practical Application of This Study

The studies of which the thesis consist of, proposes methodologies which can be used together and/or individually to ones who focus on the interior noise level of vehicles and aim to find opportunities to improve the interior noise level of a vehicle. Besides, proposing approaches as building up analytical modelling techniques, which could be useful tools for NVH engineers in product development period.

REFERENCES

- [1] **Grosso, A., Fernandez Comesana, D. and De Bree, H.** (2012). Further Development of the PNCA: New Panel Noise Contribution Reference-Related (PNCAR). *SAE Int. J. Passeng. Cars - Mech. Syst.*, 5(2), 01-1539. Doi:10.4271/2012.
- [2] **Wolff, O., Guidati, S., Sottek, R. and Steger, H.** (2004). Binaural Auralisation of Vibrating Surfaces–Laser Scanning Vibrometry Combined with Binaural Transfer Path Analysis. In *Proceedings, CFA/DAGA* (Vol. 4).
- [3] **Fleszar, A. R., Van der Linden, P. J. G., Johnson, J. R. and Grimmer, M. J.** (2001). Combining vehicle and test-bed diagnosis information to guide vehicle development for pass-by noise (No. 2001-01-1565). *SAE Technical Paper*.
- [4] **Steel, J. A., Fraser, G. and Sendall, P.** (2000). A study of exhaust noise in a motor vehicle using statistical energy analysis. *Proceedings of the Institution of Mechanical Engineers, Part D: Journal of Automobile Engineering*, 214(1), 75-83.
- [5] **Chen, X., Wang, D., Yu, X. and Ma, Z. D.** (2009). Analysis and control of automotive interior noise from powertrain in high frequency. In *Intelligent Vehicles Symposium*, Xi'an, China: 3-5 June. (pp. 1334-1339).
- [6] **Chen, S., Wang, D., Zuo, A., Chen, Z., Zan, J. and Sun, Y.** (2010). Design and optimization of vehicle interior sound package. In *Computer Design and Applications (ICCD), 2010 International Conference on* (Vol. 4, pp. V4-30). IEEE.
- [7] **Keller, H. P., Huang, L. and Pelzer, H. P.** (1998). SEA model to improve sound transmission loss of a car door. In *NOISE CON* (pp. 559-564). NOISE CONTROL FOUNDATION.
- [8] **Sarradj, E.** (2004). Energy-based vibroacoustics: SEA and beyond. In *CFA/DAGA*.
- [9] **Seddeq, H. S.** (2009). Factors influencing acoustic performance of sound absorptive materials. *Australian Journal of Basic and Applied Sciences*, 3(4), 4610-4617.
- [10] **Bai, G., Zhan, P., Sui, F. and Yang, J.** (2014). Research on sound insulation of multiple-layer structure with porous material and air-layer. In *INTER-NOISE and NOISE-CON Congress and Conference Proceedings* (Vol. 249, No. 1, pp. 6368-6373). Institute of Noise Control Engineering.

- [11] **Abid, M., Abbas, M. S., Chazot, J. D., Hammemi, L., Hamdi, M. A. and Haddar, M.** (2012). Acoustic response of a multilayer panel with viscoelastic material. *International Journal of Acoustics and Vibration*, 17(2), 82.
- [12] **Shah, S. and Belsus, S. M.** (2010). Air intake system optimization for acoustic advantage on automotive vehicles. *SAE International Journal of Commercial Vehicles*, 3(2010-01-1985), 221-229.
- [13] **Athavale, S. M. and Sajanpawar, P. R.** (1999). Analysis and Development of Inline Helmholtz Resonator through Computer Simulation for Elimination of Low Frequency Intake Noise Character (No. 1999-01-1662). *SAE Technical Paper*.
- [14] **Erol, H. and Meriç, C.** (2009). Application of resonators and a side branch duct with an expansion chamber for broadband noise control. *Noise Control Engineering Journal*, 57(5), 476-492.
- [15] **Happian-Smith, J.** (2001). *An introduction to modern vehicle design*. Elsevier.
- [16] **Meriç, C., Erol, H. and Özkan, A.** (2016). On the sound absorption performance of a felt sound absorber. *Applied Acoustics Journal*, 114, 275-280. Doi: <http://dx.doi.org/10.1016/j.apacoust.2016.08.003>.
- [17] **Munjaj, M. L.** (1987). *Acoustics of ducts and mufflers with application to exhaust and ventilation system design*. John Wiley & Sons.
- [18] **Lee, C. H., Oh, J. E., Joe, Y. G. and Lee, Y. Y.** (2004). The performance improvement for an active noise control of an automotive intake system under rapidly accelerated conditions. *JSME International Journal Series C Mechanical Systems, Machine Elements and Manufacturing*, 47(1), 314-320.
- [19] **Nishio, Y., Kohama, T. and Kuroda, O.** (1991). New approach to low-noise air intake system development (No. 911042). *SAE Technical Paper*.
- [20] **Smith, P. H. and Morrison, J. C.** (1971). *The scientific design of exhaust and intake systems*. Bentley Pub.
- [21] **Peat, K. S., Callow, G. D. and Bannister, P. A.** (1990). Improving the acoustic performance of an intake system. *Proc. I. Mech. E. C420*, 21.
- [22] **Mclean, I.** (2005). Optimized Herschel-Quincke acoustic filter (No. 2005-01-2360). *SAE Technical Paper*.
- [23] **Alt, N. W., Wiehagen, N. and Schlitzer, M. W.** (2001). Interior noise simulation for improved vehicle sound (No. 2001-01-1539). *SAE Technical Paper*.
- [24] **Castillo, M. S. and Schuhmacher, A.** (2009). Optimization of sound packages for commercial vehicles using panel contribution analysis (No. 2009-01-2241). *SAE Technical Paper*.
- [25] **Zhang, Y. K., Lee, M. R., Stanecki, P. J., Brown, G. M., Allen, T. E., Forbes, J. W. and Jia, Z. H.** (1995). Vehicle noise and weight reduction using panel acoustic contribution analysis (No. 951338). *SAE Technical Paper*.

- [26] **Rust, A., Schiffbaenker, H. and Brandl, F. K.** (1989). Complete NVH optimisation of a passenger vehicle with a DI diesel engine to meet subjective market demands and future legislative requirements (No. 890125). *SAE Technical Paper*.
- [27] **Bron-van der Jagt, G. S.** (2007). *Sound Transmission through Pipe Systems and into Building Structures* (Doctoral dissertation, PhD thesis, Eindhoven, The Netherlands).
- [28] **Burroughs, C. B., Fischer, R. W. and Kern, F. R.** (1997). An introduction to statistical energy analysis. *The Journal of the Acoustical Society of America*, 101(4), 1779-1789.
- [29] **Atalla, N. and Panneton, N.** (2012). Propagation of Sound in Porous Media: Modelling Sound Absorbing Materials. *ASME NCAD Workshop, Inter-noise 2012*.
- [30] **Biot, M. A.** (1956). Theory of propagation of elastic waves in a fluid-saturated porous solid. I. Low-frequency range. *The Journal of the acoustical Society of America*, 28(2), 168-178.
- [31] **Biot, M. A.** (1956). Theory of propagation of elastic waves in a fluid-saturated porous solid. II. Higher frequency range. *The Journal of the Acoustical Society of America*, 28(2), 179-191.
- [32] **Allard, J., & Atalla, N.** (2009). *Propagation of sound in porous media: modelling sound absorbing materials 2e*. John Wiley & Sons.
- [33] **Brouard, B., Lafarge, D. and Allard, J. F.** (1995). A general method of modelling sound propagation in layered media. *Journal of Sound and Vibration*, 183(1), 129-142.
- [34] **Delany, M. E. and Bazley, E. N.** (1970). Acoustical properties of fibrous absorbent materials. *Applied acoustics*, 3(2), 105-116.
- [35] **ESI Group** (2008). VA One User's Guide.
- [36] **Majithiya, K., Park, C.B. and Naguib, H.E.** (2011). Acoustic Behavior of Perforated Expanded Polypropylene Foam. *ANTEC Technical Paper*, 911-915.
- [37] **Chu, R.K.M., Naguib, H.E. and Atalla, N.** (2008), *SPE ANTEC Technical paper*, 1029-1033.
- [38] **Cox, T. J. and D'antonio, P.** (2009). *Acoustic absorbers and diffusers: theory, design and application*. Crc Press.
- [39] **Heed, C.** (2008). Sound absorption and acoustic surface impedance. *Stockholm, October*.



CURRICULUM VITAE



Name Surname : Cem Meriç
Place and Date of Birth : Bursa 14.07.1983
E-Mail : cem.meric@outlook.com

EDUCATION:

- **B.Sc.** : 2005, Istanbul Technical University, Mechanical Engineering
- **M.Sc.** : 2008, Istanbul Technical University, Mechanical Engineering

PROFESSIONAL EXPERIENCE AND REWARDS:

- 2007-2008 İstanbul Technical University / Project Assistant
- 2008-2011 Ford Otosan / NVH Engineer
- 2011-present TOFAŞ / NVH Engineer

PUBLICATIONS

- H.Erol and **C. Meriç** (2009). Application of resonators and a side branch duct with an expansion chamber for broad band noise control. *Noise Control Engineering Journal*, 57 (5), 476-492. Doi: <https://doi.org/10.3397/1.3148102>.

PUBLICATIONS, PRESENTATIONS AND PATENTS ON THE THESIS:

- **C. Meriç**, H. Erol and A. Özkan (2016). Noise contribution analysis of a vehicle passenger compartment. *Noise Control Engineering Journal*, 64(5), 646-657. Doi: <https://doi.org/10.3397/1/376409>.
- **C. Meriç**, H. Erol and A. Özkan (2016). On the sound absorption performance of a felt sound absorber. *Applied Acoustics*, 114, 275–280. Doi: <http://dx.doi.org/10.1016/j.apacoust.2016.08.003>.
- **C. Meriç**, H. Erol and A. Özkan (2018). Design and application of a compact helical air intake system resonator for broadband noise control. *Applied Acoustics*, 131, 103-111. Doi: <http://dx.doi.org/10.1016/j.apacoust.2017.10.022>.

